DETECTION OF HYDROGEN PEROXIDE AND ETHANOL IN EXHALED BREATH USING BIOSENSORS: CONSIDERATIONS IN STANDARDIZING BREATH COLLECTION

BY

SHIH-FANG CHEN

DISSERTATION

Submitted in partial fulfillment of the requirements
for the degree of Doctor of Philosophy in Agricultural and Biological Engineering
in the Graduate College of the
University of Illinois at Urbana-Champaign, 2012

Urbana, Illinois

Doctoral Committee:

Assistant Professor Mary-Grace C. Danao, Chair and Director of Research
Professor Keith R. Cadwallader
Professor Richard S. Gates
Professor Yuanhui Zhang

ABSTRACT

Breath monitoring is a non-invasive, safe, and repeatable approach to determining the health status of humans and other mammals. Breath samples could be detected in two ways – directly sensing exhaled breath (EB) or chilling the EB to obtaining the exhaled breath condensate (EBC). Each has its advantages and disadvantages but they are both affected by different sampling conditions. Additionally, volatile organic compounds (VOCs) and nonvolatile organic compounds (non-VOCs) in the breath matrix are retained differently under varied sampling conditions. The dearth of information on how sampling conditions affect the intrinsic properties of biomarkers in breath and the lack of standardization information hinder the use of breath monitoring in clinical use.

The study aims to develop predictive models to standardize the varied sampling conditions of breath temperatures, flow rates, condensing temperatures, and sensing durations in EB and EBC sensing. Ethanol (VOC) and H_2O_2 (non-VOC) were chosen as model biomarkers, which were potential biomarkers of liver function and respiratory diseases, respectively. A breath output simulator was developed to simulate the conditions of exhaled breath. Screen printed carbon electrodes (SPCEs) were used solely or immobilized with alcohol oxidase as biosensors for detecting the chosen biomarkers amperometrically. Akaike's information criterion, Bayesian information criterion, and cross validation were adopted in predictive model selections, and uncertainty analyses were surveyed to further clarify the margin of doubt for the measurement of each sampling factors.

Final predictive models were developed for ethanol in EB and EBC, and H_2O_2 in EBC for specific sensing time (5 min) and full sensing duration (3-10 min). Results showed that the EBC model for ethanol in 5 min measurement performed a better regression result ($R^2 = 0.9471$) than the EB model for ethanol ($R^2 = 0.8261$) and the EBC model for H_2O_2 ($R^2 = 0.8261$). Furthermore, in 5 min predictive models, both ethanol and H_2O_2 concentrations in EBC samples were affected by condensing temperature, but only H_2O_2 detection was affected by breath temperature and breath rate. The results indicated that sampling conditions were more critical and were more constrained for non-VOC sensing than VOC sensing. Uncertainty analyses showed that the 5 min EBC predictive models had 18.53 – 26.55% percentage uncertainty and the 5 min EB predictive model had up to 44.21% percentage uncertainty. The major source of the uncertainties was due to the sensing system which included the SPCEs and used enzyme.

ACKNOWLEDGMENTS

This project and my graduate program could not be accomplished without the assistance and support from many people. First, I would like to acknowledge my advisor Dr. Mary-Grace Danao for giving me the opportunity to conduct the study. Thank you for providing me your valuable advice, patience, expertise throughout the entire project and your invaluable experience share for my professional development. Moreover, I appreciate the opportunities to be the teaching assistant in your classes that benefited me a lot about how to mentor students and teach classes. Also, I would like to thank my committee members, Drs. Keith R. Cadwallader, Richard S. Gates, and Yuanhui Zhang for your guidance and suggestions. Especially Dr. Gates, thank you for teaching me how to interpret the data from theoretical perspective to realistic aspects.

I would like to express my sincere gratitude to the faculty and colleagues in Agricultural and Biological Engineering Department. Thank you for creating such a friendly and resourceful learning environment. Dr. K.C. Ting and Susan, thank you for the excellent care given to me. Your hospitality warms the hearts of many students and colors our days with your warmest concern. Dr. Prasanta Kalita, thank you for your friendship. You are my first friend at U of I, and I am always inspired by your enthusiasm to your professional career and positive philosophy of life. Shilpa Naidu and Yun Yin, thank you for your friendship and assistance in my daily lab activity. The conversations between us brainstorm the idea for research and broaden my view in life as well. Dr. Ming-Che Hu, thank you for taking care of our need when we first got here and share your life experience in US.

I would like to extend my appreciation to all the teachers and members in BW (Bliss and Wisdom) group, your support and blessing accompany me to go through every moment that I felt lost and reminder me to develop compassion, wisdom, and bravery in my life. Yung-Chen Liao, you are the one who always tolerate me, encourages me, and remind me the right mindfulness. Thank you, you virtually made a great contribution to my work.

Lastly, I hereby want to express my deepest gratitude to my parents for their tremendous love, understanding, and support. You raise me with meticulous care and good education; cultivate my confidence and healthy personality. Your love is the most precious thing that I possess and I believe that would come with me no matter how old I am. I sincerely dedicate my work to you.

TABLE OF CONTENTS

CHAPTER 1: INTRODUCTION

Exhaled breath contains hundreds of metabolic products acting as biomarkers of animal well-being, physiological and enzyme reactions, and the onset of disease. Compared to clinical blood and urine tests, breath monitoring offers several advantages -- it is noninvasive, offers a low risk of infection, repeatable, and convenient for long-term clinical monitoring.

Breath monitoring is carried out by sensing exhaled breath (EB) in the gas phase directly or passing the EB through a chilled condenser to obtain the exhaled breath condensate (EBC) sample in aqueous phase for further sensing. Gas phase sensing captures the volatile organic compounds (VOCs) in breath firsthand and minimizes the possibility of the self-vaporizing or intermixing with an external gas source or the environment. Nonvolatile organic compounds (non-VOCs) are limitedly present in aerosolized vapor with a very low level of concentration and place a big challenge on the limit of detection. On the other hand, EBC can retain nonvolatile organic compounds such as cytokines, isoprostanes, hydrogen peroxide (H_2O_2) and water soluble VOCs such as acetone, ammonia, and ethanol. However, for both phases, sampling conditions such as temperature, flow rate and relative humidity are of great interest because they affect the different intrinsic properties of each biomarker, such as its solubility, volatility, and stability. The dearth of information on how sampling conditions affect the intrinsic properties of biomarkers hinders the use of breath monitoring in clinical use. Therefore, there is a need to develop predictive models for quantifying biomarker concentrations in breath which would be useful in standardization of breath sampling, or collection, for EB

and EBC analysis. The development of a robust, portable, low-cost biosensor for EB and EBC analysis would also advance breath monitoring in clinical applications.

The overall objective of this study was to develop an enzyme-based biosensor to detect hydrogen peroxide and ethanol in exhaled breath and its condensate while considering the effects of sampling conditions on the concentration of these biomarkers. The specific objectives of the project were to:

1. Determine the behavior of VOC in simulated exhaled breath (EB) and exhaled breath condensate (EBC) and develop a predictive model under varied sampling conditions — using ethanol as the model biomarker.
2. Determine the behavior of non-VOC in simulated exhaled breath (EB) and exhaled breath condensate (EBC) and develop a predictive model under varied sampling conditions — using hydrogen peroxide as the model biomarker.
3. Determine the uncertainties of a breath output simulator and each sampling variables to evaluate the accuracy and to identify the major source of error of the predictive models.

This work is creative and original in that standardization of breath collection remains elusive and there is a need to develop a low-cost and portable device for breath monitoring purposes. In addition, it is among the very first studies to determine the decomposition of hydrogen peroxide at low temperatures and high relative humidity. Successful completion of the research is expected to have a potentially transforming impact on the development of sampling and sensing technologies not only for breath analysis, but in other applications of trace gas analysis.

CHAPTER 2: LITERATURE REVIEW

2.1 Exhaled Breath and Exhaled Breath Condensate

Breath detection, first proposed by Linus Pauling in 1970, involved using gas chromatography to analyze more than 200 compounds in the breath matrix (Miekisch et al., 2004). Some of those metabolic compounds are promising to be indicators for disease diagnosis, symptom exacerbation, or drug effects.

EB represents the first-hand information in breath and avoids further dilution by water vapor, but it has the difficulties in storage. Hence, immediate sensing is necessary for preventing possible decomposition or contamination reaction. In terms of EBC, researchers have argued that EBC provides better storage options and off-line detection than EB, because both non-VOCs and water-soluble VOCs are more stable in liquid phase. Therefore, more studies of breath analysis have been conducted by detecting the concentration level of biomarker in EBC than in EB.

EBC is collected by passing EB through a device and cooled down using wet ice, dry ice or a cold liquid. EBC usually preserves non-VOCs and water-soluble VOCs at trace concentrations, nmol/l to pmol/l (ppbv to pptv) (Horváth et al., 2005). In clinical studies, 1-3 ml of EBC is collected from patients, which takes, on average, 10-30 minutes of sampling time (Grob, et al., 2008a). The long sampling time impedes practical application for clinical diagnosis. Generally, a preconcentration step is needed to reach the detection limit of the instrument by removing excess water vapor in the breath sample. Solid-phase extraction (SPE), solid-phase microextraction (SPME) or direct cryofocusing are widely used preconcentration techniques in EBC detection (Knutson and Viteri, 1996;

Grote and Pawliszyn, 1997).

2.1.1 Biomarkers in Breath

A biomarker is a substance that can be used as an indicator of disease or well-being. Risby (2001) and Miekisch et al. (2004) reported that endogenous biomarkers can be classified into four categories: 1) hydrocarbons, such as ethane, pentane and isoprene; 2) oxygen-containing compounds, such as acetaldehyde, ethanol, and 2-propanol; 3) sulfur-containing compounds, such as methyl, ethyl mercaptanes, and dimethylsulfide; and 4) nitrogen-containing compounds, such as ammonia and dimethyl/trimethylamine. Today more than 500 biomarkers are found in breath which can provide important clinical information for assessing well-being or diagnosing disease. Changes in the biomarker concentration and overall breath composition over time can be correlated to a range of health conditions and diseases (Table 1).

Unrelated to alcohol consumption, ethanol levels in breath are associated with intake of carbohydrate (e.g., glucose) and overgrowth of bacteria or yeast in the digestive system. Ethanol and acetone are also presumed biomarkers to determine blood glucose level (Galassetti et al., 2005). Risby (2001) and Cope et al. (2000) determined that the regulation of gut bacteria and obesity in mice were correlated to breath ethanol.

H_2O_2 is one of the reactive oxygen species used to evaluate the level of oxidative stress in respiratory systems of humans and other mammals (Grob et al., 2008; Kostikas, 2003; Loukides et al., 2010; Deaton et al., 2004; Kirschvink et al., 2005). H_2O_2 levels have been correlated with lung-related inflammation, such as bronchial hyperresponsiveness, bronchoconstriction (Hulsmann et al, 1994), neutrophil priming

(Oudijk et al., 2006), and eosinophilic inflammation (Loukides et al., 2002). H_2O_2 levels in healthy adults range from 0.01 nM to 0.45 μM in EBC (Nowak et al., 2001) and increase significantly at the onset of pulmonary inflammation.

Table 1. Biomarkers in exhaled breath and its condensate are related to several health conditions and diseases

Biomarker	Typical "healthy" levels (ppb[1])	Elevated levels (ppb)	Clinical condition	Source
Acetaldehyde	244 ± 17[2]		Liver function	Turner et al. (2006b)
Acetone	477 ± 1.58[3]		Diabetes	Turner et al. (2006d)
	363			Španel et al. (2007)
Ammonia	833 ± 1.62[3]		Kidney function	Turner et al. (2006d)
	317			Španel et al. (2007)
Ethanol	196 ± 244[2]		Liver function and elevated levels of gut Bacteria	Turner et al. (2006b)
	104			Španel et al. (2007)
Hydrogen peroxide	569 ± 29.7[4]	3970 ± 868[3]	Airway inflammation, COPD[5]	Becher et al. (2005)
	310[3]	660[3]		Kostikas et al. (2003)
		480[3]		Nowak et al. (1999)
Isoprene	118 ± 68[2]		Cholesterol biosynthesis	Turner et al. (2006c)
Methanol	450± 1.62[3]		Abnormally high gut flora associated with renal failure Pancreatic insufficiency Carbohydrate malabsorption	Turner et al. (2006a)
Nitric oxide	10 to 33	6 to 98	Airway inflammation, asthma	Grob et al. (2008b)
		>19		Grob et al. (2008c)

[1]ppb = parts per billion; [2]Concentrations are reported as mean with a standard error; [3]Concentrations are reported as geometric mean with a geometric standard deviation; [4]Concentrations are reported as nmol/l; [5]COPD = chronic obstructive pulmonary disease

For simulating H_2O_2 in EB, the intrinsic properties of H_2O_2 should be considered. Commercial H_2O_2 (3-30% w/w) is relatively stable below room temperature but it has the tendency to decompose exothermically into oxygen and water. In previous studies the decomposition rate of H_2O_2 was evaluated at temperatures between 100 and 280°C, disregarding any effects from relative humidity (Lin and Smith, 1991). In exhaled breath sampling and sensing, H_2O_2 decomposition needs to be minimized or monitored for accurate measurements of H_2O_2 levels from the airway. Temperature, pH, and other impurities can affect the decomposition of H_2O_2. An increase of 10°C in the 20 to 100°C temperature range increased decomposition rates by a factor of 2.2 (Stellman, 1998). The decomposition rate of H_2O_2 is usually determined under ambient relative humidity conditions (less than 75%). Since exhaled breath is saturated (greater than 95% relative humidity) and is at lower temperatures 307-315 K (34-42°C), the decomposition rate for H_2O_2 at these conditions needs to be determined. EBC pH is also an indicator of lung inflammation or airway disease when it is lower than 7.5. For example, breath pH of 5.23 ± 2.1 is correlated to asthma exacerbation and breath pH of 6.97 has been measured for patients with chronic obstructive pulmonary disease (Horváth et al., 2005; Grob et al., 2008a).

2.1.2 Collection Techniques and Devices

Exhaled breath is usually collected by a mouthpiece or a facemask (Figure 1). It is more common to use mouthpieces for humans to obtain a larger volume of exhaled breath and shorten collection time. Cattle are mainly nose breathers and facemasks provide an easier attachment to their head and ease discomfort (Reinhold and Knobloch, 2010).

EBC is collected by user-designed or commercial devices with a cooling system to cool it down to at least 10°C and up to -70°C. Four major types of commercial devices – RTube™, ECoScreen®, TURBO-DECCS, ANACON – have been used in several studies (Figure 2). The fundamental mechanism of those devices is to provide a cooling sleeve wrapped around a collection tube to facilitate the condensation process. The mouthpieces and condensate collectors are mostly single-use, disposable tubes that do not require cleaning between sampling.

(a) (b)

Figure 1. Typical EBC sampling collection devices include (a) a mouthpiece, www.rtube.com/products-rtube.htm and (b) facemask designed for a conscious horse, www.homeofrestforhorses.co.uk/Horse-Trust-Funded-Research-Leads-to-New,-Non-Invasive-Ways-of-Assessing-Respiratory-Health-in-Horses/.

RTube™ (Respiratory Research, Inc, Charlottesville, VA) uses an aluminum jacket as a cooling sleeve which is cooled at least one hour ahead in a freezer to provide a cooling temperature of -20 or -70˚C. The sleeve is then wrapped around a condenser made of polypropylene (Prieto et al., 2007; Czebe et al., 2008; Davidsson and Schmekel, 2010). It is portable and the collection tube is disposable, but collection time increases with the temperature of the cooling sleeve. RTube™ is more commonly used in breath analysis research conducted in the U.S. (Hunt, 2007).

ECoScreen® (Erich Jaeger GmbH, Wűrzburg, Germany) uses an aluminum tube with double lumen lamellar Teflon-coating and a condenser made of polypropylene. Refrigeration via an electric system is turned on at least 40 minutes before sampling (Czebe et al., 2008, Davidsson and Schmekel, 2010). Cleaning is necessary between sample collections. Most EBC research conducted in Europe chooses ECoScreen® as their collection device (Hunt, 2007). A transportable unit for research on biomarkers obtained from disposable exhaled condensate collection systems (TURBO-DECCS, ItalChill, Pharma, Italy) uses a Peltier module to adjust the condensing temperature of a condenser down to -10°C (Goldoni et al., 2005).

ANACON (Biostec, Valencia, Spain) applies a thermoelectric pump to cool a glass-surface condenser (Romero et al., 2006; Czebe et al., 2008). In condensing temperature regulation, ECoScreen® and ANACON presented a better stability than RTube™ and Turbo Deccs (Goldoni et al., 2005; Czebe et al., 2008; Hoffmeyer et al., 2009). Comparatively, RTube™ and ECoScreen® are referred to in EBC publications more than TURBO-DECCS and ANACON in EBC publications (Hunt, 2007).

The effect of different materials used in collection devices on EBC quality and a comparison among the commercial collectors are well-documented. Soyer et al. (2006) found ECoScreen® was more sensitive and larger volumes of EBC could be collected for protein and lipid analysis. Condensers made of glass, silicon and EcoScreen® significantly affected the condensate volume and biomarker detection, and glass presented better efficiency than other two (Rosias et al., 2008). Moreover, the inner coating of the condenser also interferes with the biomarker concentrations. Rosias et al. (2006) found higher 8-isoprostane and albumin concentrations were collected when silicone or glass coating were used instead of EcoScreen®, aluminium, polypropylene and Teflon. Although the materials used in the condenser significantly affected the biomarker level in exhaled breath condensate, no particular device can deliver ideal results for a wide range of analytes (Liu et al., 2007).

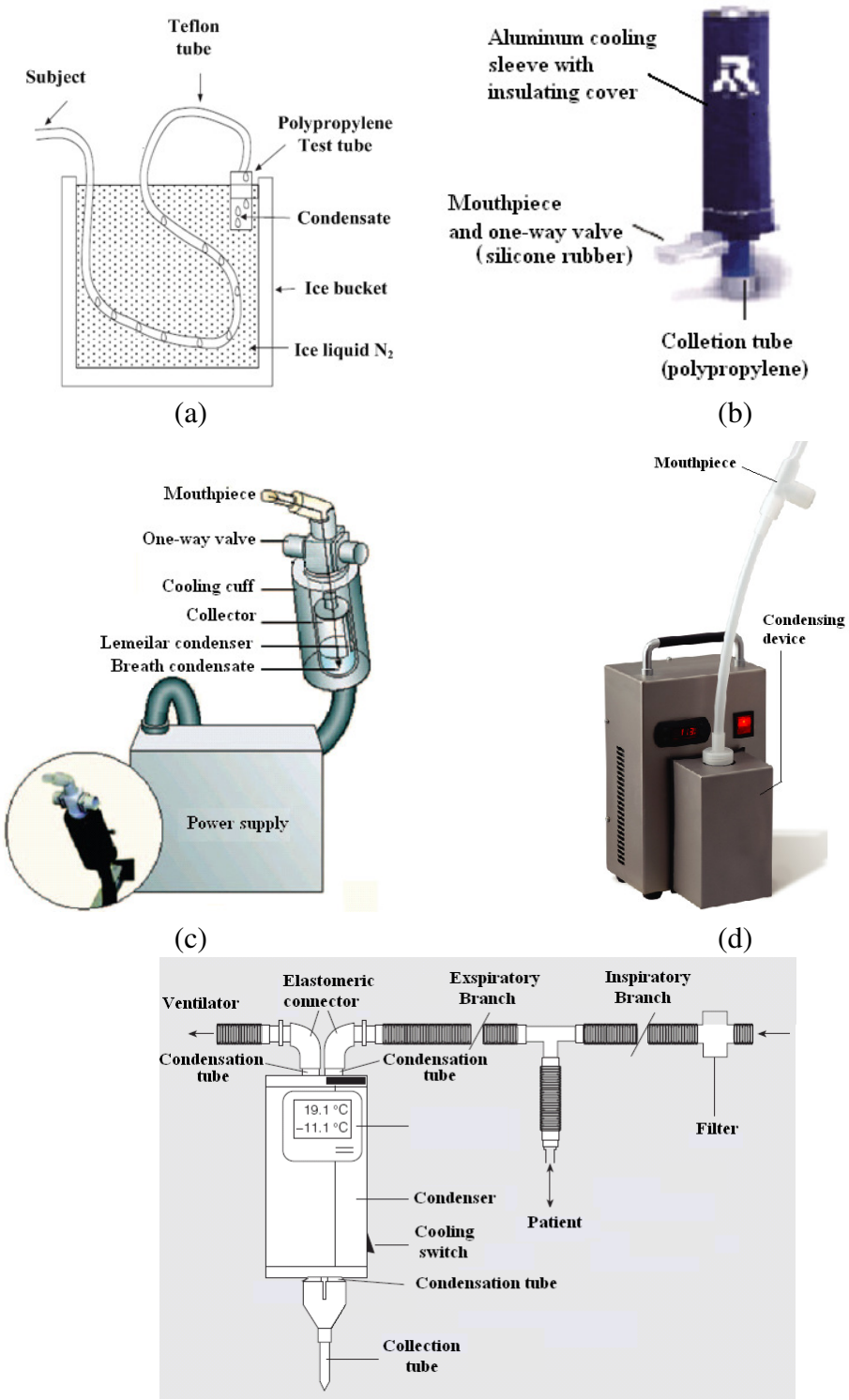

Figure 2. EBC collection device. (a) user-designed condensing device (Mutlu et al., 2001); (b) R-Tube (Chapman et al., 2010); (c) ECoScreen® (Montusch, 2007); (d) TurboDECCS, source: ttp://www.ascencia.com.au/brochures/English%20Brochure%20Turbo%20Deccs-%20%20EBC.PDF); (e) ANACON (Romero et al., 2006).

2.2 Factors that Influence Breath Collection

Direct EB collection produces less exogenous contamination but it is difficult to capture non-VOCs which are only present in small droplets. Non-VOCs are better retained in the EBC but large amounts of water vapor significant dilute non-VOCs. Several studies have been conducted to determine how a number of factors affect the concentrations of both VOC and non-VOC biomarkers.

In general, factors that could influence breath biomarker concentrations can be classified into three categories – conditions of subject, sampling conditions, and post analytical processes. Conditions of subject include temperature and pH of airway lining fluid, breathing rate or breath flow rate, contamination by upper airways and mouth, and intra-subject diurnal activities (Montuschi, 2007; Chapman, 2010). Temperature and pH lead to changes in intrinsic properties of biomarkers, such as its volatility and solubility (Hunt, 2007). Bell and Flack (1995a,b) reported breath alcohol levels can vary with EB temperature. Reinhold et al. (2006) measured breath pH and carbon dioxide levels and found them to be affected by airflow rate during EBC collection. Schleiss et al. (2000) noted hydrogen peroxide concentrations were also flow-dependent, while others reported malondialdehyde and adenosine levels in breath were flow-independent (Huszar et al., 2002; Corradi et al., 2003).

Sampling conditions are related to condensing temperature, collection device materials, collection time, dilution, pH of EBC, contamination from ambient air, and cross reactions in EBC matrix (Hunt, 2007; Montuschi, 2007; Chapman, 2010). Horváth et al. (2005) found that lower condensing temperatures stabilized unstable mediators, such as leukotrienes and purines, and the solubility of ammonia was proportional to the

sampling temperature. Higher acetone concentrations were found in condensate when a lower condensing temperature (-50, -20, and 0 °C) was applied (Loyola et al., 2008). Conversely, H_2O_2 were present at lower concentrations in the condensate when collected at lower temperatures (-10, -5, 0, and +5 °C) (Goldoni et al., 2005). For varied sampling time (3-20 min), no significant difference was found between pH, concentrations of H_2O_2, 8-isoprostane, adenosine, nitrite/nitrate, and malondialdehyde (Vaughan et al, 2003; Horváth et al., 2005). Hunt (2007) claimed the level of VOC was irrelevant with turbulent status of breath and dilution factors. Post analytical processes cover possible pretreatment procedure (e.g., preconcentration, separation), reference standard using in quantification device (e.g. mass spectrometry), and validation method (Montuschi, 2007).

2.3 Analytical Methods

Early breath research relied on gas chromatography (GC) and mass spectrometry (MS) for quantifying biomarker concentrations with great sensitivity at ppb to ppm level. Since 2000, several techniques and improvements over traditional GC and MS have been developed to improve the sensitivity and specificity of bench-scale analytical instruments, such as PTR (proton transfer reaction)-MS and optical absorption, or to improve real-time sensing with a portable device, such as and electronic nose or biosensor.

2.3.1 Laboratory Techniques

GC is one of the most commonly used methods to measure trace concentrations (parts per billion (ppb) to parts per trillion (ppt) levels) of VOC in breath (Mueller et al., 1998). It can be coupled to other instruments, such as flame ionization detection (GC-FID), mass spectrometry (GC-MS), and ion mobility spectrometry (GC-IMS) to

improve sensitivity and selectivity. Preconcentration procedures (e.g., SPE, SPME, cryofocusing) are necessary by using suitable adsorbents or fibers before injecting sample into GC-related instruments (Francesco et al., 2005).

The principle behind proton transfer reaction mass spectrometry (PTR-MS) and selected ion flow tube mass spectrometry (SIFT-MS) is the ionization of trace gas analytes by proton transfer with generating precursor ion in a flow-drift tube. The quantification results are obtained from the ratios of ion count rates using the known reaction rate constants which are analyzed by a quadrupole mass spectrometer. SIFT-MS has been used in longitudinal studies where key biomarkers (ethanol, methanol, acetone, acetaldehyde, and isoprene) were monitored to determine the base concentrations for "healthy" individuals (Dahnke et al., 2001; Turner et al., 2006a-d). The main difference between these two methods is that PTR-MS can only generate H_3O^+ as the precursor ion while SIFT-MS can generate multiple precursors, such as H_3O^+, NO^+, and O_2^+, to present a better chemical resolution in identifying sample species and concentration level (Ross, 2008).

Optical absorption spectroscopy has the virtue of real-time sensing and high sensitivity (ppb-level). Niox Mino® (Aerocrine AB, Solna, Sweden) is a handheld commercial product based on chemiluminescent reaction for sensing nitric oxide in exhaled breath (Alvin et al., 2006). Colorimetric assays can also be performed to measure 8-isoprostane, H_2O_2, and nitrate and nitrite concentration on collected EBC samples (Van Hoydonck et al., 2004; Cruz et al., 2009).

An electronic nose, a single chemical sensor for certain substance or an array-designed sensor for multiple substances, can be used to measure trace biomarkers in breath by monitoring changes in electrical signal, such as resistance, electron-volt, or vibration frequency (Fleischer et al., 2002; Dragonieri et al., 2009). The detection limits of electronic noses vary according to the type of polymer sensors used and the different VOC concentrations (Biller et al., 2011). Cyranose 320® (Smiths Detections, Pasadena, CA, US) is a commercially available electronic nose that has been demonstrated to be effective for lung cancer detection (Machado et al., 2005). In addition to the methods mentioned above, a summary of their advantages, disadvantages and sensitivities are listed in Table 2.

Table 2. A comparison of analytical methods used in breath analysis

Analytical Method		Advantages	Disadvantages	Sensitivity	Reference
GC					
	GC-FID	Quantitative High Sensitivity Low noise Large linear response range Reproducible	Sample destroyed	ppb	Phillips and Greenberg (1991) Cheng and Lee (1999) Cao and Duan (2007)
	GC-MS	Qualitative Identify isotope compound	Off-line detection	sub-picomolar ppb - ppm	Cheng and Lee (1999) Daughtrey et al. (2001) Giardina and Olesik (2003) Cao and Duan (2007)
	GC-IMS	Quantitative High selectivity Reproducible Relatively portable and Inexpensive		0.4 and 0.5 μg/L (acetone and ethanol) ppb	Lord et al. (2002) Cao and Duan (2007)
PTR-MS		Quantitative High sensitivity No concentration and separation procedures Real-time	Proton affinity of the analyte needs to be higher than water to be detected	ppt-ppb	Hansel et al. (1995) Boschetti et al. (1999) Karl et al. (2001) Williams et al. (2001) Cao and Duan (2007)
SIFT-MS		Quantitative No preconcentration and separation procedures Real-time Able to measure water saturated samples		ppb 83 ppb (SD ± 45 ppb) (isoprene)	Cheng and Lee (1999) Španel et al. (1999) Smith and Španel (2005) Cao and Duan (2007)
Optical Absorption		Real-time Portable	Lower specificity than MS	100 ppt (Ethane)	Skeldon et al. (2005) Cao and Duan (2007)
	High-resolution mid-IR[1] TLAS[2]	Real-time		1.5 ppb (NO)	Roller et al. (2002a, b) Cao and Duan (2007)

Table 2. (Continued)

Analytical Method		Advantages	Disadvantages	Sensitivity	Reference
	IR absorption spectroscopy	Cheaper than LARA[3] and IRMS[4]	Few breath samples at a time		Gisbert and Pajares (2004) BreathTek UBiT system (2006)
	UV absorption spectroscopy	High linearity High accuracy			Baum et al. (2003) Cao and Duan (2007)
	Cavity ringdown spectroscopy	Portable	Sensitive to high moisture	1.5 ppm (acetone)	Wang et al. (2004) Cao and Duan (2007)
	Chemiluminesence	High sensitivity Portable		ppb	Cheng and Lee (1999)
	FTIR[3]	Real-time	Can't differentiate compounds with same functional group	ppb	Cheng and Lee (1999)
Electrochemical Sensor		Portable Easy to operate Small volume sample	Limited sensitivity	0.1 ppm	Cheng and Lee (1999) Wilson and Baietto (2009)
Biosensor		High sensitivity High specificity Real-time		ppt-ppb	Cheng and Lee (1999)
	Electronic nose	High sensitivity Portable		2-100ppb (NO) ppm	Fleischer et al. (2002) Biller et al., (2011)
	QCM/QMB (Quartz crystal microbalance)	High sensitivity High selectivity Reproducible Real-time for multi-Components	Poor signal-to noise ratio Sensitive to humidity Sensitive to temperature		Huang et al. (2005) Cao and Duan (2007) Wilson and Baietto (2009) Wilson and Baietto (2009)
	Micro-Plasma	No preconcentration and separation Less matrix effects Low construction and maintenance cost No influence of the large amount of water vapor		ppb (acetone)	Cao and Duan (2007)

[1]IR= Infrared spectroscopy; [2]TLAS=Tunable-laser-absorption spectroscopy; [3]LARA=Laser-assisted ratio analyzer;
[4]IRMS= Isotope ratio mass spectrometer; [5]FTIR= Fourier transform infrared spectroscopy.

2.3.2 Biosensor

A biosensor is an analytical device that is composed of two parts – a bioreceptor (e.g. enzyme, antibody, tissue, or receptor) and a transducer (e.g. electrochemical, optical, piezo-electric, or thermal sensors). A bioreceptor reacts with a specific analyte while the transducer is used to measure the changes in properties or quantities in the form of current, frequency, heat, etc. (Figure 3).

The bioreceptor is typically immobilized on the transducer to enhance the specificity and sensitivity of the device. Immobilization methods are mainly categorized in five types – adsorption, entrapment, covalent bonding, crosslinking, and microencapsulation (or membrane confinement) (Figure 4) (Eggins, 2002; Chaplin, 2004). Adsorption is the simplest method for implementation but is also very weak, relying solely on van der Waals bond through electrostatic force. Entrapment involves mixing the bioreceptor in a gel or polymer (e.g., polyacrylamide, starch, agarose, gelatin) to trap bioreceptors in the resulting film matrix. The matrix typically acts as a diffusion barrier and can slow down the sensing mechanism. Covalent bonding involves coupling functional groups, such as carbonyl, amino, or hydroxyl groups, between bioreceptors and the transducers. Immobilization by covalent bonding offers the most stable form, lasting from 4-14 months (Eggins, 2002). Crosslinking reagents, such as glutaraldehyde, bis(succinimidyl esters), and diacid chlorides (Haugland, 2002) can be used to bind bioreceptors to a supporting material or directly to the transducer. Crosslinking is widely used in conjunction with other methods, such as entrapment and microencapsulation, in stabilizing enzymes and preventing leakage (Palmer, 2001). Microencapsulation forms a semi-permeable membrane to trap the bioreceptors inside a membrane and prevents its

leakage while allowing the substrate or analyte to pass through. Alginate, cellulose acetate, polycarbonate and collagen are commonly used biomaterials to form the membrane (Eggins, 2002; Taqieddin and Amiji, 2003). The loading of bioreceptor, immobilization method, pH, and interference due to cross reactions between molecules with similar conformation greatly affect a biosensor's sensitivity, selectivity, accuracy, response time and working lifetime.

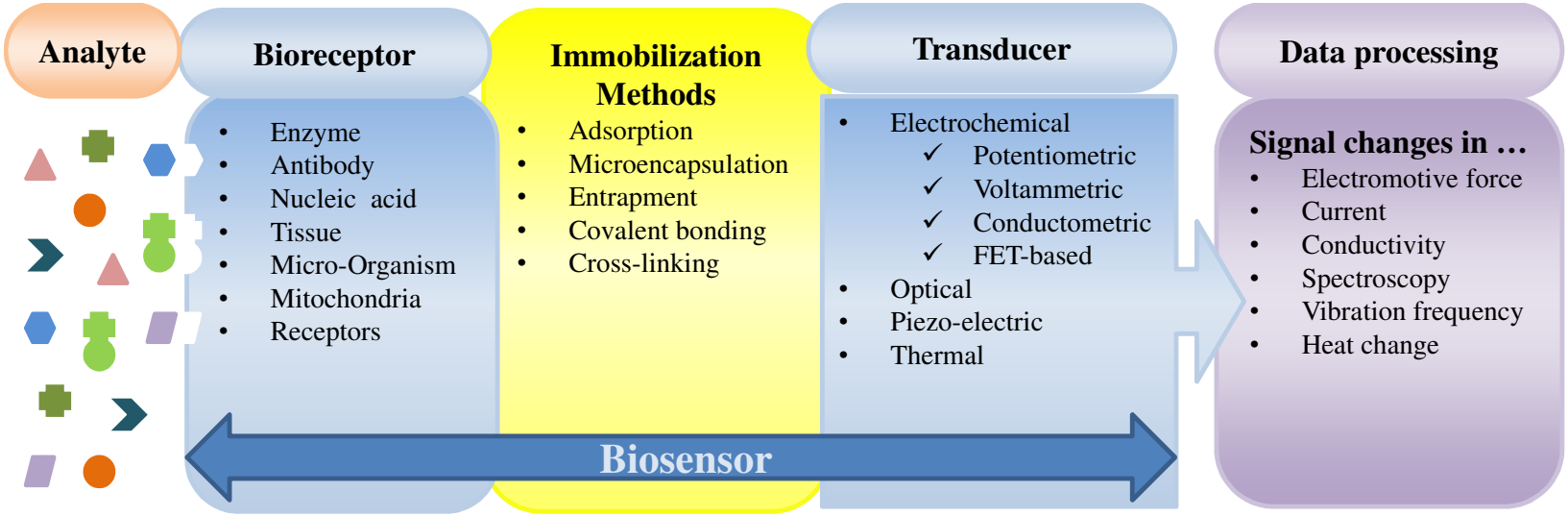

Figure 3. Biosensors are composed by bioreceptors and transducers which are bound with each other using immobilization techniques. The measured level of target analyte is presented by types of signal change due to different transducers.

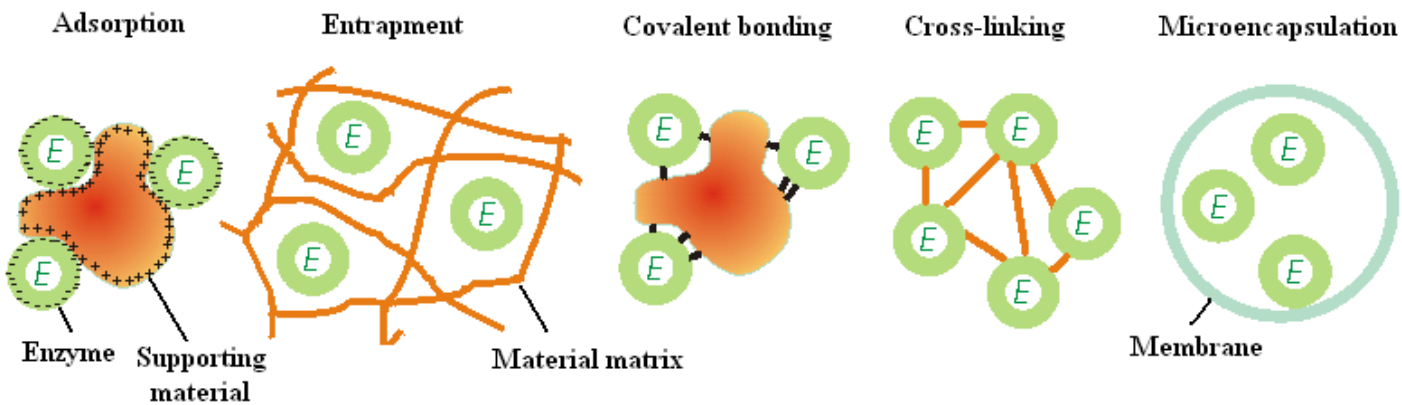

Figure 4. Enzyme immobilizations were mostly categorized in five types. Adapted from www.lsbu.ac.uk/biology/enztech/immethod.html#tab3_3.

CHAPTER 3: MATERIALS AND METHODS

3.1 Reagents

Alcohol oxidase (AOX, E.C. 1.1.3.13, 30 U/mg protein) from *Pichia pastoris* was purchased from Sigma Aldrich (St. Louis, MO). Bovine serum albumin (BSA, 96% w/w), glutaraldehyde (25% w/w), potassium phosphate monobasic, methanol (99.8% w/w), ethanol (99.5% w/w), acetone (≥99.5% w/w), acetaldehyde (99% w/w), and hydrogen peroxide (30% w/w) were of analytical reagent grade and purchased from Sigma-Aldrich (St. Louis, MO). Potassium phosphate buffer solution (100 mM, pH 7.4) was prepared using deionized water and stored at 4°C until use. Immediately before testing, all the biomarker solutions were prepared in potassium phosphate buffer solution to hold a neutral pH condition.

3.2 Breath Output Simulators

A breath output simulator was designed and built to simulate the expiration of breath biomarkers, such as ethanol and hydrogen peroxide (Figure 5). A volume of compressed air was humidified by bubbling it through an aqueous solution containing one of these biomarkers. The humidified air exiting the bubbler was considered as the simulated exhaled breath.

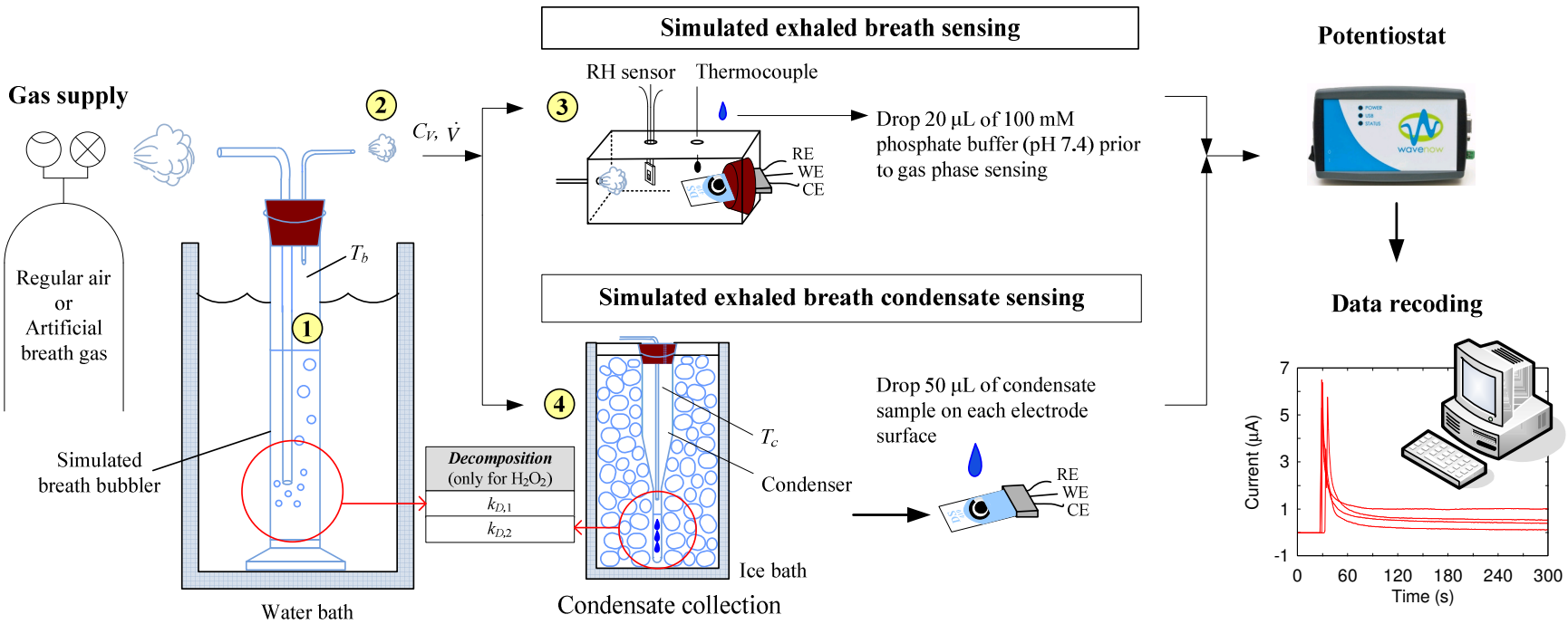

Figure 5. The breath output simulator was used to simulate exhaled breath by humidifying compressed air using an aqueous solution of a biomarker. The concentrations of the biomarkers in the simulated exhaled breath sample were measured amperometrically at the gas phase and condensed (liquid) using enzyme-coated electrodes.

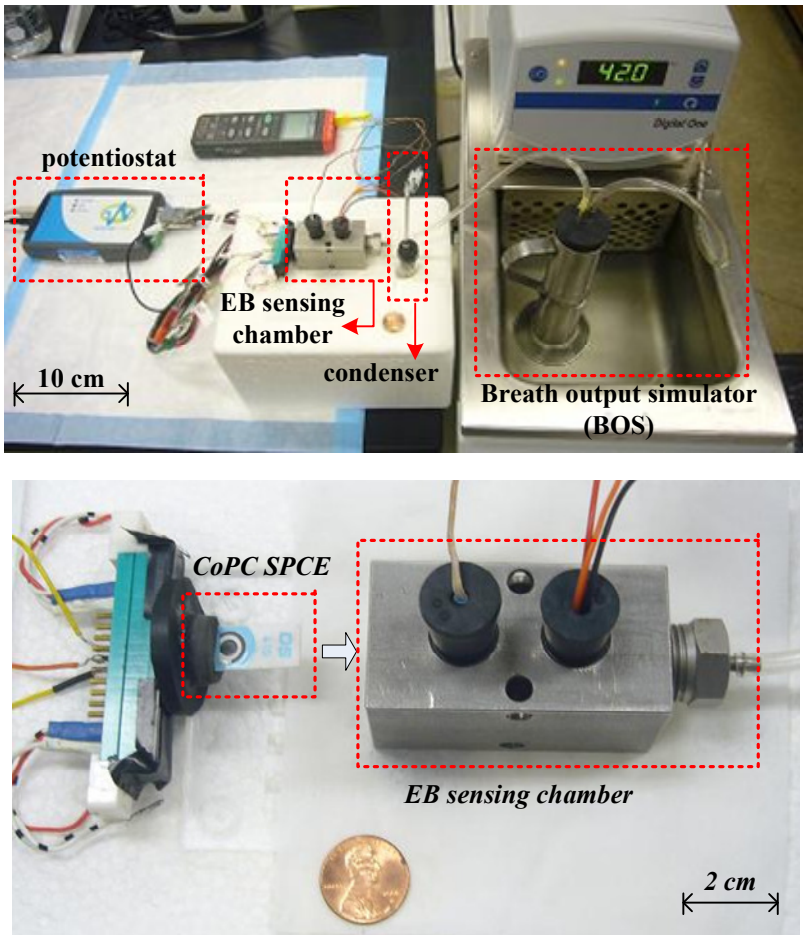

Figure 6. The overall diagram of sampling and sensing system was shown.

Flow rate was manually controlled using a valve and measured using a shielded flow meter (GF-1260 and GF-1360, Gilmont, Barrington, IL). Typically, exhaled breath flows through the trachea of a healthy person under laminar conditions and the Reynolds number is estimated to be around 1600 to 2000 (Chang and Mortola, 1981; Ultman, 1985). The Reynolds number of the simulated exhaled breath in this study was set at 957 and 1833 to simulate laminar conditions for average, healthy individuals.

The simulated breath was maintained at saturated conditions (> 95% relative humidity) through the bubbler, which was monitored using a humidity sensor (HIH-4000, Honeywell Sensing and Control, Valley, MN). The bubbler was submerged in a water

bath (DigitalOne, Thermo Scientific, Newington, NH) and the temperature was adjustable to 295, 307, 310, and 315 K. The temperature of the humidified air was monitored using a datalogging thermometer (HH309A, MEGA Engineering, INC., Stamford, CT). These temperatures corresponded to room temperature, exhaled breath temperature from the mouth, blood and alveolar air temperature, and extremely high fever temperature that can cause brain damage (Begg et al., 1964; Jones, 1982 and 1995; Yamamoto and Ueda, 1972). The simulated exhaled breath either passed through a chamber for vapor phase sensing or was delivered to a condenser to cool it down to 274 K or 256 K in an ice bath. The latter condition was achieved using a condenser bath containing 1:8 weight ratio of sodium chloride and ice mixture. Sodium chloride was purchased from Sigma-Aldrich (St. Louis, MO). The condensate was collected in 10 minutes to obtain 105-700 µl samples in the case of H_2O_2 (Figure 7).

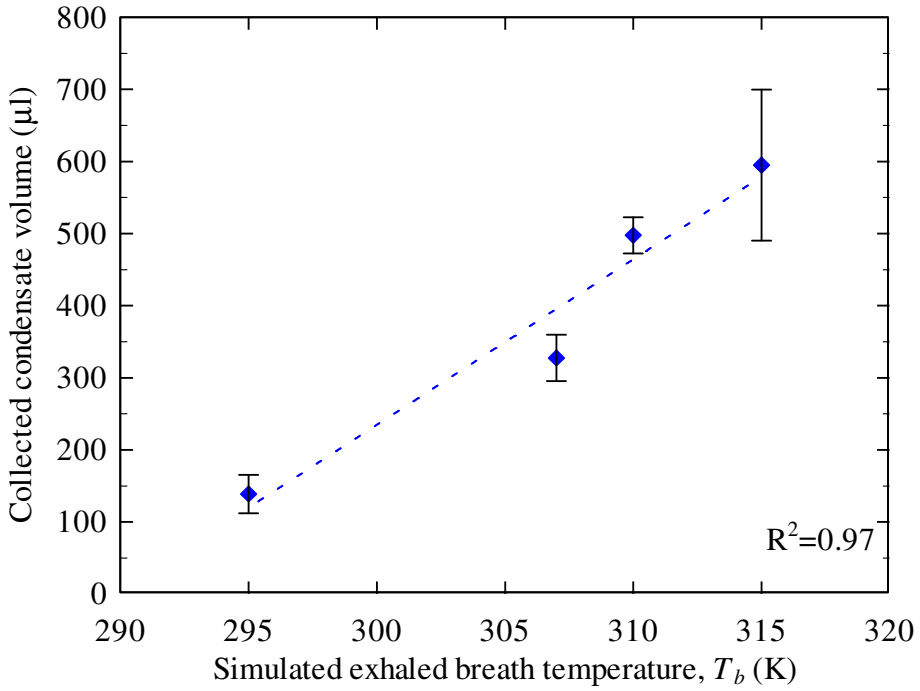

Figure 7. EBC volumes collected for 10 min increased with increasing simulated exhaled breath temperature at T_c = 274 K.

3.3 Biomarker Measurements

3.3.1 Henry's law

The concentrations of the biomarkers in the simulated exhaled breath were calculated using Henry's law. Henry's law states that at a constant temperature, the amount of a given solute (or gas) dissolved in a given type and volume of liquid is directly proportional to the partial pressure of that gas in equilibrium with that liquid:

$$k_H = \frac{c}{P}, \tag{1}$$

where k_H is Henry's law constant for a given solute (mol/L·atm); c is the concentration of the solute (mol/L); and P is the partial pressure of the solute in the gas above the solution (atm). k_H is used for describing the solubility of the solute in water and it is related to the solute volatility, $k_{H,inv}^{px}$ by

$$k_{H,inv}^{px} = \frac{p}{x_a} = \frac{\rho_{H_2O}}{M_{H_2o} \times k_H}, \tag{2}$$

where x_a is the molar mixing ratio in aqueous phase; ρ_{H2O} is the density of water; M_{H2O} is the molar mass of water.

Henry's law constant k_H varies with temperature (Equation 3). k_H at 298.15K and $\Delta_{soln}H/R$ values for ethanol and hydrogen peroxide may be estimated using the average values collected from previous studies (Sander, 1999). The empirical values are shown in APPENDIX A.

$$k_{H,T_2} = k_{H,T_1} \times \exp\left(\frac{\Delta_{soln}H}{R}\left(\frac{1}{T_2} - \frac{1}{T_1}\right)\right), \tag{3}$$

where $\Delta_{soln}H$ is the enthalpy of solution; R is the universal gas constant, 8.314 J/K·mol; T_1 is the temperature under standard condition (298.15K); and T_2 is the sample temperature.

Based on the published k_{H,T_1} and $\Delta_{soln}H/R$ values, aqueous ethanol and hydrogen peroxide were prepared and used as stock solutions in the bubbler (① in Figure 6) to produce the expected concentrations of biomarkers. The conversion between aqueous and gas phases was calculated under standard conditions (298.15K, 1 atm) (Tables 3).

Table 3. The Henry's law constant of ethanol and H_2O_2 under different temperatures

Ethanol (ρ = 0.789 g/ml, FW = 46.07 g/mol, $\Delta_{soln}H/R$ = 6500 K, $k_{H,T=298.15K}$ =184 M/atm)					
Breath Temperature, T_b (K)	**k_H (M/atm)**	**$k_{H,inv}^{px}$ (atm)**	**Aqueous Concentration % (w/w) in the bubbler**	**Aqueous Concentration (mM) in the bubbler**	**Vapor Concentration, C_V (ppm)**
295	221.29	0.00025	0.00517	0.885	4
			0.00646	1.106	5
			0.00969	1.660	7.5
307	97.08	0.00057	0.00227	0.388	4
			0.00283	0.485	5
			0.00425	0.728	7.5
310	79.09	0.00070	0.00185	0.316	4
			0.00231	0.395	5
			0.00346	0.593	7.5
315	56.70	0.00098	0.00132	0.388	4
			0.00166	0.485	5
			0.00248	0.728	7.5
H_2O_2 (ρ=1.463 g/ml, FW=34.015 g/mol, $\Delta_{soln}H/R$=7062.5 K, $k_{H,T=298.15K}$ =77888.89 M/atm)					
Breath Temperature, T_b (K)	**k_H (M/atm)**	**$k_{H.inv}^{px}$ (atm)**	**Aqueous Concentration % (w/w) in the bubbler**	**Aqueous Concentration (mM) in the bubbler**	**Vapor Concentration, C_V (ppb)**
295	99101	0.00056	0.058	24.8	250
			0.115	49.6	500
			0.230	99.1	1000
307	38898	0.00143	0.023	9.7	250
			0.045	19.4	500
			0.090	38.9	1000
310	31139	0.00178	0.018	7.8	250
			0.036	15.6	500
			0.072	31.1	1000
315	21695	0.00256	0.013	5.4	250
			0.025	10.8	500
			0.050	21.7	1000

3.3.2 Sensor Preparation

Screen-printed carbon electrode (SPCE), DRP-410, purchased from Metrohm USA Inc. (Riverview, FL), was composed of three parts – a carbon-based working electrode containing cobalt phthalocyanine (CoPC) (12.56 mm^2) as electrochemical mediator, a counter electrode made of carbon paste (1.45 mm^2), and a reference electrode (2.2 mm^2 area) made of silver paste (Figure 7). The oxidation of H_2O_2 was measured through the oxidation of $2Co^+$ to Co^{2+}. Hence, the bare SPCE was directly used as a H_2O_2 sensor. For the ethanol sensor, AOX was immobilized on the cell by dropcoating a 2 µl aliquot of mixture containing glutaraldehyde and the enzyme on the working electrode of a CoPC SPCE. The immobilization process stabilized AOX on SPCE and favored higher current responses than non-immobilized AOX assays (APPENDIX B). Glutaraldehyde concentration was 1.5 % (v/v) to present a better performance (APPENDIX C). The mixture was allowed to dry for 2 to 2.5 h at room temperature (Figure 8). AOX is an enzyme that catalyzes oxidation of alcohols and us unable to bind with ketones or aldehydes. During the AOX-catalyzed oxidation of ethanol, H_2O_2 was measured using the CoPC SPCE. Therefore, the concentration of ethanol could be detected indirectly.

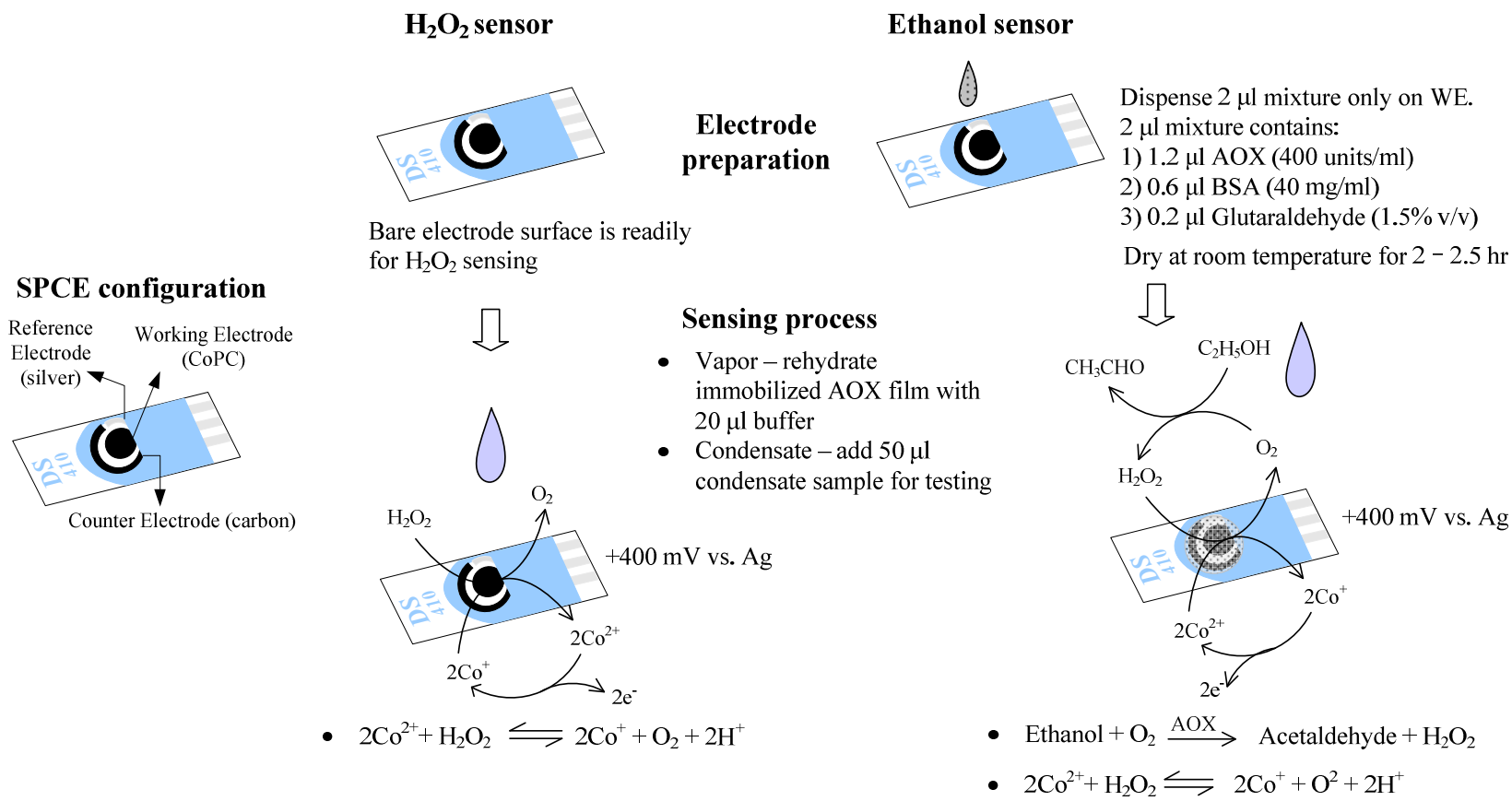

Figure 8. Sensor preparation and sensing process were involved dropcoating enzyme solutions on the working electrodes of the screen printed carbon electrodes.

3.3.3 Amperometric Measurements

A portable USB potentiostat (WaveNow, Pine Research Instrumentation, Raleigh, NC) was used to measure the redox reaction occurring on the sensor surface. In preliminary tests and previous studies, hydrogen peroxide showed a cathodic (reduced) peak around +400 mV vs. Ag/AgCl (Boujtita et al., 2000; Danao et al., 2007), resulting in a linear response to increasing concentrations of hydrogen peroxide in amperometric measurement (Figure 9 a,b).

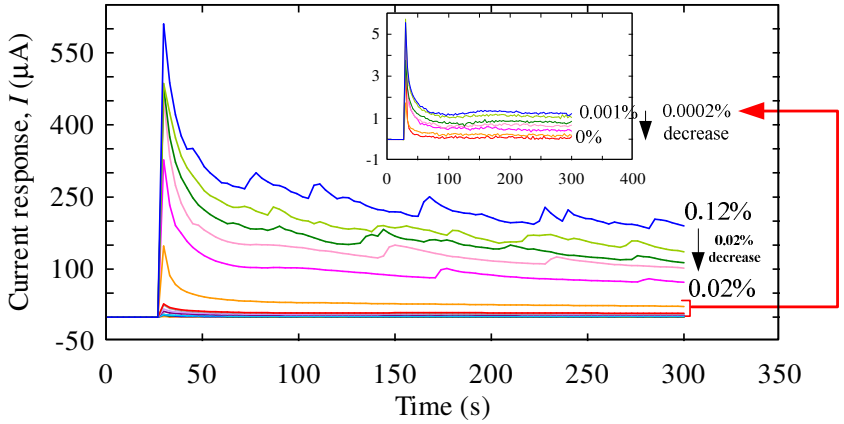

(a)

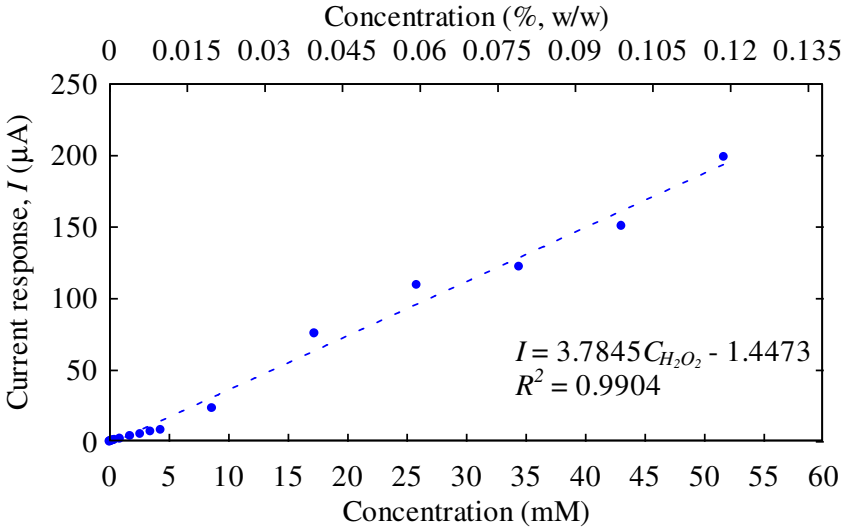

(b)

Figure 9. (a) Amperometric measurement of H_2O_2 solutions increased linearly with increasing levels of H_2O_2 from 0-0.12% (w/w) and (b) the corresponded calibration curve.

3.4 Data Analysis

3.4.1 Signal Processing

For vapor phase measurements, the electrode was exposed to ambient air for a period of 30 s prior to coating the electrode with 20 µl of potassium phosphate buffer. After 60 s, the electrode was inserted into the test chamber and the amperometric response for the simulated exhaled breath sample was recorded for the rest of 8 minute and 30 s (Figure 10). Similarly, for condensate (liquid) phase measurements, the electrode was exposed to ambient air for 30 s prior to coating the electrode with 50 µl of condensate sample in biomarker sensing.

In most condensate samples, the current response gradually stabilized after 5 min, but the current did not fully stabilize after 5-10 min measurement in vapor samples. The sampling rate of current response was set at 3 s. In order to minimize the background noise, the current response at X s is averaged from the current response from (X - 3) s to (X + 3) s, or central averaging (Equation 4).

$$I_{\overline{X}s} = \frac{\left(I_{(X-3)s} + I_{Xs} + I_{(X+3)s}\right)}{3} \tag{4}$$

For signal extraction of different sensing duration, current from t = 3, 4,…, 10 min, I_{tmin}, was considered as a signal from the sample, and noise (or background value) was taken from current at 2 min (I_{2min}) for vapor and at 15 s (I_{15s}) for condensate. The data were processed in three ways – subtraction, ratio, and slope (or differentiation) (Figure 11) for filtering out noises from signals.

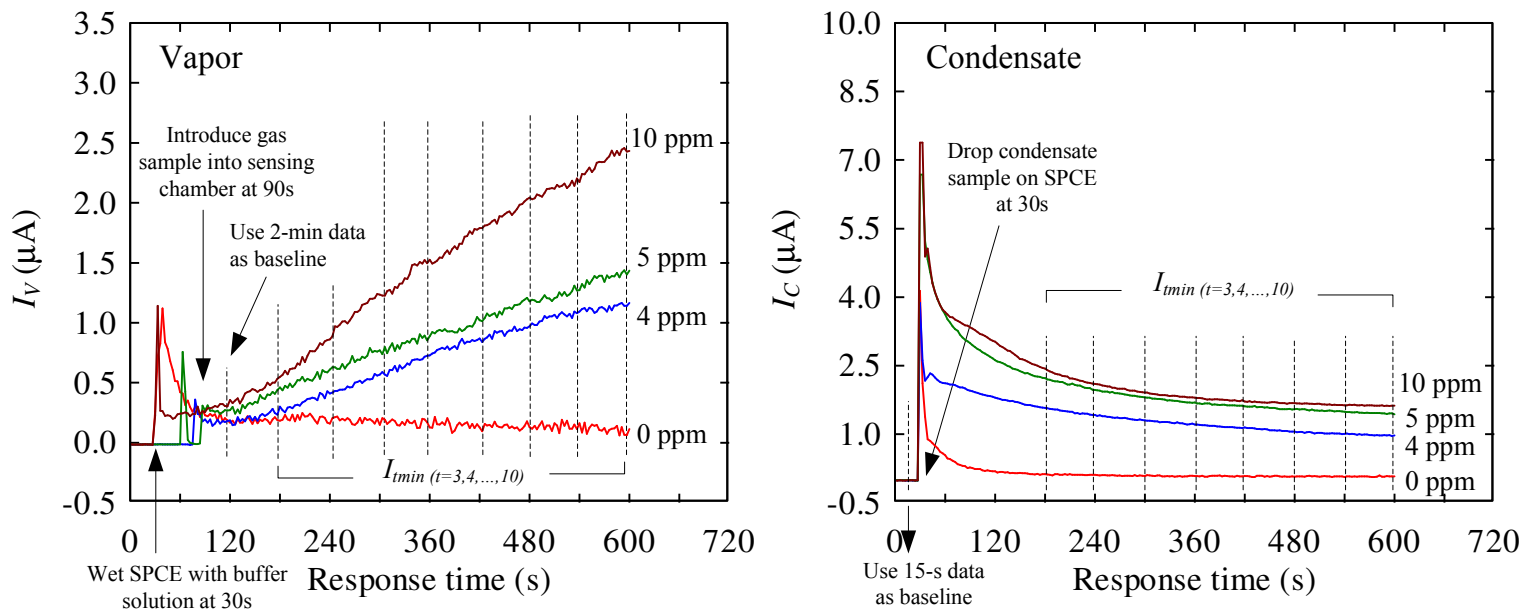

Figure 10. The current response, $I_{V/C}$, for the breath biomarker was recorded for 10 min. I_V at 2 min (120 s) and I_C at 15 s were taken as baseline values (background signals) for vapor and condensate samples individually. The case here was from the results of ethanol samples.

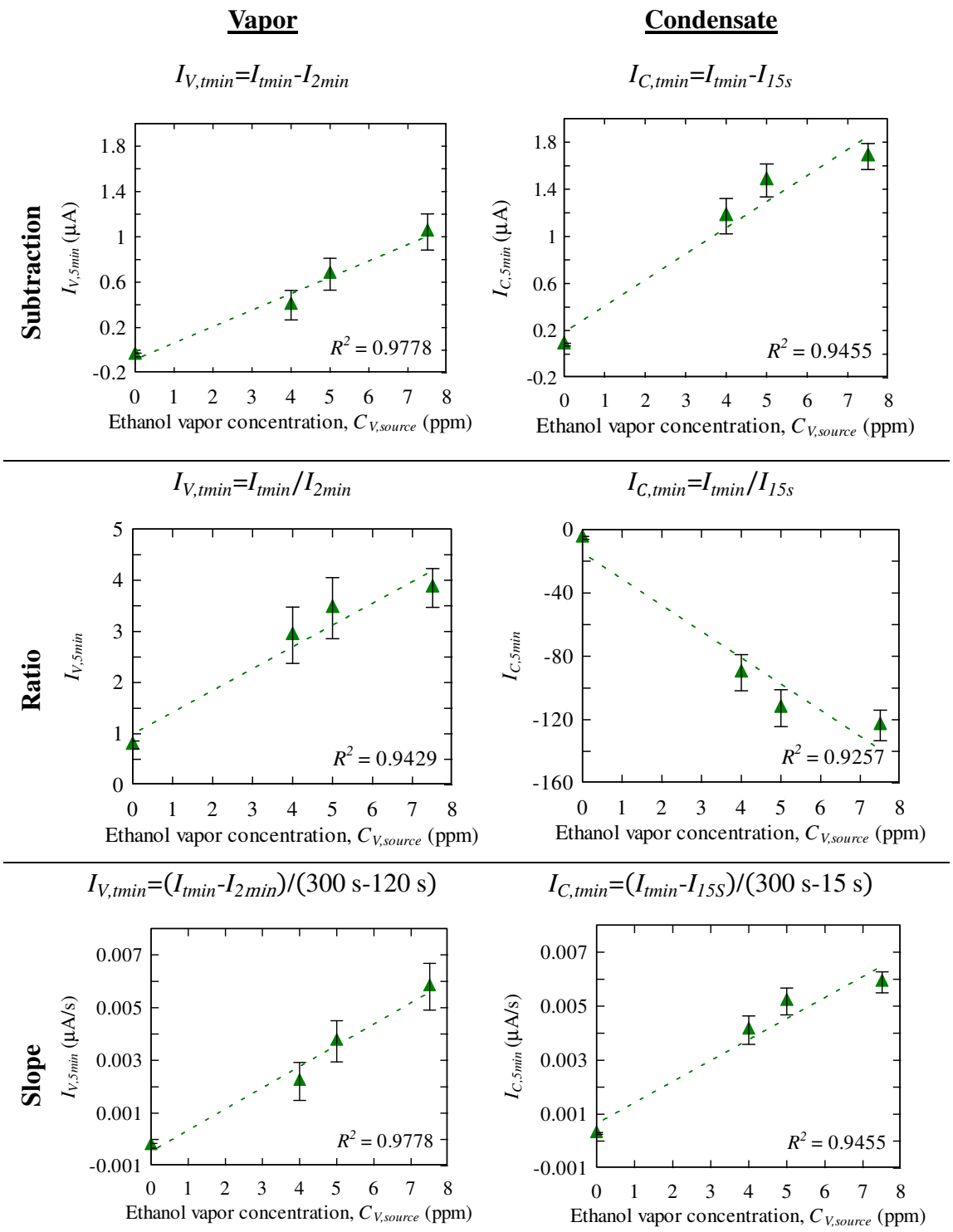

Figure 11. Three ways of signal processing were evaluated for data collected from vapor and condensate samples. Ethanol vapor concentrations were calculated based on Henry's law. The case here was from the results of ethanol samples at 5 min from T_b = 310 K. Dashed lines represent linear regression results.

3.4.2 Model Selections

Current responses were determined to be a function of parameters (variables) of the sampling conditions. Initial models, which included the sampling/sensing parameters and the two-way interaction terms from the parameters, were tested through a model selection process using Akaike's information criterion (AIC), Bayesian information criterion (BIC, or Schwarz criterion, SBC), or cross validation (CV).

AIC, which was first published by Hirotsugu Akaike in 1974, is used for comparing nested models and provides a criterion to choose the best compromised model between the goodness of fit and the numbers of parameters included in the model based on the theories of maximum likelihood, information and entropy (Akaike, 1974; Motulsky and Christopoulos, 2004). AIC is calculated as:

$$AIC = -2\ln(L) + 2k \tag{4}$$

where L is the maximized likelihood of the estimated model; k is the number of parameters in the model. If the model presented constant variance, then it also can be written as:

$$AIC = n\ln(\frac{RSS}{n}) + 2k \tag{5}$$

where RSS denotes residual sum of squares and n is the number of data. Burnham & Anderson (2002) proposed to use AICc instead of AIC when k is larger and n is small.

$$AICc = AIC + \frac{2k(k+1)}{n-k-1} \tag{6}$$

For the data in this project, the number of k and n were of adequate size for employing the AIC method. A set of models containing all possible combinations of sampling/sensing parameters and the two-way interaction terms were created and the AIC value for each combination was calculated. Models with low AIC values were pursued

further in developing the predictive model.

The BIC was proposed by Gideon E. Schwarz in 1978 and is presented as:

$$BIC = -2\ln(L) + k\ln(n) \tag{7}$$

BIC is more stringent than AIC due to the heavier penalty term of $k \cdot \ln(n)$ than $2k$ in AIC. There are some arguments about whether AIC or BIC can provide a better fitting in data explanation and the possibility of overfitting or underfitting. However, there is no clear answer and is case-dependent.

Cross validation, which was also a means of prediction error estimation, was carried out by the k-fold cross validation here. The original dataset was partitioned into k fold nearly equally and $k = 10$ was commonly used in the field of data mining (Refaeilzadeh et al., 2009). (k - 1) fold was randomly chosen in a certain times of iterations to serve as a training (learning) set to develop a predictive model and the remaining one fold was used as a test set for validating the predictive model. In each iteration, the sum of mean squared error in the test set was calculated. By comparing the values, the model with a minimum sum of mean squared error was pursued further in developing the predictive models.

Models selected by AIC, BIC, and CV were subjected to a multifactor analysis of variance (or factorial ANOVA) that contained factors of vapor concentration of model biomarker (C_V, ppb or ppm, at ② in Figure 5), temperature of the simulated exhaled breath from the bubbler (T_b, K, at ① in Figure 5), breath (flow) rate ($\dot{V}$, liter per minute (LPM), at ② in Figure 5), temperature drop in vapor sensing (ΔT = temperature at ① – temperature at ③, in Figure 5, K), condensing temperature (T_c, K, at ④ in Figure 5) in

condensate sensing. In each case, three replications were taken in each test. Three methods of data processing (subtraction, ratio, slope) and four sensing duration (3, 5, 10, and 3-10 min) were evaluated. All the statistical analyses were computed in R environment (version 2.11) and the complete codes are listed in APPENDIX D. The final predictive models were chosen in consideration of a shorter sensing duration and a bigger R^2 (Figure 12).

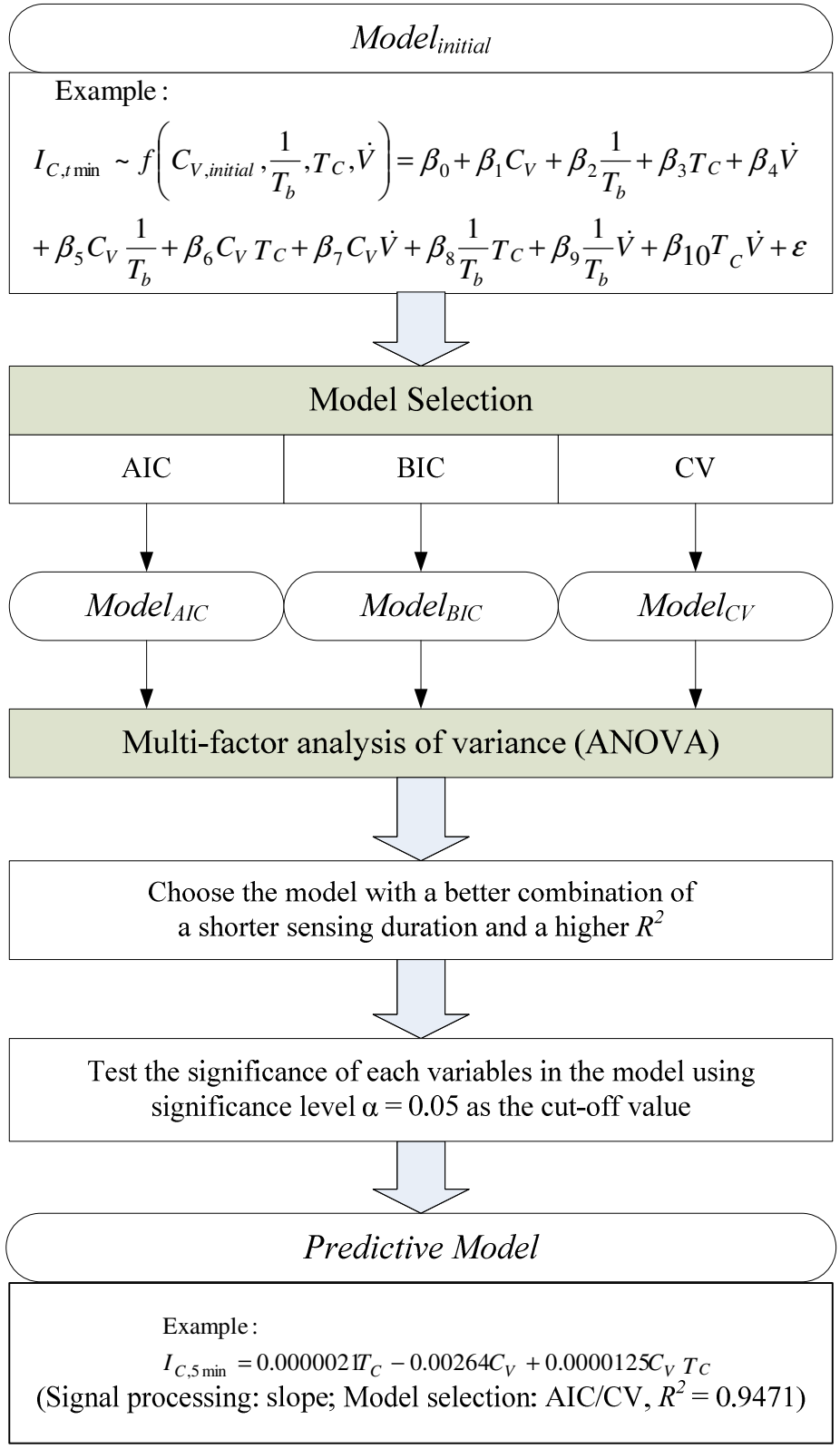

Figure 12. A predictive model was chosen based on the results of model selections and ANOVA tests. (The example is from ethanol condensate sample in 5-min sensing time.

CHAPTER 4: RESULTS AND DISCUSSION

Ethanol and H_2O_2 were chosen as model biomarkers in EB and EBC sampling and sensing. Vapor and condensate samples were collected at four simulated concentrations (C_V) and breath temperatures (T_b) – 295, 307, 310, and 315 K. Samples collected at 310 K were also sampled from two flow rates($\dot{V}$), 3.438 and 6.876 LPM (Reynolds numbers are equal to 957 and 1833), and condensate samples were condensed at two condensing temperature (T_C), 276 and 264 K. The effect of sensing duration was determined at 5 and 10 min.

4.1 VOC Detection in Breath — Ethanol as the Model Biomarker

Ethanol vapor with concentration of 4, 5 and 7.5 ppm (② in Figure 5) were produced from the prepared stock ethanol solution in the bubbler (① in Figure 5). The concentrations of stock solutions were calculated based on Henry's law (Table 3). As the concentration of ethanol in the stock solution increased, the current response increased. The concentrations of stock ethanol solutions at each simulated breath temperature and the current responses are demonstrated a linear trend and shown in Figure 13a. The x-axis can be converted into corresponding calculated vapor concentrations for comparison Lower current responses were found at higher T_b even when they were calculated to present the same vapor concentration (Figure 13b).

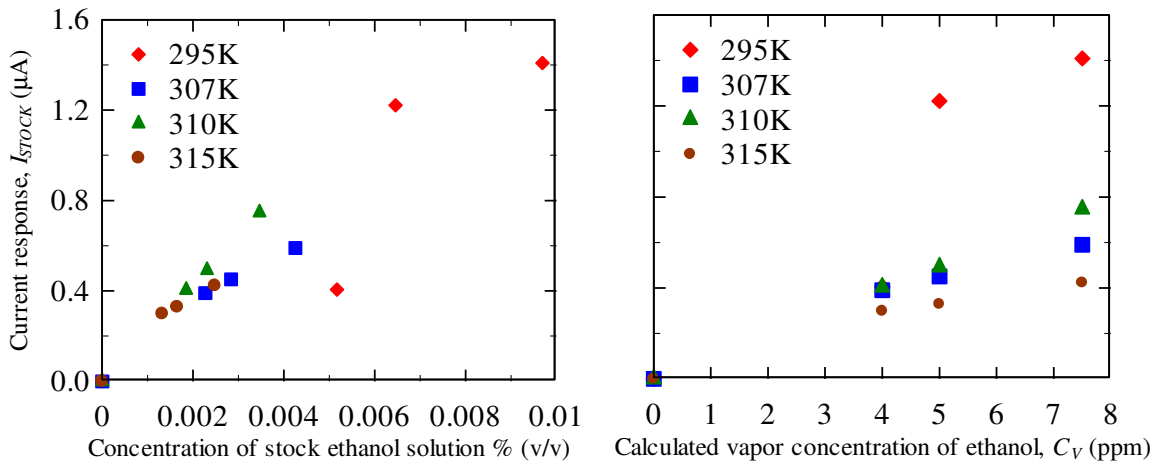

(a) (b)

Figure 13. The relationship between current response and (a) stock ethanol concentration and (b) calculated ethanol vapor concentration in simulated exhaled breath sample across the range of temperatures used in this study was linear. Results shown are for one test replication.

4.1.1 Temperature

Current measurements due to ethanol vapor and condensate typically increased linearly as C_V increased (Figures 14). In general, the higher the T_b, the lower the current response derived for the same C_V. The results were possibly due to further water condensation with increasing T_b. Moreover, higher current responses were found in the results from 10 min sensing duration compared to 5 min sensing duration for vapor samples, but the effect was not seen with condensate samples.

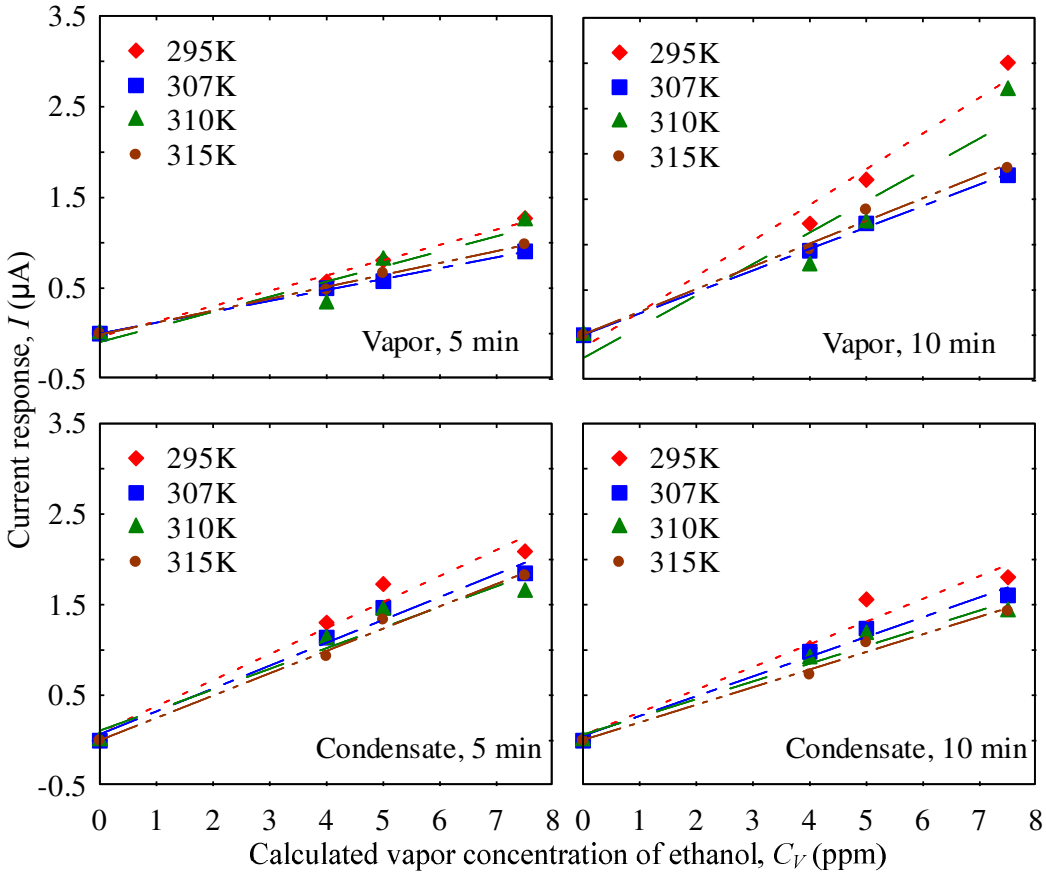

Figure 14. Current measurements due to the level of ethanol present in the vapor and condensate samples increased with increasing temperature. All points were averaged from three replicate samples. Dashed lines represent linear regression results.

Current responses for condensate samples were higher than the current responses for vapor and stock solution after 5 min of sensing (Figure 15). When the sensing time was extended to 10 min, vapor samples had the highest current responses, followed by condensate and stock solution, respectively.

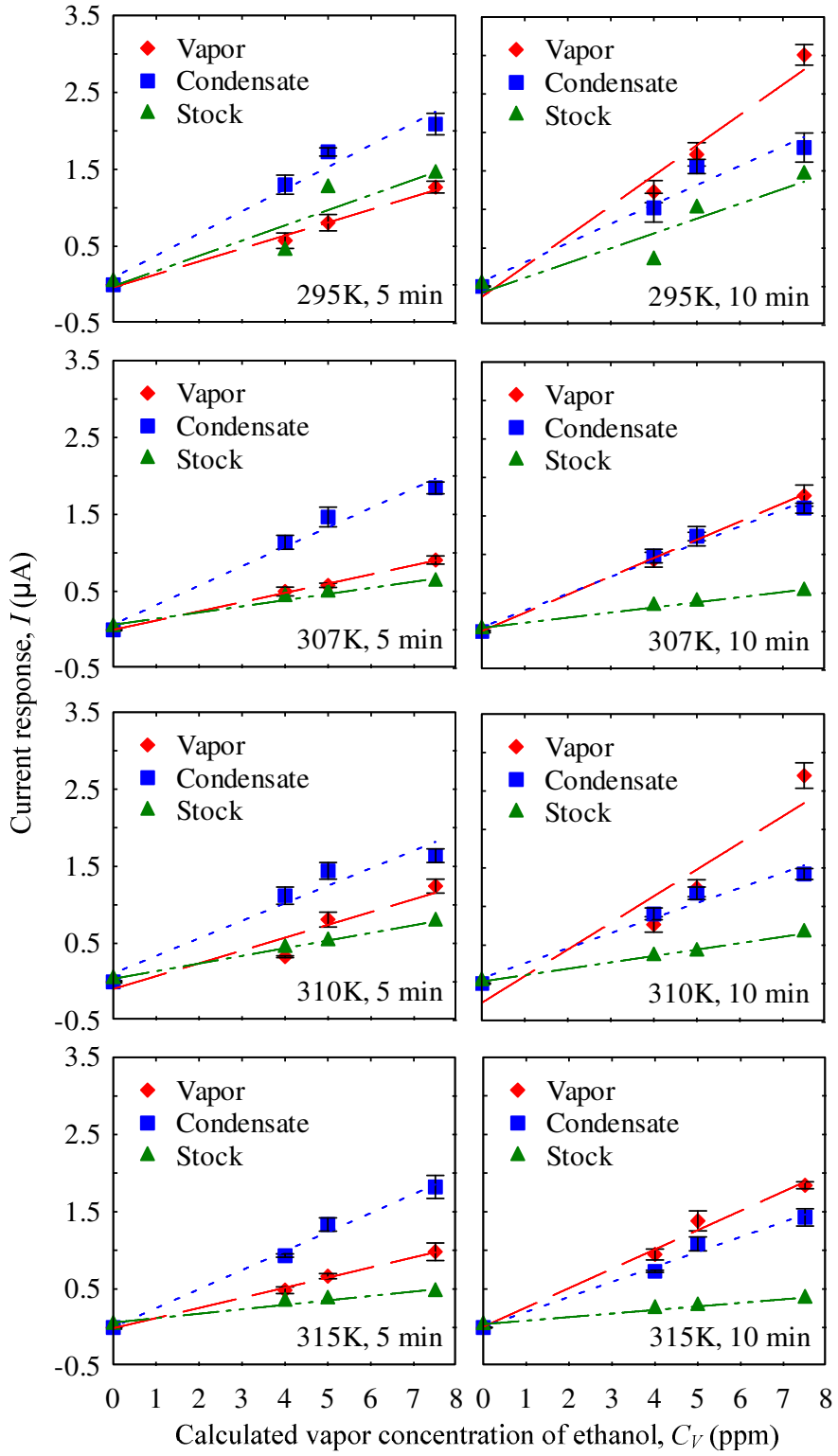

Figure 15. Current measurements due to the level of ethanol present in vapor, condensate, and stock solution samples were affected by sensing durations. Vapor and condensate samples were sampled three times. One replication was conducted for stock solution.

Error bars and dashed lines represent ± one S.E and linear regression results, respectively.

Ethanol molecules in the vapor were present as aerosol particles that randomly deposited on the sensor surface. As sensing duration increased, the chances of aerosol deposition increased. With the condensate sample, the composition was fixed after collection by directly dropcoating the sensor with the condensate sample. Hence, a shorter sensing duration was needed in condensate sensing.

The current responses for the stock solution were lower than those for vapor and condensate samples. Since the boiling point of ethanol is 78.4^{o}C, which is lower than the boiling point of water and water-based solvents (100°C), ethanol readily evaporated in the bubbler than water and higher levels of ethanol were detected in both vapor and condensate samples.

4.1.2 Flow Rate

Whether the sensing durations or flow rate changed, current responses presented comparable values in condensate samples. Although higher current responses were measured at the higher flow rate for vapor samples (Figure 16), but the responses were not statistically different (p_{5min}=0.355, p_{10min}=0.518).

4.1.3 Condensing Temperature

In condensate sensing, lower current responses were measured for samples collected from lower condensing temperature at T_C = 256 K (-17°C) (Figure 17). The melting point of ethanol is -114°C which is much lower than 0°C, the melting point of water. Therefore more water was condensed than ethanol and a diluted sample was collected. However, no statistically significant difference was found (p_{5min}=0.522, p_{10min}=0.540).

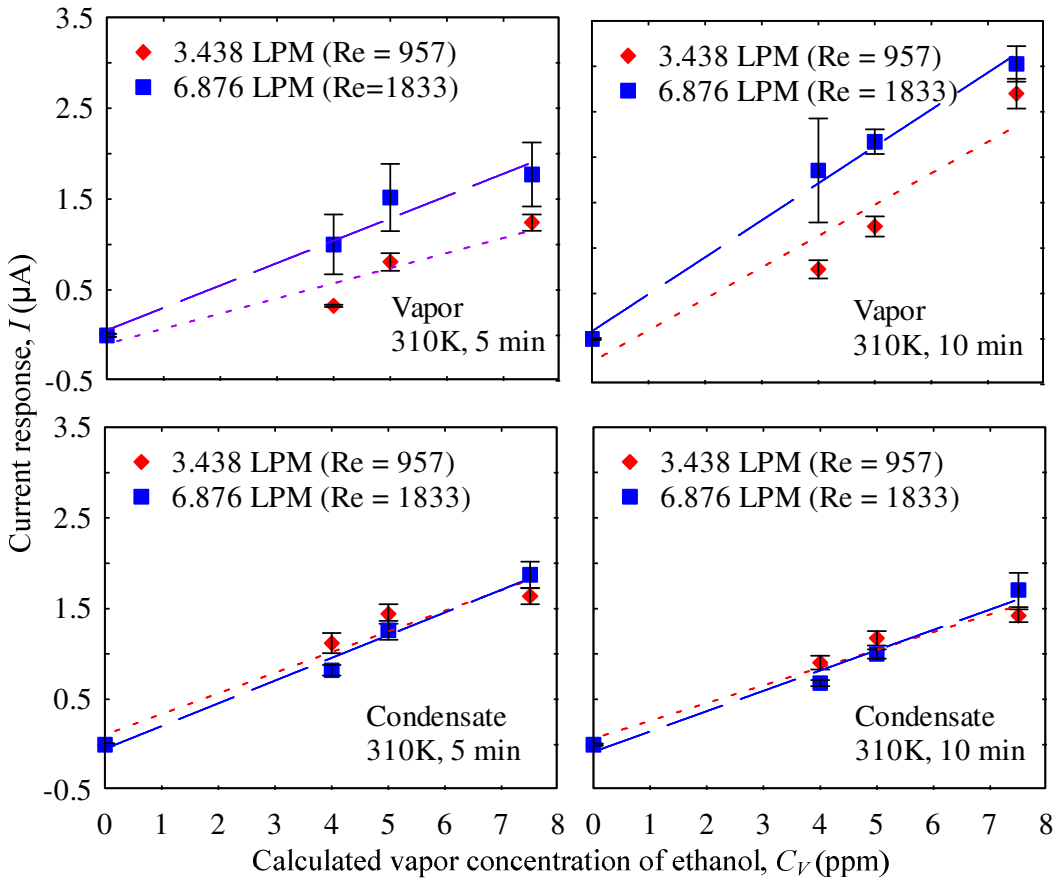

Figure 16. Current measurements due to the level of ethanol present in vapor and condensate samples were compared with changing flow rate in 5 min or 10 min sensing. All vapor and condensate samples were sampled three times. Error bars and dashed lines represent ± one S.E and linear regression results, respectively.

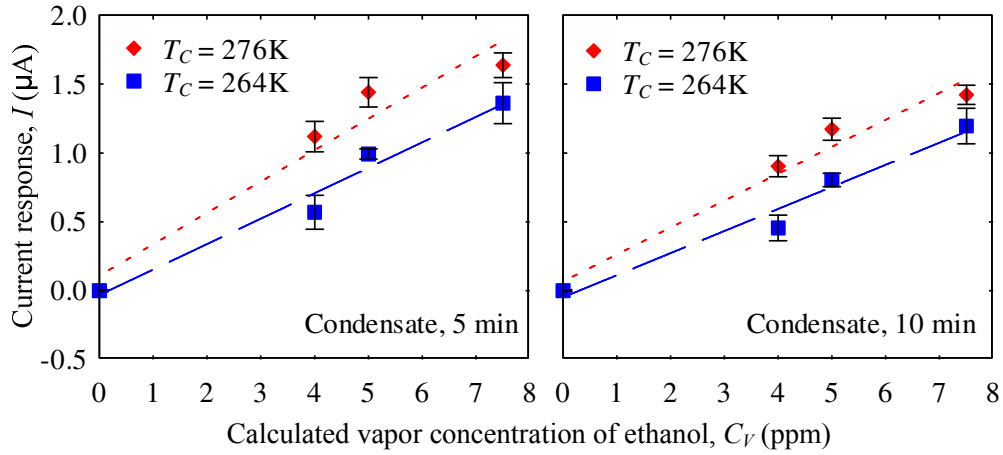

Figure 17. Condensate sampled from T_C = 256 K had a lower current response than it sampled from T_C = 274 K. All samples were sampled three times. Error bars and dashed lines represent ± one S.E and linear regression results, respectively.

4.2 Non-VOC Detection in Breath — H_2O_2 as the Model Biomarker

H_2O_2 vapor with concentration of 250, 500, and 1000 ppb (② in Figure 5) were produced from the prepared stock H_2O_2 solution in the bubbler (① in Figure 5). Henry's law was applied to calculate the concentrations of stock solutions (Table 3). The concentrations of stock H_2O_2 solutions and corresponding vapor concentrations at each simulated breath temperature and the current responses are shown in Figure 18.

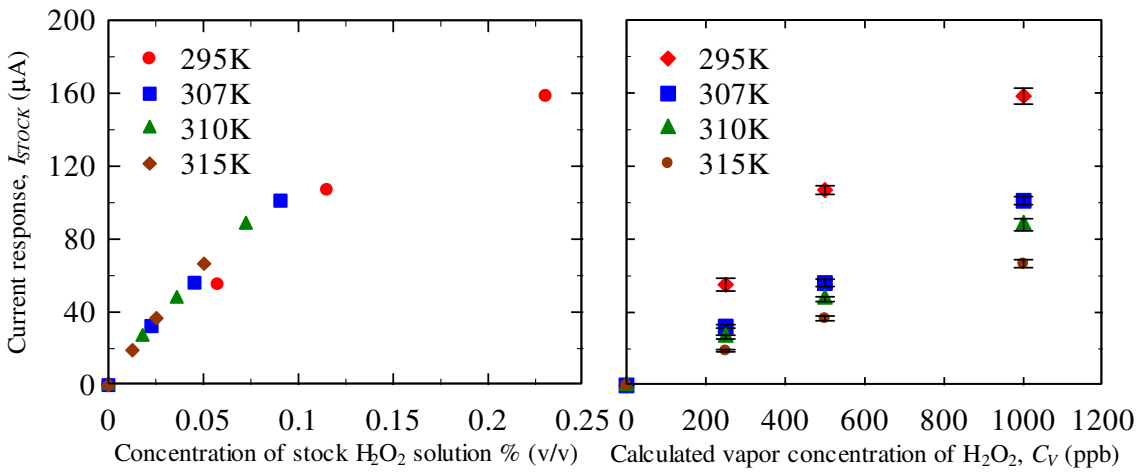

Figure 18. Amperometric tests were measured for stock solution in the bubbler and associated H_2O_2 vapor concentration that it produced. All samples were sampled three times and present with ± one S.E.

Although the current measurements for H_2O_2 vapors in the sensing chamber were linear, they were too low and below the limit of detection of the potentiostat. The current responses need to be amplified to provide clearer trend from measured signals. All the results from H_2O_2 vapor sensing including determining its decomposition rate and sampling condition effect are listed in APPENDIX E.

4.2.1 Decomposition

4.2.1.1 Decomposition of H_2O_2 in Stock Solution

The effect of temperature on the decomposition constant of stock solution (② in Figure 5), the decomposition constant $k_{D,1}$ in stock solution was conducted by monitoring the concentration of H_2O_2 every 10 min at 295, 307, 310, 315 K. H_2O_2 decomposes into water and oxygen exothermically:

$$H_2O_2 \rightarrow 2H_2O + O_2 \tag{8}$$

Except for the samples taken at 295 K, the amperometric response due to H_2O_2 concentration decreased over time (Figure 19) and supported the hypothesis that H_2O_2 decomposed faster with increasing temperature.

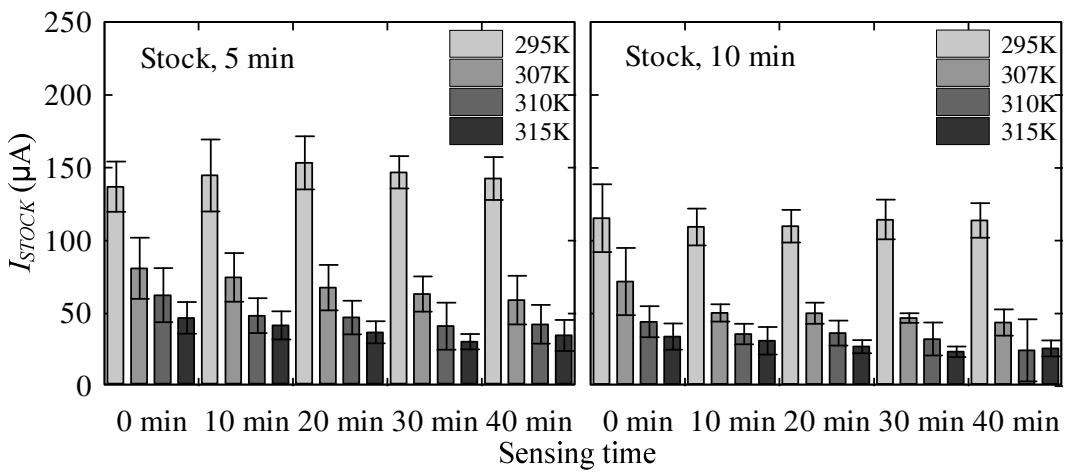

Figure 19. Current responses of H_2O_2 stock solution decreased over time at elevated T_b. Error bars represent ± one S.E

The decomposition reaction is a first-order reaction because the reaction rate only depends on the concentration of H_2O_2 at the same temperature:

$$\frac{dC_{V,t}}{dt} = k_{D,1}C_{V,t} \tag{9}$$

where t is sampling time (minute) and $C_{V,t}$ is the vapor concentration of H_2O_2 (ppb) at

time t. After integration, H_2O_2 concentration can be described as

$$C_{V,t} = C_{V,0} e^{-k_{D,1} t} \tag{10}$$

where $C_{V,0}$ is the initial concentration of H_2O_2 (ppb). Rearranging Equation 10,

$$\ln \frac{C_{V,t}}{C_{V,0}} = -k_{D,1} t \tag{11}$$

The decomposition rate constant $k_{D,1}$ can be obtained from the slope of the $\ln \frac{C_{V,t}}{C_{V,0}}$ vs. time curve (Figure 20).

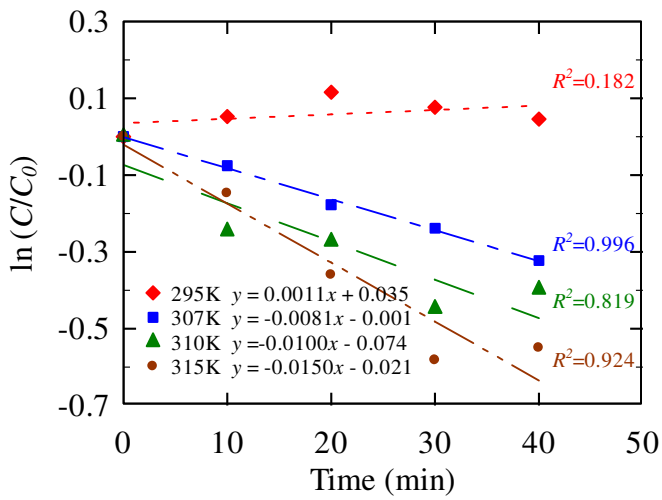

Figure 20. The decomposition rate $k_{D,1}$ increased with increasing temperature. Each test contained two to four replications taken at 3.438 LPM. Dashed lines represent linear regression results.

The general form of $k_{D,1}$ can be determined using the Arrhenius equation which is used to evaluate the effect of temperature on reaction rates:

$$\ln k_{D,1} = \ln A - \frac{E}{RT_b} \tag{12}$$

where A is reaction frequency factor (s^{-1}); E is activation energy (kcal/mol); R is gas constant, 8.314 kcal/mol/K; T_b is breath temperature (K). $k_{D,1}$ was directly proportional to

the increasing temperature and A and E values were determined to be 4.63 x 10^8 s^{-1} and 63,142 kcal/mol from the regression (Figure 21).

$$k_{D,1} = 4.63 \times 10^8 \times \exp\left(-\frac{631412}{RT}\right) \tag{13}$$

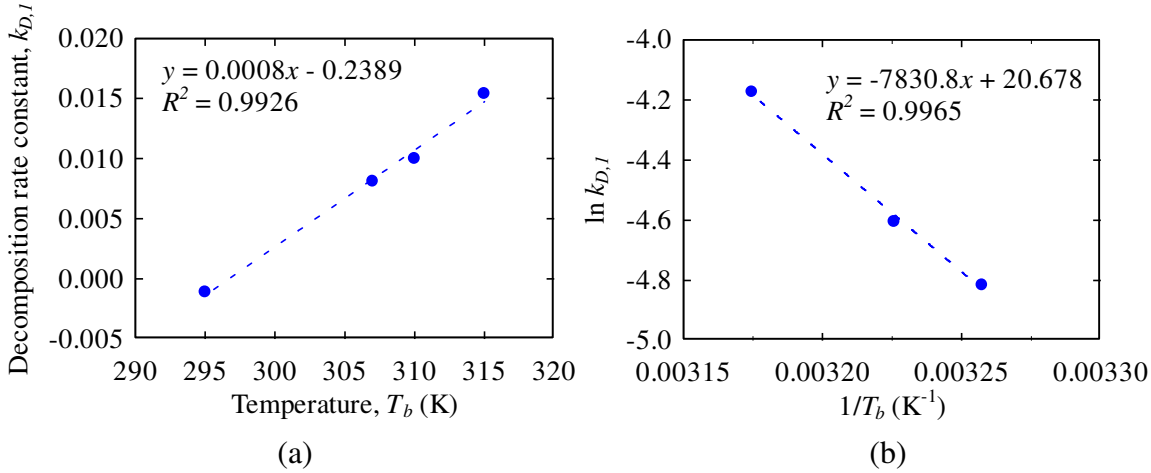

(a) (b)

Figure 21. (a) $k_{D,1}$ increased with increasing temperature and (b) the slope and intercept of the Arrhenius plot was used to derive the reaction frequency factor A and activation energy E of the decomposition of H_2O_2 in the bubbler. Each test contained 2-4 replications taken at 3.438 LPM. Dashed lines represent linear regression results.

4.2.1.2 Decomposition of H_2O_2 in the Condensate

The decomposition constant of the collected condensate, $k_{D,2}$ was determined from the concentration of H_2O_2 over time (④ in Figure 5). Due to the high water vapor content in simulated exhaled breath, H_2O_2 levels were diluted 125-275 times (Figure 22) the H_2O_2 levels in the stock solution in the bubbler (Figure 19). Since no significant difference ($p > 0.05$) was seen between 5 and 10 min measurements of H_2O_2 in collected condensate samples, the 5 min sensing duration were used to estimate $k_{D,2}$ and develop predictive models.

Opposite of the trend seen with H_2O_2 levels in stock solution, $k_{D,2}$ decreased with increasing temperature as a result of more water evaporating at higher temperatures (Figure 23), thereby increasing the dilution of H_2O_2 in the condensate (Figure 24). The Arrhenius plot yielded the following general form of $k_{D,2}$ of H_2O_2 in the condensate:

$$k_{D,2} = 2.28\times10^{-8}\times\exp\left(\frac{30950}{RT_b}\right) \tag{14}$$

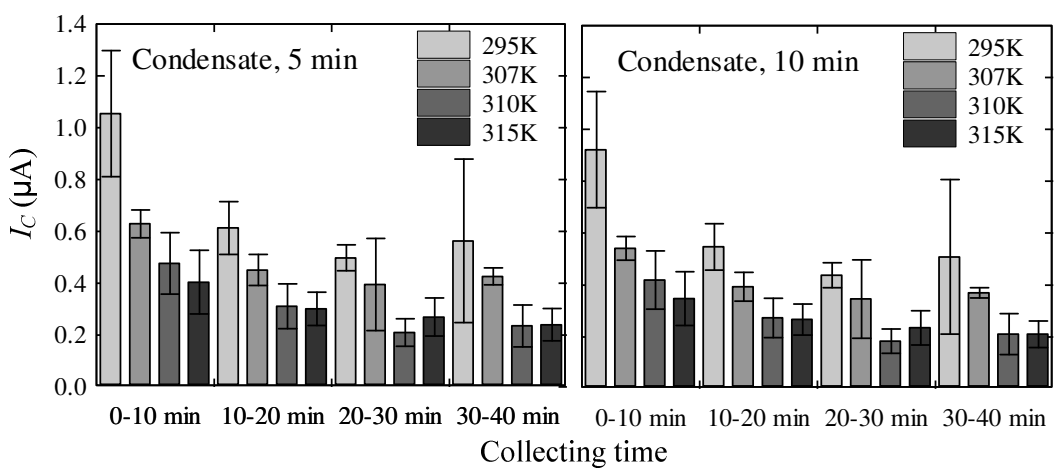

Figure 22. The decomposition of H_2O_2 in condensate samples were determined by monitoring the sensing duration in 5 min and 10 min at different bubbler temperatures and 3.438 LPM. Each test contained three replications. Error bars represent ± one S.E.

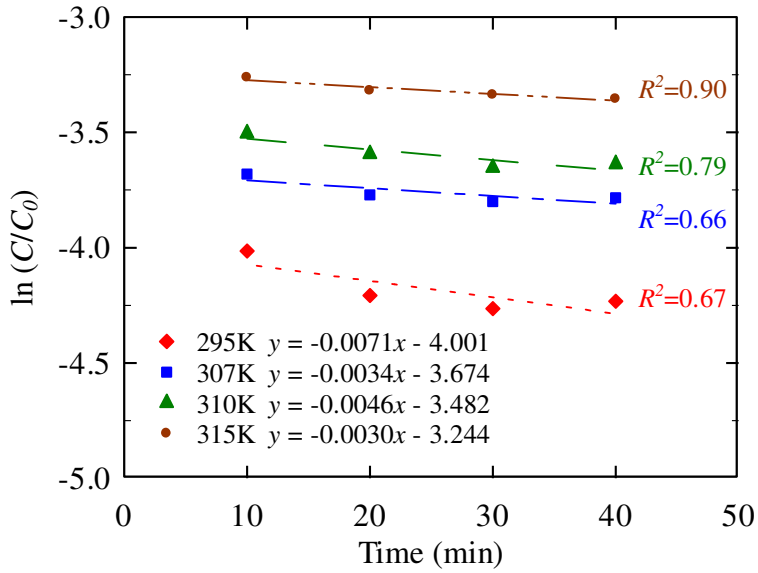

Figure 23. The decomposition rate constant $k_{D,2}$ decreased with increasing temperature. Condensate samples from sampling time interval of 0-10 min were used to estimate $k_{D,2}$. Each test contained three replications taken at 3.438 LPM. Dashed lines represent linear regression results.

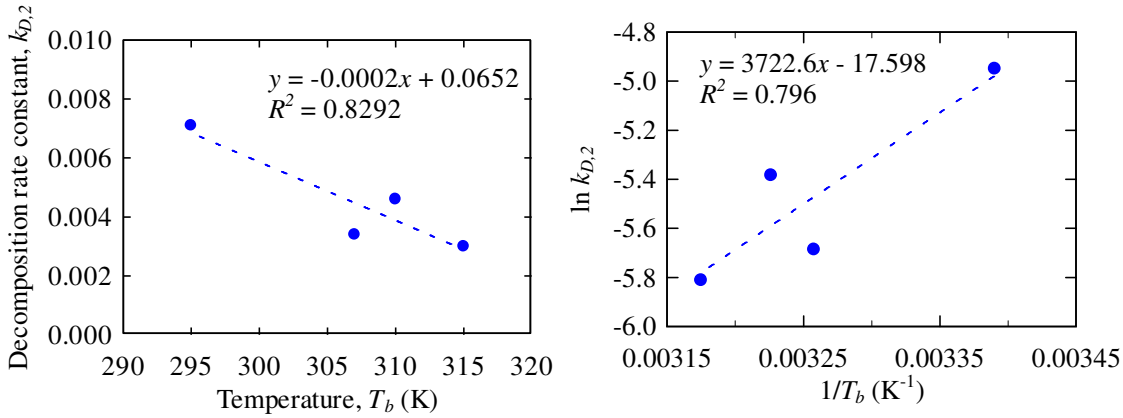

Figure 24. $k_{D,2}$ decreased with increasing temperature and the slope and intercept of the Arrhenius plot was used to derive the reaction frequency factor A and activation energy E of the decomposition of H_2O_2 in the condenser. Each test contained 2-4 replications taken at 3.438 LPM. Dashed lines represent linear regression results.

4.2.2 Temperature

4.2.2.1 Condensate

H_2O_2 concentration in the EBC decreased linearly as T_b increased (Figures 25) as a result of further dilution of H_2O_2 and higher decomposition rates with increasing T_b.

Since the boiling point of water is less than the boiling point of H_2O_2, when T_b increased, the amount of water vapor increased more than the amount of H_2O_2. Therefore, when the breath sample was condensed, the EBC collected at higher breath temperatures became more diluted.

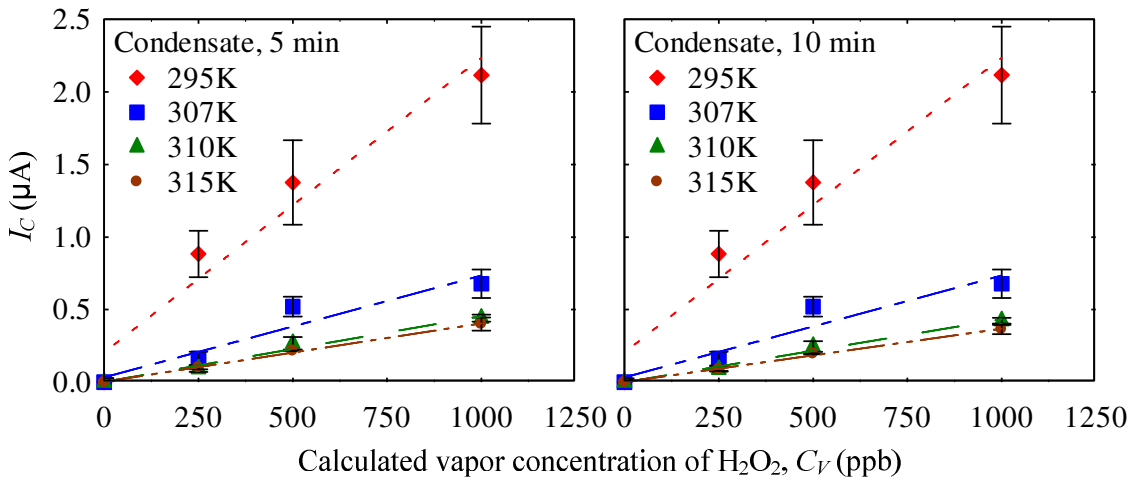

Figure 25. Linear trends were found between amperometric responses due to H_2O_2 levels in the condensate and H_2O_2 levels in the vapor at 295, 307, 310 and 315 K. Each test contained three replications of condensate samples collected at 274K and 3.438 LPM. Error bars and dashed lines represent ± one S.E and linear regression results, respectively.

4.2.3 Flow rate

4.2.3.1 Condensate

At a condensing temperature of 274 K, condensate samples collected at 6.876 LPM had higher levels of H_2O_2 compared to samples collected at 3.438 LPM (Figure 26). This was due to the higher vaporization rate with increasing flow rate. Higher flow rates also generated higher pressure which further increased the solubility of H_2O_2 into the condensate (Equation 1, $P = k_H \times c$).

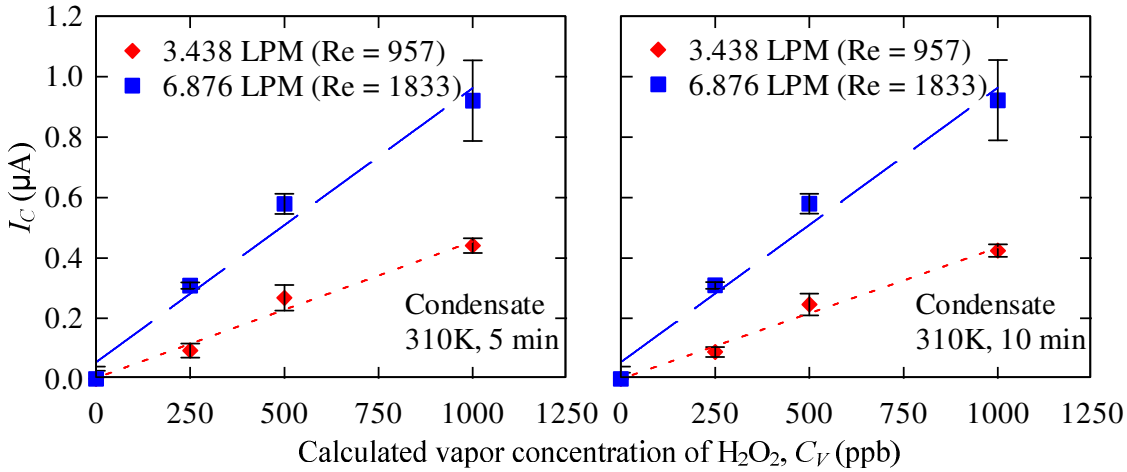

Figure 26. Amperometric tests were performed to monitor the effect of flow rate change with $\dot{V}$ = 3.438 and 6.876 LPM at T_b = 310K in H_2O_2 condensate samples. Increasing trend was present with increasing flow rate. Three replicate samples were measured. Error bars and dashed lines represent ± one S.E and linear regression results, respectively.

4.2.4 Condensing Temperature

When the condensing temperature was decreased to 256 K, H_2O_2 levels further decreased as a result of condensing more water vapor and enhancing the dilution of condensed H_2O_2 in the condensate (Figure 27).

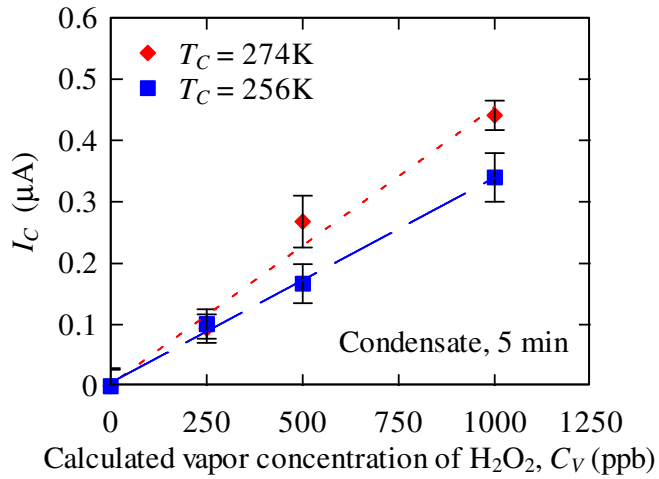

Figure 27. H_2O_2 collected in the EBC increased with increasing flow rate but decreased with decreasing condensing temperature. Each test contained three replications. Error bars and dashed lines represent ± one S.E and linear regression results, respectively.

4.3 Predictive Model Development

Breath sampling and measurement could be viewed as a three-part process (Figure 28):

1. Breath output simulator (BOS). Biomarkers in the simulated breath were affected by the empirical constants used in Henry's law and the decomposition reaction.
2. Sampling conditions. The concentrations of the biomarker in collected samples were changed with the input concentration and also varied with the changing flow rates and the sampling temperatures.
3. Sensing system, which, in this study, was an enzyme-based biosensor. Current responses resulted from a set of factors, such as the concentrations of the breath samples, the process of enzyme immobilization, and the uniformity of screen-printed electrodes from the manufacturer. The current response can be used to calculate the concentration of the sample by using an empirical calibration curve (Figure 9b).

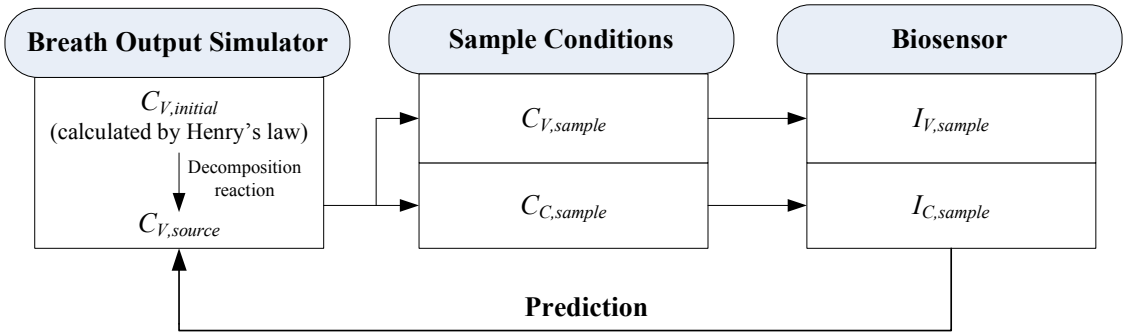

Figure 28. Concept diagram of predictive model development presents sampling and sensing system could be broken down into three subsystems.

4.3.1 Breath Output Simulator (BOS)

Depending on the sensing duration and decomposition rate, the concentration of the biomarker in the simulated breath vapor at the moment when it leaves the BOS was

$C_{V,source}$ could differ from the initial concentration of the biomarker in simulated breath vapor – $C_{V,initial}$. $C_{V,initial}$, could be expressed as a function of Henry's law constant, k_{H,T_b}, and the partial pressure of the solute in the gas above the solution, P (Equation 1). k_{H,T_b} is a function of $k_{H,T=298.15K}$, $\Delta_{soln}H$, and $1/T_b$ (Equation 3). Since $k_{H,T=298.15K}$ and $\Delta_{soln}H$ are empirical values from previous studies (Sandy, 1999), k_{H,T_b} could be simplified to be a function of $1/T_b$ only while P is directly proportional to flow rate $\dot{V}$. Consequently, $C_{V,initial}$ is expressed as

$$C_{V,initial} \sim f\left(\frac{1}{T_b}, \dot{V}\right) \tag{15}$$

At simulated breath temperatures of 295-315 K, decomposition rateof $C_{V,initial}$ for ethanol samples were negligible. However, decomposition was observed with the H_2O_2 samples and the decomposition constant $k_{D,1}$ and reaction time t needed to be included in the function (Equations 10 and 13). Hence, the $C_{V,source}$ for ethanol and H_2O_2 were derived as:

$$\text{Ethanol:}\quad C_{V,source} \sim f\left(C_{V,initial}\right) \sim f\left(\frac{1}{T_b}, \dot{V}\right) \tag{16}$$

$$H_2O_2\text{:}\quad C_{V,source} \sim f\left(C_{V,initial}, k_{D,1}, t\right) \tag{17}$$

$k_{D,1}$ was obtained from H_2O_2 decomposition reactions in a 40 min sensing duration with a 10 min sampling rate. However, since H_2O_2 measurements were taken within 10 minutes of breath simulation, H_2O_2 decomposition was not observed and the effect of $k_{D,1}$ was negligible. For a specific sensing time (t = 3 min, 4 min, …, 10 min), t was the same. The function of $C_{V,source}$ could therefore be rewritten as

$$H_2O_2\text{:}\quad C_{V,source} \sim f\left(C_{V,initial}\right) \tag{18}$$

4.3.2 Sampling Conditions

Sampling conditions, which are of great importance for solubility of biomarkers, were affected by the concentrations ($C_{V,source}$) and the temperature (T_b) of samples from the source. T_b was found to have a negative correlation with sample concentration ($C_{V/C,sample}$). A higher flow rate ($\dot{V}$) resulted in higher pressure that increased the solubility of the sample. A direct proportion was assumed between $\dot{V}$ and $C_{V/C,sample}$. The temperature drop (ΔT) between the simulated breath and the vapor sensing chamber in vapor sampling, and the condensing temperature (T_C) also contributed to $C_{V/C,sample}$ by the varying condensing conditions. Large ΔT favored water vapor condensation and caused further dilution to $C_{V/C,sample}$. Hence, ΔT was inversely proportional to $C_{V/C,sample}$. If the chosen biomarker had a tendency to decompose, then the decomposition effect on $C_{V/C,sample}$ needed to be taken into account. Accordingly, the functions of $C_{V/C,sample}$ were derived as

Ethanol: (vapor)

$$C_{V,sample} \sim f\left(C_{V,source}, \frac{1}{T_b}, \frac{1}{\Delta T}, \dot{V}\right) \tag{19}$$

(condensate)

$$C_{C,sample} \sim f\left(C_{V,source}, \frac{1}{T_b}, T_C, \dot{V}\right) \tag{20}$$

H_2O_2: (condensate)

$$C_{C,sample} \sim f\left(C_{V,source}, \frac{1}{T_b}, T_C, \dot{V}, k_{D,2}, t\right) \tag{21}$$

Similarly with $k_{D,1}$, the decomposition constant of H_2O_2 condensate, $k_{D,2}$, was also negligible in a 10-min sample collection period. For a specific sensing time, t was the same. The function of $C_{C/V,sample}$ of H_2O_2 became:

H_2O_2: (condensate)

$$C_{C,sample} \sim f\left(C_{V,source}, \frac{1}{T_b}, T_C, \dot{V}\right) \tag{22}$$

4.3.3 Biosensor

Finally, the output signals of the biosensor were directly proportional to concentrations of the analyte. When an enzyme was involved in the reaction, as was the case for ethanol sensing, it was necessary to control the effect of enzyme loading, enzyme kinetics, the thickness of enzyme layers (a key factor in the rate of mass transfer), and the conditions of enzyme immobilization processes that affect the retention of enzymatic activity. Factors due to manufacturer – the uniformity of the sensor coating (e.g. the percentage of each reagent element in the paste), the thickness of the layer, and the size of reaction area were possible sources of signal noise and instability of the SPCEs. In this project, errors due to enzyme immobilization and electrode were minimized by preparing all the biosensors in a similar manner. The SPCE from Metrohm USA Inc. (Riverview, FL) were assumed to hold a good uniformity. As a result, the current responses, $I_{V/C,sample}$, were only affected by the concentrations of the collected samples $C_{V/C,sample}$:

$$I_{V/C,sample} \sim f\left(C_{V/C,sample}\right) \tag{23}$$

The final predictive models contained these three main factors (Figure 29). For ethanol vapor samples, the predictive model in a specific sensing duration of $I_{V/C,sample}$ was derived from Equations 16, 19, and 23:

$$I_{V,t\min} = I_{V,sample\ \text{at tmin}} \sim f\left(C_{V,initial}, \frac{1}{T_b}, \frac{1}{\Delta T}, \dot{V}\right) \tag{24}$$

In the same manner, the predictive model for ethanol condensate samples in a specific sensing duration, $I_{C,sample}$ was derived from Equations 16, 20, and 23:

$$I_{C,t\min} = I_{C,sample\ \text{at tmin}} \sim f\left(C_{V,initial}, \frac{1}{T_b}, T_C, \dot{V}\right) \tag{25}$$

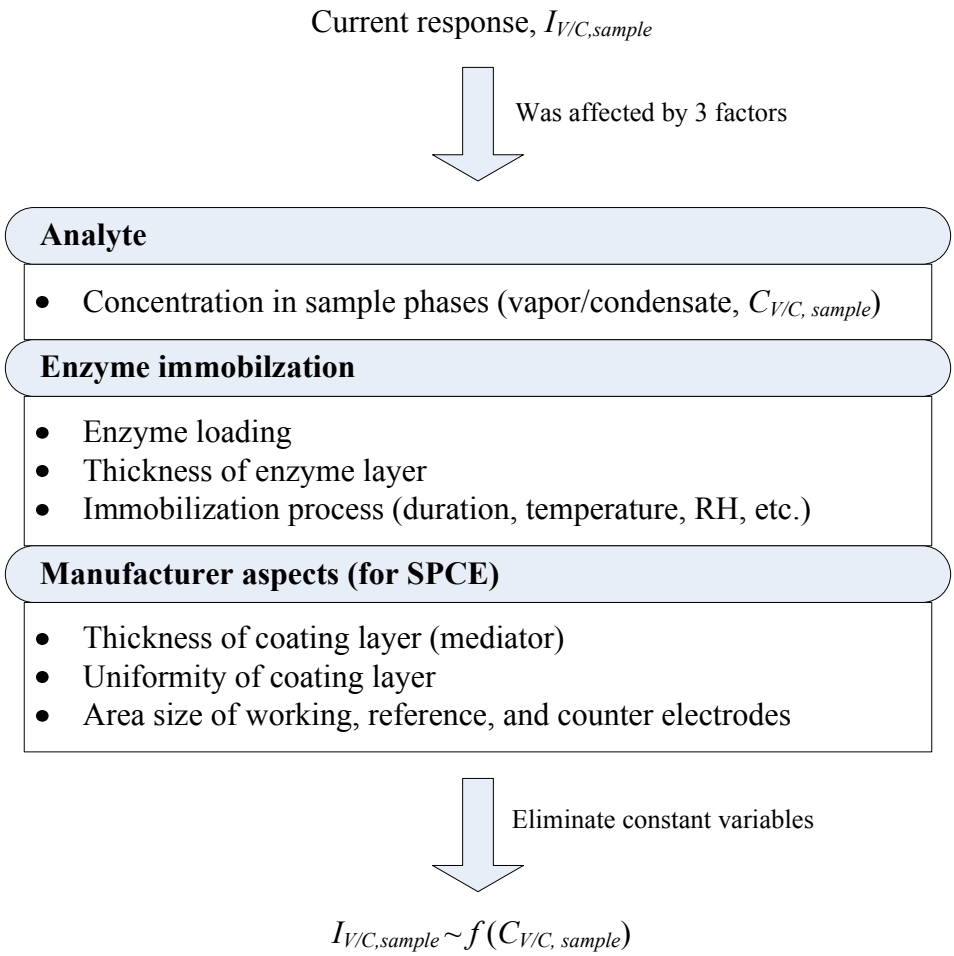

Figure 29. Contributing factors considered in the biosensor subsystem.

By considering Equations 17, 22, and 23, the predictive model for H_2O_2 condensate samples in a specific sensing duration, $I_{C,sample}$ had the same form as Equation 25. Full models that included reaction time t as one of the variables were also developed for ethanol and H_2O_2 separately (Figures 30 and 31).

	Dependent Variables	Influence Factors	Models
Breath Output Simulator	$C_{V,initial}$	• Henry's law constant, $k_{H,Tb}$ • Pressure, P	• $k_{H,Tb} \sim f(k_{H,T=298.15K}, \Delta_{soln}H, 1/T_b)^1 \sim f(1/T_b)$ • $P \sim f(\dot{V})$ • $C_{V,initial} \sim f(k_{H,Tb}, P) \sim f(1/T_b, \dot{V})$
	Decomposition reaction	No decomposition	
	$C_{V,source}$	• $C_{V,initial}$	• $C_{V,source} \sim f(C_{V,initial}) \sim f(1/T_b, \dot{V})$
Sample Condition	$C_{V,sample}$	• $C_{V,source}$ • Simulated breath temperature T_b • Temperature drop, ΔT • Flow rate, $\dot{V}$	• $C_{V,sample} \sim f(C_{V,source}, 1/T_b, 1/\Delta T, \dot{V})^2$ $\sim f(C_{V,initial}, 1/T_b, 1/\Delta T, \dot{V})$
	$C_{C,sample}$	• $C_{V,source}$ • Simulated breath temperature T_b • Condensing temperature, T_C • Flow rate, $\dot{V}$	• $C_{C,sample} \sim f(C_{V,source}, 1/T_b, T_C, \dot{V})$ $\sim f(C_{V,initial}, 1/T_b, T_C, \dot{V})$
Biosensor	$I_{V,sample}$	• $C_{V,sample}$ • Other factors	• $I_{V,sample} \sim f(C_{V,sample}) \sim f(C_{V,initial}, 1/T_b, 1/\Delta T, \dot{V})$
	$I_{C,sample}$	• $C_{C,sample}$ • Other factors	• $I_{C,sample} \sim f(C_{C,sample}) \sim f(C_{V,initial}, 1/T_b, T_C, \dot{V})$
Final model (Biomarker: ethanol)		In specific sensing duration	• $I_{V,tmin} \sim I_{V,sample\ at\ t\ min} \sim f(C_{V,initial}, 1/T_b, 1/\Delta T, \dot{V})$ • $I_{C,tmin} \sim I_{C,sample\ at\ t\ min} \sim f(C_{V,initial}, 1/T_b, T_C, \dot{V})$
		In full-time (time-series)	• $I_{V,3\text{-}10min} \sim f(t, C_{V,initial}, 1/T_b, 1/\Delta T, \dot{V})$ • $I_{C,3\text{-}10min} \sim f(t, C_{V,initial}, 1/T_b, T_C, \dot{V})$

Figure 30. Models for ethanol prediction were derived from three subsystems. ([1]$k_{H,T=298.15K}$ and $\Delta_{soln}H$ were constant values from empirical results. [2]T_b and ΔT were found to have reverse trends with sample concentration in experimental results. Hence, reciprocal forms were used. [3]Other factors (Figure 13) were negligible when they held constant.)

	Dependent Variables	Influence Factors	Models
Breath Output Simulator	$C_{V,initial}$	• Henry's law constant, $k_{H,Tb}$ • Pressure, P	• $k_{H,Tb} \sim f(k_{H,T=298.15K}, \Delta_{soln}H, 1/T_b)^1 \sim f(1/T_b)$ • $P \sim f(\dot{V})$ • $C_{V,initial} \sim f(k_{H,Tb}, P) \sim f(1/T_b, \dot{V})$
	Decomposition reaction	• Decomposition reaction in $C_{V,initial}$ - Decomposition constant, $k_{D,1}$ - Reaction time, t	• $k_{D,1} \sim f(1/T_b)$
	$C_{V,source}$	• $C_{V,initial}$ • Decomposition reaction in $C_{V,initial}$	• $C_{V,source} \sim f(C_{V,initial}$, Decomposition reaction in $C_{V,initial})$ $\sim f(C_{V,initial}, \dot{V}, k_{D,1}, t) \sim f(C_{V,initial})^2$
Sample Condition	$C_{C,sample}$	• $C_{V,source}$ • Simulated breath temperature, T_b • Condensing temperature, T_C • Flow rate, $\dot{V}$ • Decomposition reaction in $C_{C,sample}$ - Decomposition constant, $k_{D,2}$ - Reaction time, t	• $C_{C,sample} \sim f(C_{V,source}, 1/T_b, T_C, \dot{V}$, Decomposition reaction in $C_{C,sample})$ $\sim f(C_{V,source}, 1/T_b, T_C, \dot{V}, k_{D,2}, t)^{3,4}$ $\sim f(C_{V,source}, 1/T_b, T_C, \dot{V})^3$
Biosensor	$I_{C,sample}$	• $C_{C,sample}$ • Other factors[5]	• $I_{C,sample} \sim f(C_{C,sample}) \sim f(C_{V,source}, 1/T_b, T_C, \dot{V})$ $\sim f(C_{V,initial}, 1/T_b, T_C, \dot{V})$
	Final model (Biomarker: Hydrogen Peroxide)	In specific sensing duration	• $I_{C,tmin} \sim I_{C,sample\ at\ tmin} \sim f(C_{V,initial}, 1/T_b, T_C, \dot{V})$
		In full-time (time-series, adding t)	• $I_{C,3\text{-}10min} \sim f(t, C_{V,initial}, 1/T_b, T_C, \dot{V})$

Figure 31. Models for H_2O_2 prediction were derived from three subsystems. ([1]$k_{H,T=298.15K}$ and $\Delta_{soln}H$ were constant values from empirical results. [2]For the first 10 min sampling, $k_{D,1}$ were the same. [3]T_b was found to have a reverse trend with sample concentration in experimental results. Hence, a reciprocal form was used. [4]In10-min sample collecting, $k_{D,2}$ were the same. [5]Other factors (Figure 13) were negligible when they were held constant.)

4.3.4 Predictive Models

Final predictive models established in Section 4.3.3 were selected through statistical processes (Figure 12). Both specific sensing time (5 min) and full time (3-10 min) models were developed.

Modeling the current responses based on a 5 min sensing time for ethanol vapor samples required $1/T_b$, C_V, and the interaction term, C_V/T_b. For ethanol condensate samples, the model contained T_c and C_V, and the interaction term was replaced by T_cC_V. For full time (3-10 min) models, additional parameters and interaction terms were included in the models to better explain the change of current response with different time period (Tables 4 through 6). Higher complexities in full time models resulted in lower R^2 values ($R^2 = 0.6706$ in ethanol EB, 0.8878 in ethanol EBC, and 0.6924 in H_2O_2 EBC) compared to models based on specific sensing times ($R^2 = 0.8261$ in ethanol EB, 0.9471 in ethanol EBC, and 0.9348 in H_2O_2 EBC). In addition, EB models (Table 4) were less accurate than the EBC models (Table 5) respectively. It also demonstrated that vapor sensing was more unstable and more challenging than condensate sensing.

Ethanol, a VOC, could be retained in a more stable form when condensed and resulted in predictive models higher R^2 values compared to predictive models for H_2O_2 , a non-VOC. This was especially true for predictive models based on full time sensing (R^2 = 0.8878 for ethanol and $R^2 = 0.6924$ for H_2O_2).

Table 4. Predictive EB models for ethanol

Type		Model selection	Signal processing	R^2	Model						
Vapor (EB)	Ethanol condensate, specific sensing time	AIC	Subtraction, 5 min	0.8261	$I_{V,5\min} = \frac{\beta_0}{T_b} + \beta_1 C_V + \beta_2 \frac{C_V}{T_b}$						
						β_0	β_1	β_2			
						-20.70	-0.72	267.42			
					SE	19.89	0.30	92.07			
	Ethanol condensate, full time (time-series)	AIC	Subtraction, 3-10 min	0.6706	$I_{V,3-10\min} = \beta_0 + \beta_1 t + \frac{\beta_2}{T_b} + \frac{\beta_3}{\Delta T} + \beta_4 \dot{V} + \beta_5 C_V + \beta_6 \frac{t}{T_b} + \beta_7 t \times C_V + \frac{\beta_8}{T_b \times \Delta T} + \beta_9 \frac{C_V}{T_b} + \beta_{10} \frac{\dot{V}}{\Delta T} + \beta_{11} \dot{V} \times C_V$						
						β_0	β_1	β_2	β_3	β_4	β_5
						14.03	-1.16	-4064	-41.28	-0.22	-0.98
					SE	3.64	0.35	1086	11.29	0.19	0.30
						β_6	β_7	β_8	β_9	β_{10}	β_{11}
						348.8	0.036	11440	315.8	1.39	0.0403
					SE	107.8	0.003	3194	90.1	0.68	0.0011

Table 5. Predictive EBC models for ethanol

Type		Model selection	Signal processing	R^2	Model							
Condensate (EBC)	Ethanol condensate, specific sensing time	AIC/CV	Slope 5 min	0.9471	$I_{C,5\min} = \beta_0 T_C + \beta_1 C_V + \beta_2 \times C_V$							
						β_0	β_1	β_2				
						2.1E-6	-0.00264	1.25E-5				
					SE	7.8E-7	0.00093	3.44E-6				
	Ethanol condensate, full time (time-series)	AIC/CV	Slope 3-10 min	0.8878	$I_{C,3-10\min} = \beta_0 t + \frac{\beta_1}{T_b} + \beta_2 T_C + \beta_3 \dot{V} + \beta_4 C_V + \beta_5 t \times T_C + \beta_6 t \times C_V$							
						β_0	β_1	β_2	β_3	β_4	β_5	β_6
						0.0030	2.592	-1.35E-5	-0.0016	0.0016	-1.13E-5	-0.00014
					SE	0.0011	0.978	1.11E-5	0.0003	7E-5	3.92E-6	0.00001

Table 6. Predictive models for EBC H_2O_2

Type	Model selection	Signal processing	R^2	Model									
H_2O_2 condensate, specific sensing time	AIC	Subtraction 5 min	0.9348	$I_{C,5\min} = \frac{\beta_0}{T_b} + \beta_1 T_C + \beta_2 \dot{V} + \beta_3 C_V + \beta_4 \frac{C_V}{T_b} + \beta_5 T_C \times C_V$									
					β_0	β_1	β_2	β_3	β_4	β_5			
					-98.9	0.0011	0.0540	-0.0165	3.928	1.61E-5			
				SE	228.8	0.0027	0.0213	0.0027	0.844	4.37E-6			
H_2O_2 condensate, full time (time-series)	AIC	Subtraction 3-10 min	0.6924	$I_{C,3\text{–}10\min} = \beta_0 + \beta_1 t + \frac{\beta_2}{T_b} + \beta_3 T_C + \beta_4 \dot{V} + \beta_5 C_V + \beta_6 \frac{T_C}{T_b} + \beta_7 \frac{C_V}{T_b} + \beta_8 \dot{V} \times C_V$									
					β_0	β_1	β_2	β_3	β_4	β_5	β_6	β_7	β_8
					-59.5	-0.0082	18330	0.22	0.0082	-0.013	-67.68	4.01	1.24E-4
				SE	25.4	0.0029	7878	0.01	0.0162	0.002	29.17	0.61	2.54E-5

CHAPTER 5: UNCERTAINTY ANALYSIS

5.1 Fundamental Principle

In all kinds of measurement and prediction, errors inevitably result from various sources. After deriving the predictive models, they were further analyzed to clarify the margin of doubt for the measurement of each variable (condition) by running uncertainty analysis. Uncertainty analysis was estimated using two categories – Type A and Type B uncertainties. Type A uncertainty (u) was evaluated from repeated measurements which scatter around the mean of all readings and represent unpredictable random effects, such as imperfect repeatability of instrument or measurement and slight changes in experimental conditions. This type of error could be reduced by increasing the number of replications and the standard uncertainty, which represents the margin from the range of ± one standard deviation,

$$u = \frac{\sigma}{\sqrt{n}} \tag{26}$$

where n was the number of measurements.

Type B uncertainty, which is correlated to systematic errors, was determined from manufacturer's specifications, calibration reports, previous data and known uncertainties of reference data (GUM, 1995). Based on the nature of test data, Type B uncertainty could be assumed in several probability distributions – normal, rectangular, triangular, U-shaped, lognormal, quadratic and others (NIST, 2000; ISO/IEC, 2008; Castrup, 2010), with the first three types of distribution are more commonly seen (Figure 16). Normal probability distributions are widely applied for errors resulting from random events; rectangular (uniform) probability distribution, for errors occurring with equal possibility

between the range of upper and lower bounds, such as the resolution of an instrument; and triangular probability distribution, for errors that are more likely to happen near the center portion, such as simulation in business decision making. In this simulated breath project, only normal and rectangular probability distributions were applied.

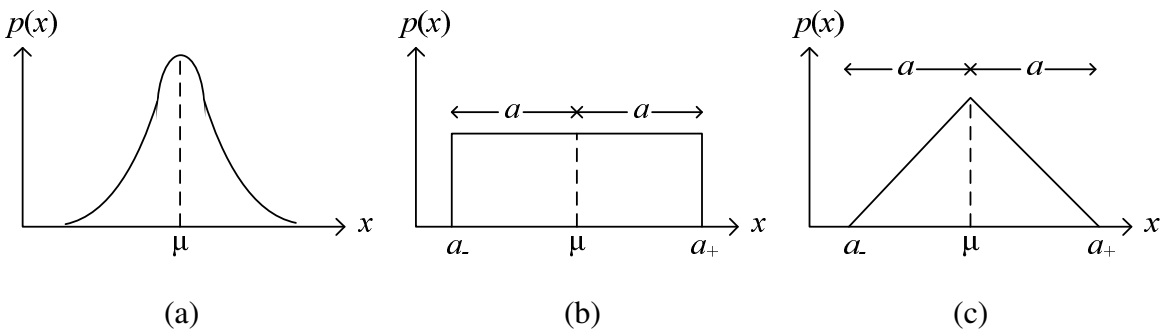

Figure 32. Most probability distributions are (a) normal, (b) rectangular, and (c) triangular shapes. The function $p(x)$ is the probability density function where μ is the mean value and a is the half width between the upper and lower bounding limits.

With an estimated value x_i of a true input value X_i, the standard uncertainty of x_i from different probability distributions result from the integration of $p(x)$:

Normal: $$u(x_i) = \frac{a}{2} \tag{27}$$

Rectangular: $$u(x_i) = \frac{a}{\sqrt{3}} = \frac{w}{\sqrt{12}} \tag{28}$$

Triangular: $$u(x_i) = \frac{a}{\sqrt{6}} = \frac{w}{\sqrt{24}} \tag{29}$$

where w is the full-width between the upper and lower bounding limits, or $2a$.

By considering both Type A and B uncertainties, the summation in quadrature (root sum of the squares) is called the combined standard uncertainty, u_c (Kirkup and Frenkel, 2006). In general, a measurand Y is a function of N variables (X_1, X_2, …, X_N) that could indicate different input/sampling conditions, and the associated estimates are denoted by

$$y = f(x_1, x_2, ..., x_N) \tag{30}$$

where y and x_1, x_2, …, x_N are the output and input estimates respectively.

When x_1, x_2, …, x_N are independent of each other, the uncertainty of y are presented as:

$$u_c^2(y) = \left(\frac{\partial y}{\partial x_1}\right)^2 u^2(x_1) + \left(\frac{\partial y}{\partial x_2}\right)^2 u^2(x_2) + \cdots + \left(\frac{\partial y}{\partial x_N}\right)^2 u^2(x_N) \tag{31}$$

or

$$u_c(y) = \sqrt{\left(\frac{\partial y}{\partial x_1}\right)^2 u^2(x_1) + \left(\frac{\partial y}{\partial x_2}\right)^2 u^2(x_2) + \cdots + \left(\frac{\partial y}{\partial x_N}\right)^2 u^2(x_N)} \tag{32}$$

After deriving the standard uncertainty, rescaling the uncertainty according to the level of confidence is necessary to express the margin of the output estimate y. The rescaling factor is called the coverage factor, $k_{coverage}$. By multiplying it by the combined standard uncertainty u_c, the expanded uncertainty U is obtained (Bell, 1999).

$$U = k_{\text{cov}\,erage} \times u_c \tag{32}$$

Some commonly used $k_{coverage}$ are 1, 2, and 3 which correspond to confidence levels of 68%, 95%, and 99.7%, respectively. The measured (estimated) value could be expressed as $y \pm U$ under an associated confidence level. Moreover, the percentage uncertainty could be calculated as:

$$\text{Percentage uncertainty} = \frac{\text{expanded uncertainty}, U}{\text{(measured) mean value}} = \frac{k_{coverage} \times u_c}{\text{(measured) mean value}} \tag{33}$$

Through all the uncertainty estimation in this study, $k_{coverage} = 2$ was applied.

5.2 Uncertainty in BOS and Sampling System

The uncertainties in the settings of experimental parameters (e.g. T_b, T_C, C_V.) which were varied to simulate different sampling conditions were derived based on using different devices or empirical principles/coefficients. For T_b and T_C, the measurands were affected by the water/ice bath and thermometer as their Type B uncertainties. The repeated readings taken every minute in a 10-minute time span were considered as the Type A uncertainty. Referring to Bell's (1999) spreadsheet model, the uncertainty of the condition at T_b = 310 K (37°C) and $\dot{V}$ =1.779 LPM was 1.2°C (details are listed in Table 7). In comparing the standard uncertainty of each component, the standard uncertainty for calibration of the thermometer was 0.54 K, which was relatively larger than the uncertainty for calibrating the water bath (0.25 K) and for the resolutions of both thermometer (0.03 K) and water bath (0.03 K). This resulted in the calibration of the thermometer accounting for 81% of the total uncertainty of T_b measurement. Using a similar approach, uncertainty analysis of other temperature measurements (T_b, T_C, ΔT), and $\dot{V}$ under different conditions could be accomplished (APPENDIX F).

Table 7. Uncertainty analysis for T_b at 310K with $\dot{V}$ = 1.779 LPM

T_b = 310K, $\dot{V}$ = 1.779 LPM				
Source of uncertainty	Value	Probability distribution	Divisor	Standard uncertainty (K)
Water bath				
calibration (±)	0.5	Normal, 2σ	2	0.25
Resolution	0.1	Uniform	$\sqrt{12}$	0.03
Thermometer				
calibration (±)	1.07	Normal, 2σ	2	0.54
Resolution	0.1	Uniform	$\sqrt{12}$	0.03
Correction	0.06			
SE from 11 repeated readings	0.08	Normal, 1σ	1	0.08
Combined standard uncertainty, u_c				0.60
Coverage factor, $k_{coverage}$[1]		2		
Expanded uncertainty, U				1.20
Mean from 11 repeated readings	310.31			
The measurement result and the uncertainty		310.37[2]	±	1.20

[1]Coverage factor, $k_{coverage}$ is equal to 2 which correspond to confidence levels of 95%.

[2]The measurement result = mean from 11 repeated readings + correction from the thermometer

The uncertainty of C_V was calculated using Henry's law, a combination of the empirical values of $k_{H,T_1=298.15K}$ and $\Delta_{soln}H/R$ in Equation 3, and also the possible errors made during the preparation of the stock solution. C_V was considered in units of ppm which was converted through unit conversion and Henry's law constant $k_{H,T_2=T_b}$ to have the unit of molarity:

$$1\ \text{ppm} = 10^{-6} \times 1\ \text{atm} = 10^{-6}\ \text{atm} \tag{34}$$

$$[M] = 10^{-6}\ \text{atm} \times k_{H,T_2=T_b} \frac{\text{M}}{\text{atm}} \tag{35}$$

where [M] is the molar concentration of ethanol. Hence C_V was derived as

$$C_V\,(\text{ppm}) = \frac{10^6 \times [M]}{k_{H,T_2=T_b}} = \frac{10^6 \times [M]}{k_{H,T_1=298.15K} \times \exp\left[\frac{\Delta_{soln}H}{R}\left(\frac{1}{T_b} - \frac{1}{298.15}\right)\right]} \tag{36}$$

and its uncertainty would be

$$u(C_V) = 10^6 \times \left\{ \left(b \times e^{cQ}\right)^{-2} u^2(a) + \frac{a^2}{\left(b \times e^{cQ}\right)^4} \times \left[\left(e^{cQ}\right)^2 u^2(b) + \left(bQ \times e^{cQ}\right)^2 u^2(c) + \left(\left(\frac{-bc}{T_b^{\,2}}\right) \times e^{cQ}\right)^2 u^2(T_b) \right] \right\}^{1/2} \tag{37}$$

where a, b, c, Q represent [M], $k_{H,T_1=298.15K}$, $\Delta_{soln}H/R$, and ($1/T_b$ - 1/298.15), respectively.

The standard uncertainties of b, c, T_b were estimated in the following manner:

- $u(b)$ and $u(c)$, which were 11.01 and 70.71, respectively, were calculated from empirical results presented in previous studies (Sander, 1999). .
- $u(T_b)$ could be estimated using the spreadsheet model shown in Table 7 for different T_b.

The standard uncertainty of a was based on a desired molar concentration [M], which was converted to volume concentration V_{ratio} to facilitate solution preparation,

$$V_{ratio} = \frac{V_A}{V_A + V_B} = [M]\frac{\text{mol}}{1} \times F.W.\frac{\text{g}}{\text{mol}} \times \frac{1}{\rho}\frac{\text{ml}}{\text{g}} \times \frac{1}{10^3}\frac{1}{\text{ml}} \tag{38}$$

where V_A is the volume of solute (ethanol solution) concentration; V_B is the volume of solvent (buffer solution); $F.W.$ and ρ are the formula weight and density of ethanol, respectively. Rearranging Equation 38,

$$[M] = \frac{10^3 P \times \rho}{F.W.} \tag{39}$$

the uncertainty of it was obtained as:

$$u([M]) = \sqrt{\left(\frac{\partial [M]}{\partial V_{ratio}}\right)^2 u^2(V_{ratio})} = \left(\frac{10^3 \rho}{F.W.}\right) u(V_{ratio}) \tag{40}$$

$u(V_{ratio})$ was estimated through a preparation process that was correlated to how the experimenter takes solution using different pipettes and each individual accuracy of the pipettes. For example, if 135 µl solvent is taken, using the pipette ranging from 20 – 200 µl will introduce calibration uncertainty of ± 1.6 µl and using the pipette ranging from 100 – 1000 µl will bring higher calibration uncertainty of ± 8 µl. The different combination of pipettes used resulted in varying uncertainties in solution preparation. The uncertainty of $u(V_{ratio})$ was:

$$\begin{aligned} u(V_{ratio}) &= \sqrt{\left(\frac{\partial V_{ratio}}{\partial V_A}\right)^2 u^2(V_A) + \left(\frac{\partial V_{ratio}}{\partial V_B}\right)^2 u^2(V_B)} \\ &= \sqrt{\left[\frac{V_B}{(V_A + V_B)^2}\right]^2 u^2(V_A) + \left[\frac{-V_A}{(V_A + V_B)^2}\right]^2 u^2(V_B)} \end{aligned} \tag{40}$$

The estimation of the total standard uncertainty for producing 4 ppm ethanol vapor

at 310 K is shown in Table 8. The uncertainty analyses for the rest of conditions are listed in Appendix F.2 and F.3. In all the cases (four T_b and three C_V), the percentage uncertainties of the volume concentration were within ±2% range of the measurement results. With this information, the uncertainties of C_V at three levels of ethanol vapor concentration, four simulated exhaled temperatures, and two flow rates were calculated using Equation 36. Results showed the percentage uncertainty was ±16.62% from the calculated ethanol concentration (Table 9). In the same manner, the percentage uncertainty was ±15.45% in H_2O_2 samples (Table 10). The largest source of uncertainty in ethanol and H_2O_2 samples were from the $u^2(b)$ associated term, or $\left(e^{cQ}\right)^2 u^2(b)$ in Equation 37. It indicated that the variation of $k_{H,T_1=298.15\,K}$ was the major source of uncertainty.

Table 8. Uncertainty analysis of the concentration of ethanol solution for producing 4ppm ethanol vapor at 310 K

Ethanol solution preparation for producing 4 ppm ethanol vapor at 310K				
Source of uncertainty	Value ± (μl)	Probability distribution	Divisor	Standard uncertainty (μl)
A (solute, use 0.1% (v/v) ethanol solution)				1478
1 ml	8	Rectangular	$\sqrt{3}$	4.62
uncertainty from 0.1% ethanol[1]				7.06
combined uncertainty of 1ml				*8.43*
450 μl	8	Rectangular	$\sqrt{3}$	4.62
uncertainty from 0.1% ethanol				3.18
combined uncertainty of 450 μl				*5.60*
28 μl	0.5	Rectangular	$\sqrt{3}$	0.29
uncertainty from 0.1% ethanol				0.20
combined uncertainty of 28μl				*0.35*
Combined standard uncertainty $u_c(A)$				*10.13*
B (solvent, use buffer)				78522
78 ml	600	Rectangular	$\sqrt{3}$	346.41
500 μl	8	Rectangular	$\sqrt{3}$	4.62
22 μl	0.5	Rectangular	$\sqrt{3}$	0.29
Combined standard uncertainty $u_c(B)$				*346.44*
Standard uncertainty of ethanol solution $u(P)$				**0.000148**
Coverage factor, $k_{coverage}$		2		
The measurement result and the uncertainty (in 0.1% ethanol based)		0.0185	±	0.0003
Percentage uncertainty[2]				**1.60%**

[1]Standard uncertainty for 0.1% ethanol was 0.000706% (calculated by same principle).

[2]In this case, the percentage uncertainty = $\frac{0.0003}{0.0185}$=1.60%.

Table 9. Uncertainty of C_V in ethanol samples under different experimental conditions

T_b (K)	C_V (ppm)	V (LPM)	$u(C_V)$ (ppm)	Percentage uncertainty (%)	T_b (K)	C_V (ppm)	V (LPM)	$u(C_V)$ (ppm)	Percentage uncertainty (%)
	4		0.2889	14.45%		4		0.4904	24.52%
295	5	1.779	0.3606	14.42%	315	5	1.779	0.6128	24.51%
	7.5		0.5401	14.40%		7.5		0.9191	24.51%
	4		0.2924	14.62%		4		0.2990	14.95%
307	5	1.779	0.3652	14.61%	310	5	3.407	0.3734	14.94%
	7.5		0.5509	14.69%		7.5		0.5598	14.93%
	4		0.2923	14.62%					
310	5	1.779	0.3650	14.60%		Average		0.45715	16.62%
	7.5		0.5473	14.59%					

Table 10. Uncertainty of C_V in H_2O_2 samples under different experimental conditions

T_b (K)	C_V (ppb)	V (LPM)	$u(C_V)$ (ppb)	Percentage uncertainty (%)	T_b (K)	C_V (ppb)	V (LPM)	$u(C_V)$ (ppb)	Percentage uncertainty (%)
	250		15.33	12.27%		250		36.03	28.82%
295	500	1.779	31.45	12.58%	315	500	1.779	56.38	22.55%
	1000		61.70	12.34%		1000		78.54	15.71%
	250		17.62	14.09%		250		18.06	14.45%
307	500	1.779	34.71	13.89%	310	500	3.407	36.30	14.52%
	1000		68.88	13.78%		1000		72.18	14.44%
	250		17.59	14.07%					
310	500	1.779	35.33	14.13%		Average		43.3571	15.45%
	1000		70.27	14.05%					

5.3 Uncertainties Analysis in Predictive Ethanol Models

Based on the predictive models in Table 4 and 5 for vapor and condensate samples, the related uncertainty analyses and the uncertainty equations were derived (Table 11 through 14). In the analysis, two percentage uncertainties were calculated – one was based solely on Type B uncertainty, which was calculated based on the listed uncertainty equation. The associated uncertainties were resulted from the model selection processes. The other uncertainty was the combined Type (A+B) uncertainties that included one more standard uncertainty which was contributed from the sensing system and could be calculated from the repeated readings of current response ($I_{V/C}$). The major source of uncertainties of predictive models could be recognized by comparing Type (A+B) and Type B uncertainties.

For both vapor and condensate specific time sensing, Type (A+B) percentage uncertainties, which were 44.21% for vapor and 18.20% for condensate, were greater than Type B percentage uncertainties that presented 18.53% for vapor and 0.05% for condensate. The observed increases in percentage uncertainties suggested the sensing system had a higher contribution of uncertainty on the final sensor output ($I_{V/C}$) than the BOS system and sampling conditions did. Factors that contributed to the uncertainties in the sensing system were the AOX enzyme layer and SPCE of the biosensor and the potentiostat.

For the predictive model for EB ethanol with 5 min sensing time, uncertainty increased as T_b, ΔT and $\dot{V}$ increased or when C_V decreased. For the time series predictive model, the total uncertainty was about 6.89 x 10^8% (Table 11), with the coefficient of the term of ΔT contributing > 99% of the total uncertainty. Hence, the EB time series

predictive model from current results was not accurate enough to provide credible information. For the EBC models, smaller percentage uncertainties, 0.05-18.20%, were achieved. Additionally the uncertainty of T_c increased as T_c decreased, owing to a greater degree of condensation by the water vapor than the ethanol at cooler condensing temperatures.

Table 11. Uncertainty analyses for ethanol EB predictive models

Type	Model selection	Signal processing	Uncertainty Analysis							
Ethanol vapor, specific sensing time	AIC	Subtraction, 5 min	$u^2(I_{V,5\min}) = \underbrace{\left(\frac{-\beta_0+\beta_2 C_V}{T_b{}^2}\right)^2}_{c_1} u^2(T_b) + \underbrace{\left(\beta_1+\frac{\beta_2}{T_b}\right)^2}_{c_2} u^2(C_V)$							
			Percentage uncertainty (%)		Major sources of $u(I_{V,5min})$	Trend				
			Type B	18.53	C_V	Variable	$T_b\uparrow$	$\dot{V}\uparrow$	$\Delta T\uparrow$	$C_V\uparrow$
						$u(I_{V,5min})$	↑[1]	---	↑	↓
			Type (A+B)	44.21	1) SE from repeated readings 2) C_V	Variable	$T_b\uparrow$	$\dot{V}\uparrow$	$\Delta T\uparrow$	$C_V\uparrow$
						$u(I_{V,5min})$	---[2]	↑	---	↓
Ethanol vapor, full time (time-series)	AIC	Subtraction, 3-10 min	$u^2(I_{V,3-10\min}) = \underbrace{\left(\beta_1+\frac{\beta_6}{T_b}+\beta_7 C_V\right)^2}_{c_1} u^2(t) + \underbrace{\left(-\frac{\beta_2+\beta_6 t+\frac{\beta_8}{\Delta T}+\beta_9 C_V}{T_b{}^2}\right)^2}_{c_2} u^2(T_b) + \underbrace{\left[-\frac{\beta_3+\frac{\beta_8}{\Delta T}+\beta_9 C_V}{(\Delta T)^2}\right]^2}_{c_3} u^2(\Delta T)$ $+ \underbrace{\left(\beta_4+\frac{\beta_{10}}{\Delta T}+\beta_{11} C_V\right)^2}_{c_4} u^2(\dot{V}) + \underbrace{\left(\beta_5+\beta_7 t+\frac{\beta_9}{T_b}+\beta_{11}\dot{V}\right)^2}_{c_5} u^2(C_V)$							
			Percentage uncertainty (%)		Major sources of $u(I_{V,3-10min})$	Trend				
			Type B	6.89E8	1) ΔT 2) flow rate	Variable	$T_b\uparrow$	$\dot{V}\uparrow$	$\Delta T\uparrow$	$C_V\uparrow$
						$u(I_{V,3-10min})$	↓	↑	↓	↓
			Type (A+B)	6.89E8		Variable	$T_b\uparrow$	$\dot{V}\uparrow$	$\Delta T\uparrow$	$C_V\uparrow$
						$u(I_{V,3-10min})$	↓	↑	↓	↓

[1]↑: increasing trend. [2] ---: no obvious trend found

Table 12. Related coefficients and standard uncertainties of 5-min ethanol EB predictive models

Ethanol vapor, 5-min, predictive model												
								Mean of	Type B		Type (A+B)	
T_b (K)	C_V (ppm)	$\dot{V}$ (LPM)	c_1	$u(T_b)$ (K)	c_2	$u(C_V)$ (ppm)	S.E. of $I_{V,5min}$	$I_{V,5min}$ (μA)	$u(I_{V,5min})$ (μA)	Percentage uncertainty[1] (%)	$u(I_{V,5min})$ (μA)	Percentage uncertainty (%)
	4		1.56E-04			0.2878	0.0948	0.6286	0.0535	17.03%	0.1089	34.63%
295.29	5	1.779	2.42E-04	0.58	3.40E-02	0.3593	0.0944	0.8669	0.0668	15.42%	0.1157	26.69%
	7.5		5.40E-04			0.5391	0.1977	1.4438	0.1003	13.89%	0.2216	30.70%
	4		1.33E-04			0.2918	0.1023	0.4526	0.0440	19.46%	0.1114	49.24%
307.24	5	1.779	2.07E-04	0.59	2.22E-02	0.3646	0.0270	0.5575	0.0550	19.74%	0.0613	21.99%
	7.5		4.61E-04			0.5491	0.0705	0.9087	0.0828	18.23%	0.1088	23.94%
	4		1.28E-04			0.2915	0.1298	0.3967	0.0416	20.98%	0.1363	68.70%
310.19	5	1.779	1.99E-04	0.60	1.98E-02	0.3642	0.1405	0.6709	0.0520	15.50%	0.1498	44.67%
	7.5		4.44E-04			0.5465	0.1599	1.0425	0.0780	14.96%	0.1779	34.14%
	4		1.21E-04			0.4897	0.0512	0.5617	0.0630	22.44%	0.0812	28.92%
314.89	5	1.779	1.88E-04	0.61	1.64E-02	0.6122	0.0870	0.7657	0.0788	20.57%	0.1173	30.65%
	7.5		4.18E-04			0.9185	0.1229	1.0161	0.1182	23.26%	0.1705	33.57%
	4		1.28E-04			0.2982	0.1213	0.4378	0.0423	19.31%	0.1285	58.69%
310.53	5	3.407	1.98E-04	0.60	1.96E-02	0.3726	0.1978	0.6908	0.0528	15.29%	0.2047	59.28%
	7.5		4.42E-04			0.5591	0.4185	0.7255	0.0792	21.83%	0.4259	117.41%

[1]Percentage uncertainty = $\frac{k_{coverage} \times u(I_{V,5\min})}{\text{mean of } I_{V,5\min}}$, $k_{coverage} = 2$ was applied here with the confidence level at 95%.

Table 13. Uncertainty analyses for ethanol EBC predictive models

Type	Model selection	Signal processing	Uncertainty Analysis							
Ethanol condensate, specific sensing time	AIC/CV	Slope, 5 min	$u^2(I_{C,5\min}) = \underbrace{(-\beta_0 + \beta_2 C_V)^2}_{c_1} u^2(T_C) + \underbrace{(\beta_1 + \beta_2 T_C)^2}_{c_2} u^2(C_V)$							
			Percentage uncertainty (%)		Major sources of $u(I_{C,5min})$	Trend				
			Type B	0.05	C_V	Variable	$T_b \uparrow$	$\dot{V} \uparrow$	$T_C \uparrow$	$C_V \uparrow$
						$u(I_{C,5min})$	↑	---	---	↑
			Type (A+B)	18.20	1) SE from repeated readings 2) C_V	Variable	$T_b \uparrow$	$\dot{V} \uparrow$	$T_C \uparrow$	$C_V \uparrow$
						$u(I_{C,5min})$	---	↓	↑	↑
Ethanol condensate, full time (time-series)	AIC/CV	Slope, 3-10 min	$u^2(I_{C,3-10\min}) = \underbrace{(\beta_0 + \beta_5 T_C + \beta_6 C_V)^2}_{c_1} u^2(t) + \underbrace{\left(\frac{-\beta_1}{T_b^{\,2}}\right)^2}_{c_2} u^2(T_b) + \underbrace{(\beta_2 + \beta_5 t)^2}_{c_3} u^2(T_C)$							
			: $+ \underbrace{(\beta_3)^2}_{c_4} u^2(\dot{V}) + \underbrace{(\beta_4 + \beta_6 t)^2}_{c_5} u^2(C_V)$							
			Percentage uncertainty (%)		Major sources of $u(I_{C,3-10min})$	Trend				
			Type B	0.06	C_V	Variable	$T_b \uparrow$	$\dot{V} \uparrow$	$T_C \uparrow$	$C_V \uparrow$
						$u(I_{C,3-10min})$	↑	---	↓	↑
			Type (A+B)	18.20	1) SE from repeated readings 2) C_V	Variable	$T_b \uparrow$	$\dot{V} \uparrow$	$T_C \uparrow$	$C_V \uparrow$
						$u(I_{C,3-10min})$	---	↓	↑	---

Table 14. Related coefficients and standard uncertainties of 5-min ethanol EBC predictive models

Ethanol condensate, 5-min, predictive model													
T_b (K)	C_V (ppm)	$\dot{V}$ (LPM)	T_C (K)	c_1	$u(T_C)$ (K)	c_2	$u(C_V)$ (ppm)	S.E. of $I_{C,5min}$	Mean of $I_{C,5min}$ (μA)	Type B		Type (A+B)	
										$u(I_{C,5min})$ (μA)	Percentage uncertainty (%)	$u(I_{C,5min})$ (μA)	Percentage uncertainty (%)
	4			2.30E-09			0.2878	0.2421	1.4410	0.0002	0.03%	0.2421	33.61%
295.29	5	1.779	274.25	3.66E-09	0.53	6.25E-07	0.3593	0.0825	1.7697	0.0003	0.03%	0.0825	9.32%
	7.5			8.42E-09			0.5391	0.0865	1.7821	0.0004	0.05%	0.0865	9.70%
	4			2.30E-09			0.2918	0.1386	1.1632	0.0002	0.04%	0.1386	23.84%
307.24	5	1.779	274.25	3.66E-09	0.53	6.25E-07	0.3646	0.2378	1.3999	0.0003	0.04%	0.2378	33.97%
	7.5			8.42E-09			0.5491	0.1996	1.6477	0.0004	0.05%	0.1996	24.23%
	4			2.30E-09			0.2915	0.1501	1.1719	0.0002	0.04%	0.1501	25.63%
310.19	5	1.779	274.25	3.66E-09	0.53	6.25E-07	0.3642	0.1405	1.4751	0.0003	0.04%	0.1405	19.05%
	7.5			8.42E-09			0.5465	0.1103	1.6777	0.0004	0.05%	0.1103	13.15%
	4			2.30E-09			0.4897	0.0301	1.0010	0.0004	0.08%	0.0301	6.01%
314.89	5	1.779	274.25	3.66E-09	0.53	6.25E-07	0.6122	0.1305	1.3936	0.0005	0.07%	0.1305	18.73%
	7.5			8.42E-09			0.9185	0.2429	1.6312	0.0007	0.09%	0.2429	29.78%
	4			2.30E-09			0.2982	0.0415	0.9099	0.0002	0.05%	0.0415	9.12%
310.53	5	3.407	274.25	3.66E-09	0.53	6.25E-07	0.3726	0.0755	1.3261	0.0003	0.04%	0.0755	11.39%
	7.5			8.42E-09			0.5591	0.1298	1.9473	0.0004	0.05%	0.1298	13.33%
	4			2.30E-09			0.2915	0.0912	0.6266	0.0002	0.05%	0.0912	29.11%
310.53	5	1.779	256.04	3.66E-09	0.50	3.17E-07	0.3642	0.0084	1.0056	0.0002	0.04%	0.0084	1.67%
	7.5			8.42E-09			0.5465	0.1126	1.4121	0.0003	0.04%	0.1126	15.95%

5.4 Uncertainties Analysis in Predictive H_2O_2 Models

In contrast to the percentage uncertainties (0.05-18.2%) shown in 5-min ethanol condensate models (Table 13), H_2O_2 model had relatively higher percentage uncertainties (12.67-26.55%) (Table 15). One of the major sources of uncertainties in both ethanol and H_2O_2 models was from C_V, but the percentage uncertainty of C_V for H_2O_2 samples was 15.45% (Table 10), which was in the same order for ethanol samples, 16.62% (Table 9). Hence, the greater uncertainties were possibly due to the relatively smaller $I_{C,5min}/I_{C,3\text{-}10min}$ (0.1-0.8 μA, in Table 16) for H_2O_2 samples than for ethanol samples (0.6-2 μA, in Table 14). The mean of $I_{C,5min}/I_{C,3\text{-}10min}$ was the divisor in the calculation of the percentage uncertainty, so that the smaller $I_{C,5min}/I_{C,3\text{-}10min}$ made the percentage uncertainty larger when the numerator had the same order of magnitude. Furthermore the smaller $I_{C,5min}/I_{C,3\text{-}10min}$ were due to applying a lower concentration level (250-1000 ppb) for H_2O_2 samples. The nonvolatile nature of H_2O_2 coupled with its accelerated decomposition with increasing temperature contributed to ppb-levels of H_2O_2 samples and presented low $I_{C,5min}$ and $I_{C,3\text{-}10min}$ values. Therefore, non-VOCs sensing posed more constraints and resulted in larger uncertainties in the EB predictive models.

Table 15. Uncertainty analyses for H_2O_2 EBC predictive models

Type	Model selection	Signal processing	Uncertainty Analysis							
H_2O_2 condensate, specific sensing time	AIC	Subtraction, 5 min	$u^2(I_{C,5\min}) = \underbrace{\left(-\frac{\beta_0+\beta_4 C_V}{T_b^{\,2}}\right)^2}_{c_1} u^2(T_b) + \underbrace{(\beta_1+\beta_5 C_V)^2}_{c_2} u^2(T_C) + \underbrace{(\beta_2)^2}_{c_3} u^2(\dot{V}) + \underbrace{\left(\beta_3+\frac{\beta_4}{T_b}+\beta_5 T_C\right)^2}_{c_4} u^2(C_V)$							
			Percentage uncertainty (%)		Major sources of $u(I_{C,5min})$	Trend				
			Type B	12.67	C_V	Variable	$T_b\uparrow$	$\dot{V}\uparrow$	$T_C\uparrow$	$C_V\uparrow$
						$u(I_{C,5min})$	$\uparrow$	$\downarrow$	$\downarrow$	$\uparrow$
			Type (A+B)	26.55	1) SE from repeated readings 2) C_V	Variable	$T_b\uparrow$	$\dot{V}\uparrow$	$T_C\uparrow$	$C_V\uparrow$
						$u(I_{C,5min})$	$\downarrow$	$\uparrow$	$\downarrow$	---
H_2O_2 condensate, full time (time-series)	AIC	Subtraction, 3-10 min	$u^2(I_{C,3-10\min}) = \underbrace{(\beta_1)^2}_{c_1} u^2(t) + \underbrace{\left(-\frac{\beta_2+\beta_6 T_C+\beta_7 C_V}{T_b^{\,2}}\right)^2}_{c_2} u^2(T_b) + \underbrace{\left(\beta_3+\frac{\beta_6}{T_b}\right)^2}_{c_3} u^2(T_C)$ $+ \underbrace{(\beta_4+\beta_8 C_V)^2}_{c_4} u^2(\dot{V}) + \underbrace{(\beta_5+\beta_8 \dot{V})^2}_{c_5} u^2(C_V)$							
			Percentage uncertainty (%)		Major sources of $u(I_{C,3-10min})$	Trend				
			Type B	301.68	C_V	Variable	$T_b\uparrow$	$\dot{V}\uparrow$	$T_C\uparrow$	$C_V\uparrow$
						$u(I_{C,3-10min})$	$\uparrow$	$\uparrow$	$\downarrow$	---
			Type (A+B)	303.24	1) SE from repeated readings 2) C_V	Variable	$T_b\uparrow$	$\dot{V}\uparrow$	$T_C\uparrow$	$C_V\uparrow$
						$u(I_{C,3-10min})$	$\uparrow$	$\downarrow$	$\downarrow$	---

Table 16. Related coefficients and standard uncertainties of 5-min H_2O_2 EBC predictive models

H_2O_2 condensate, 5-min, predictive model																
T_b (K)	C_V (ppb)	$\dot{V}$ (LPM)	T_C (K)	c_1	$u(T_b)$	c_2	$u(T_C)$	c_3	$u(\dot{V})$	c_4	$u(C_V)$	S.E. of $I_{C,5min}$	Mean of $I_{C,5min}$ (μA)	$u(I_{C,5min})$ (μA)	Percentage uncertainty (%)	$u(I_{C,5min})$ (μA)	Percentage uncertainty (%)
	250			8.75E-05		2.63E-05					17.62	0.0542	0.2057	0.0132	12.84%	0.0558	54.26%
307.24	500	1.779	274.25	3.90E-04	0.59	8.37E-05	0.53	2.91E-03	0.0196	4.36E-07	34.71	0.0621	0.5994	0.0262	8.74%	0.0674	22.48%
	1000			1.65E-03		2.96E-04					68.88	0.0880	0.7567	0.0522	13.80%	0.1023	27.04%
	250			8.42E-05		2.63E-05					17.59	0.0179	0.2419	0.0113	9.33%	0.0212	17.52%
310.19	500	1.779	274.25	3.76E-04	0.60	8.37E-05	0.53	2.91E-03	0.0196	2.90E-07	35.33	0.0341	0.4105	0.0229	11.13%	0.0411	20.02%
	1000			1.58E-03		2.96E-04					70.27	0.0189	0.5816	0.0457	15.71%	0.0495	17.01%
	250			7.93E-05		2.63E-05					36.03	0.0093	0.1813	0.0140	15.48%	0.0169	18.60%
314.89	500	1.779	274.25	3.54E-04	0.61	8.37E-05	0.53	2.91E-03	0.0196	1.22E-07	56.38	0.0006	0.2934	0.0233	15.91%	0.0233	15.92%
	1000			1.49E-03		2.96E-04					78.54	0.0344	0.4746	0.0373	15.73%	0.0508	21.39%
	250			8.39E-05		2.63E-05					18.06	0.0293	0.3261	0.0116	7.12%	0.0316	19.35%
310.53	500	3.407	274.25	3.74E-04	0.60	8.37E-05	0.53	2.91E-03	0.0500	2.75E-07	36.30	0.1478	0.6273	0.0230	7.33%	0.1496	47.69%
	1000			1.58E-03		2.96E-04					72.18	0.0901	0.7423	0.0457	12.33%	0.1011	27.23%
	250			8.39E-05		2.63E-05					18.06	0.0226	0.1346	0.0074	11.06%	0.0238	35.29%
310.53	500	1.779	256.04	3.74E-04	0.60	8.37E-05	0.50	2.91E-03	0.0196	5.36E-08	36.30	0.0267	0.1948	0.0151	15.48%	0.0307	31.48%
	1000			1.58E-03		2.96E-04					72.18	0.0240	0.3373	0.0304	18.00%	0.0387	22.94%

CHAPTER 6: CONCLUSION AND RECOMMENDATIONS FOR FUTURE STUDIES

6.1 Conclusion

Exhaled breath analysis provides a promising method to trace, monitor, or diagnose some of the symptoms, diseases and conditions through a noninvasive way. However, the varied sampling conditions cause difficulties in comparing the results. Standardized formulas could be developed after testing the impact of each sampling factor and predictive models could be established. Four concentrations (C_V) of chosen biomarkers in simulated exhaled breath were testing under four simulated breath temperatures (T_b = 295, 307, 310, and 315 K), two flow rates ($\dot{V}$ = 3.438 and 6.876 LPM, Reynolds numbers = 957 and 1833), two condensing temperature (T_C = 276 and 264K), and sensing duration from 3 to 10 min in this study.

The different properties of VOCs and non-VOCs in breath pose a question that how the differences will affect the breath sensing and detection. In this study ethanol and H_2O_2 were employed as the VOC and non-VOC model biomarkers. Biomarkers can be successfully detected by using the mediated SPCE and cooperating with immobilized enzyme in amperometric measurements. Predictive models were developed for specific sensing time (5 min) and full time (3-10 min). The major conclusions of this study are outlined below.

1. **The behavior of VOC (ethanol, 4 - 7.5 ppm) in simulated EB and EBC and the predictive models**

   In both EB and EBC, the concentration of collected ethanol samples were more

concentrated than the concentration from the source because the boiling point of ethanol was lower than that of water in the breather and was easier to vaporize. Higher T_b and lower T_C had lower current responses, which indicated less concentration of ethanol was detected, due to the water vaporization and condensation. Increasing flow rate and sensing duration did not significantly affect the ethanol concentration in condensate, but increased the ethanol concentration in vapor sensing. Higher regression results were shown in EBC predictive models (R^2 = 0.9471 in 5 min and R^2 = 0.8878 in full time) than EB predictive models (R^2 = 0.8261 in 5 min and R^2 = 0.6706 in full time). This showed EBC sensing was more stable than EB sensing.

2. **The behavior of non-VOC (H_2O_2, 250 -1000 ppb) in simulated EB and EBC and the predictive models**

Decompositions of H_2O_2 were observed in both stock solution and condensate at T_b = 307 - 315K. At higher T_b, decomposition rate increased in stock solution and decreased in condensate. It could be attributed to the sigmoidal curve relationship between H_2O_2 concentration and decomposition rate. Hence, the condensate contained relatively low H_2O_2 concentration and had slower reaction rates.

The concentrations of H_2O_2 condensate were measured at lower concentrations than the concentration from the source because of the high boiling point of H_2O_2 compared to that of water in the breath. In terms of the effect of sampling conditions, the same trends found for ethanol held true. Results showed that less H_2O_2 was sensed with increasing T_b or decreasing T_C. As for the effect of flow rate in condensate sensing, significant increases were observed at the elevated flow rate.

Slightly decreasing H_2O_2 concentrations were found in a longer sensing duration but were not found to be significant. Predictive models were developed with $R^2 = 0.9348$ and 0.6924 for 5 min and full time sensing, respectively.

3. The uncertainty analyses of predictive models and the whole sampling and sensing system

In order to further investigate the causes of error of predictive models, uncertainty analysis was employed. In BOS, the empirical Henry's law constant $k_{H,T_1=298.15\,K}$ resulted in the major source of the percentage uncertainty (associated with 95% possibility) of C_V in ethanol (±16.62%) and H_2O_2 (±15.45%) samples. Lower C_V and T_C increased the uncertainties of T_b, $\Delta T, \dot{V}$, and T_C. Nevertheless, comparing to the uncertainties due to BOS and the settings of sampling condition, the sensing system contributed greater uncertainties, which can be observed in varied values of current responses of samples from the same source concentrations, on the predictive models. In final results, the percentage uncertainties of each model were obtained as 18.53-44.21% for 5 min ethanol vapor; 0.05-18.20% for 5 min ethanol condensate; 0.06-18.20% for full time (3-10 min) ethanol condensate; and 12.67-26.55% for 5 min H_2O_2 condensate. The percentage uncertainties of ethanol vapor and H_2O_2 EBC models in full time were both over 300%. Hence, these two models were not able to give credible prediction presently. In uncertainty analyses, varied readings from repeated data and simulated vapor concentration (C_V) were the biggest sources to furnish the uncertainties of predictive models.

The developed predictive models provided a reference formula to standardize the varied sampling factors. The behaviors of ethanol and H_2O_2 under varied sampling

conditions were explored in this study and could contribute to a further understanding in VOC and non-VOC collection and sensing in breath analysis and also in trace gas analysis.

6.2 Recommendations for Future Research

In the course of this study, several improvements could be made to advance future research and were listed below:

1. Vapor sensing

   Two parts were noted to result in higher uncertainties or ineffective readings in vapor sensing – one was the temperature difference of vapor temperature from BOS to sensing chamber (ΔT), the other was how to amplify the current signal from highly diluted samples. In the first part, ΔT increased with increasing T_b or $\dot{V}$ (see APPENDIX G for temperature drop profile). This was caused by the reduced temperature of the sensing chamber because it lacked insulation or thermostat design. Three compensation methods were employed to amend this problem, such as wrapping the sensing chamber by heating tape or water heat recycling tube, or placing part of the sensing chamber body in a water bath. However, there were still no effective solutions found. The size of the chamber was too small and the heating tape could not be tightly fitted to the surface of chamber so that it could not function well. The thickness of water tube created another barrier for transmitting the heat. The water bath only provided limited compensation to the chamber but also posed a potential risk to induce water to come into the chamber or even the connector of potentiostat. In addition to the temperature issue in the sensing chamber, a further design, such as a mixing device, will help mix biomarkers and water vapor thoroughly.

In the preliminary results of H_2O_2 vapor sensing, linear responses were found in part of the data, but the current levels were below the detection limit of the potentiostat (WaveNow, Pine Research Instrumentation, Raleigh, NC). To obtaining more credible data, amplifying current responses or applying a more precision instrument (WaveNano, Pine Research Instrumentation, Raleigh, NC, which has a practical range from 1 pA to 1 mA) would help analyze trace analyte.

2. Condensate collection

In this study, an ice bath was used to provide a cooling environment at T_C = 274 and 256 K (1 and -17 °C) with uncertainties of 1.06 and 1 K respectively. Some researchers claimed that a lower condensing temperature (down to -70 °C) can stabilize biomarkers better through the immediately freezing process. Peltier modules can provide a choice of stable and miniaturizing cooling device. In future studies, the effect of condensing temperature could be further studied by widening the range of temperature and the uncertainties could be minimized by reaching a more stable temperature control system.

3. Sensor choice and preparation

In section 5.1, the sensing system, which included biosensor and potentiostat, was identified to be one of the major sources of uncertainties. The potentiostat was calibrated before experiments. Ethanol was measured with AOX-immobilized SPCEs while H_2O_2 was measured with bare SPCEs. The varied current readings from sample with the same concentration might have originated from the enzyme layer and the SPCE. Human error (pipetting error) led to uneven thickness or unequal amount of the enzyme layer because the small volume (0.2 – 2 μl) of each

component in composing the AOX-immobilized assay. Additionally, the repeatability of SPCE should be considered. From Figures 15 and 24, larger error bars were found with H_2O_2 sensing. This implies the repeatability of the SPCE could be a stronger factor than enzyme layer and thus, led to larger variation. The enzyme layer was observed to stabilize the performance of biosensor in some way.

With regards to SPCEs, limited options for commercially are available CoPC-mediated SPCEs in the US. The shelf life and different batches affected their performance. A customized option was available through Gwent Electronic Materials (GEM, Pontypool, Gwent, UK) but a bulk order was needed and proved more costly. In preliminary experiments where CoPC-mediated SPCEs from GEM were used, higher current readings were obtained with lower enzyme loadings and smaller working electrode surface area (Chen and Danao, 2010; APPENDIX H). Because the testing number between Gwent and DropSens obtained SPCEs were limited, full testing under the same preparation procedure and the assay composition will help further understand how to choose SPCEs with better performance.

4. Other biomarkers

While ethanol and H_2O_2 were chosen as the model biomarker in this study, results provided information on the behaviors of VOC and non-VOC during exhaled breath sampling and sensing. Based on the results presented in this dissertation, biomarkers with similar properties are expected to behave in a similar manner, following the general trends, and could be quantified using the analytical methods, predictive model development, and uncertainty analyses outlined in this study. The BOS, sampling or sensing systems may need to be re-designed for other biomarkers, taking into consideration their unique properties. For example, ammonia sensing was

briefly tested and results showed the conversion between ammonia and ammonium ion and the pH preference posed difficulties to simulate ammonia in exhaled breath (APPENDIX I.1).

A portable sensing array for multi-biomarker detection is a long-term goal in breath analysis. The possible crosstalk (or interaction) between measured biomarkers and its derivatives need to be considered in designing a robust sensing system. Limited experiments to demonstrate how crosstalk between metabolites of alcohol metabolism were conducted and results showed a more comprehensive experiment need to be designed and conducted to determine the contribution of each product or byproduct (APPENDIX I.2).

REFERENCES

Akaike, H. 1974. A new look at the statistical model identification. *IEEE Transactions on Automatic Control* 19(6):716–723.

Alving, K., C. Janson and L. Nordvall. 2006. Performance of a new hand-held device for exhaled nitric oxide measurement in adults and children. *Respiratory Research* 7: 67.

Baum, M. M., S. Kumar, A. M. Lappas and P. D. Wagner. 2003. Measurement of acetylene in breath by ultraviolet absorption spectroscopy: Potential for noninvasive cardiac output monitoring. *Review of Scientific Instruments* 74(6): 3104–3110.

Begg, T. B., I. D. Hill and L. C. Nickolls. 1964. Breathalyzer and Kitagawa-Wright methods of measuring breath alcohol. *British Medical Journal* 1(5374): 9-15.

Bell, C. M. and H. J. Flack. 1995a. Examining Variables Associated with Sampling for Breath Alcohol Analysis. Australia: University of Adelaide. Available at: http://www.druglibrary.org/schaffer/misc/driving/s5p3.htm. Accessed 02 April 2010.

Bell, C. M. and H. J. Flack. 1995b. Development of a system for real-time breath alcohol analysis. Australia: University of Adelaide. Available at: http://www.druglibrary.org/schaffer/misc/driving/s30p16.htm. Accessed 02 April 2010.

Bell, S. 1999. A Beginner's Guide to Uncertainty of Measurement: Issue 2. Middlesex, United Kingdom: National Physical Laboratory.

Biller, H., O. Holz , H. Windt, W. Koch, M. Műller, R. A. Jörres, N. Krug and J. M. Hohlfeld. 2011. Breath profiles by electronic nose correlate with systemic markers but not ozone response. *Respiratory Medicine*, doi:10.1016/j.rmed.2011.03.002

Boschetti, A., F. Biasioli, M. van Opbergen, C. Warneke, A. Jordan, R. Holzinger, P. Prazeller, T. Karl, A. Hansel, W. Lindinger and S. Iannott. 1999. PTR-MS real

time monitoring of the emission of volatile organic compounds during postharvest aging of berryfruit. *Postharvest Biology and Technology* 17(3): 143–151.

Boujtita, M., J. P. Hart and R. Pittson. 2000. Development of a disposable ethanol biosensor based on a chemically modified screen-printed electrode coated with alcohol oxidase for the analysis of beer. *Biosensors & Bioelectronics* 15: 257–263.

BreathTek UBiT system. 2011. Rockville, Md.: Meretek Diagnostics Group of Otsuka America Pharmaceutical, Inc. www.meretek.com/physician_instruments.asp#UBiT. Accessed June 06, 2011.

Cao, W. and Y. Duan. 2007. Current status of methods and techniques for breath analysis. *Critical Reviews in Analytical Chemistry* 37: 3–13.

Castrup, S. 2010. Comparison of methods for establishing confidence limits and expanded uncertainties. In *Proc. of 2010 Measurement Science Conference*, 23 pages. Pasadena, Calif.: Measurement Science Conference.

Chang, H. K. and J. P. Mortola. 1981. Fluid dynamic factors in tracheal pressure measurement. *Journal of Applied Physiology* 51(1): 218-225.

Chapman, E. A., P. S. Thomas and D. H. Yates. 2010. Breath analysis in asbestos-related disorders: a review of the literature and potential future applications. *Journal of Breath Research* 4: 034001 (11pp).

Chaplin, M. 2004. Method of Immobilisation. England: London South Bank University. Available at: http://www.lsbu.ac.uk/biology/enztech/immethod.html. Accessed 02 April 2009.

Cheng, W. and W. Lee. 1999. Technology development in breath microanalysis for clinical diagnosis. *Journal of Laboratory and Clinical Medicine* 133(3): 218-228.

Cope, K., T. Risby and A. M. Diehl. 2000. Increased gastrointestinal ethanol production in obese mice: implications for fatty liver disease pathogenesis. *Gastroenterology* 119(5): 1340-1347.

Corradi, M., G. Folesani, R. Andreoli, P. Manini, A. Bodini, G. Piacentini, S. Carraro, S. Zanconato and E. Baraldi. 2003. Aldehydes and glutathione in exhaled breath condensate of children with asthma exacerbation. *American Journal of Respiratory and Critical Care Medicine* 167 (3): 395-399.

Cruz, M. J., S. Sánchez-Vidaurre, P.V. Romero, F. Morell and X. Muñoz. 2009. Impact of age on pH, 8-isoprostane, and nitrogen oxides in exhaled breath condensate. *Chest* 135 (2): 462–467.

Czebe, K., I. Barta, B. Antus, M. Valyon, I. Horváth and T. Kullmann. 2008. Influence of condensing equipment and temperature on exhaled breath condensate pH, total protein and leukotriene concentrations. *Respiratory Medicine* 102(5): 720-725.

Danao, M. C., D. Cullen, C. Turner and T. Mottram. 2007. Direct detection and monitoring of ethanol in artificial breath samples using an alcohol oxidase-based electrochemical sensor. ASABE poster. Minneapolis, Minn.: ASABE.

Dahnke, H., D. Kleine, P. Hering and M. Mürtz. 2001. Real-time monitoring of ethane in human breath using mid-infrared cavity leak-out spectroscopy. *Applied Physics B: Lasers and Optics* 72(8): 971-975.

Daughtrey, E. H., K. D. Oliver, J. R. Adams, K. G. Kronmiller, W. A. Lonneman and W. A. McClenny. 2001. A comparison of sampling and analysis methods for low-ppbC levels of volatile organic compounds in ambient air. *Journal of Environmental Monitoring* 3(1):166–174.

Davidsson, A. and B. Schmekel. 2010. Efficacy of two breath condensers. *Journal of Clinical Laboratory Analysis* 24: 219–223.

Deaton, C. M., D. J. Marlin, N. C. Smith, K. C. Smith, R. J. Newton, S. M. Gower, S. M. Cade, C. A. Roberts, P. A. Harris, R. C. Schroter and F. J. Kelly. 2004. Breath condensate hydrogen peroxide correlates with both airway cytology and epithelial lining fluid ascorbic acid concentration in the horse. *Free Radical Research* 38(2): 201-208.

Dragonieri, S., J. T. Annemaa, R. Schot, M. P.C. van der Schee, A. Spanevello, P. Carratúb, O. Restab, K. F. Rabea and P. J. Sterka. 2009. An electronic nose in the

discrimination of patients with non-small cell lung cancer and COPD. *Lung Cancer* 64: 166–170.

Eggins, B. R. 2002. Sensing Elements. In *Chemical Sensors and Biosensors*. West Sussex, UK: John Wiley & Sons Ltd.

Fleischer, M., E. Simon, E. Rumpel, H. Ulmer, M. Harbeck, M. Wandel, C. Fietzek, U. Weimar and H. Meixner. 2002. Detection of volatile compounds correlated to human diseases through breath analysis with chemical sensors. *Sensors and Actuators B: Chemical* 83(1-3): 245-249.

Francesco, F. D., R. Fuoco, M. G. Trivella and A. Ceccarini. 2005. Breath analysis: Trends in techniques and clinical applications. *Microchemical Journal* 79: 405– 410.

Galassetti, P. R., B. Novak, D. Nemet, C. Rose-Gottron, D. M. Cooper, S. Meinardi, R. Newcomb, F. Zaldivar and D. R. Blake. 2005. Breath ethanol and acetone as indicators of serum glucose levels: an initial report. *Diabetes Technology & Therapeutics* 7(1):115-123.

Giardina, M. and S. V. Olesik. 2003. Application of low-temperature glassy carbon-coated macrofibers for solid-phase microextraction analysis of simulated breath volatiles. *Analytical Chemistry* 75(7):1604–1614.

Gisbert, J. P. and J. M. Pajares. 2004. Review article: ^{13}C-urea breath test in the diagnosis of Helicobacter pylori infection—A critical review. *Alimentary Pharmacology & Therapeutics* 20(10): 1001–1017.

Goldoni, M., A. Caglieri, R. Andreoli, D. Poli, P. Manini, M. Vettori, M. Corradi and A. Mutti. 2005. Influence of condensation temperature on selected exhaled breath parameters. *BMC Pulmonary Medicine* 5(1): 10 (9 pp).

Grob, N. M., M. Aytekin and R. A. Dweik. 2008a. Biomarkers in exhaled breath condensate: a review of collection, processing and analysis. *Journal of Breath Research* 2(3): 037004 (18 pp.).

Grob, N. M. and R. A. Dweik. 2008b. Exhaled nitric oxide in asthma: progress since the introduction of standardized methodology. *Journal of Breath Research* 2: 037002 (7 pp).

Grob, N. M. and R. A. Dweik. 2008c. Exhaled nitric oxide in asthma: from diagnosis, to monitoring, to screening: are we there yet? *Chest* 133: 837-839.

Grote, C. and J. Pawliszyn. 1997. Solid-phase microextraction for the analysis of human breath. *Analytical Chemistry* 69(4): 587–596.

Hansel, A., A. Jordan, R. Holzinger, P. Prazeller,W. Vogel and W. Lindinger. 1995. Proton-transfer reaction mass spectrometry—Online trace gas analysis at the ppb level. *International Journal of Mass Spectrometry and Ion Processes* 150: 609–619.

Haugland, R. P. 2002. Chapter 5 — Crosslinking and Photoreactive Reagents. In *Handbook of Fluorescent probe and research product*. Eugene, Ore.: Molecular Probes, Inc.

Hoffmeyer, F., M. Raulf-Heimsoth, V. Harth, J. Bünger and T. Brüning. 2009. Comparative analysis of selected exhaled breath biomarkers obtained with two different temperature-controlled devices. *BMC Pulmonary Medicine* 9:48.

Horváth, I., J. Hunt, P. J. Barnes. 2005. Exhaled breath condensate: methodological recommendations and unresolved questions. *European Respiratory Journal* 26(3): 523-548.

Hulsmann, A. R., H. R. Raatgeep, J. C. Den Hollander, T. Stijnen, P. R. Saxena, K. F. Kerrebijn and J. C. De Jongste. 1994. Oxidative epithelial damage produces hyperresponsiveness of human peripheral airways. *American Journal of Respiratory and Critical Care Medicine* 149(2): 519-525.

Hunt, J. 2007. Exhaled Breath Condensate pH Assays. *Immunology and Allergy Clinics of North America* 27(4): 597-606.

Huszar, E., G. Vass, E. Vizi, Z. Csoma, E. Barat, G. Molnar Vilagos, I. Herjavecz and I. Horvath. 2002. Adenosine in exhaled breath condensate in healthy volunteers and in patients with asthma. *European Respiratory Journal* 20(6): 1393-1398.

ISO/IEC. 2008. Uncertainty of measurement: Part 3. Guide to the expression of uncertainty in measurement (GUM:1995). ISO Guide 9803:2008(E). Geneva, Switzerland: International Standards Organization.

Jones, A. W. 1982. Effects of temperature and humidity of inhaled air on the concentration of ethanol in a man's exhaled breath. *Clinical Science* 63(5): 441-445.

Karl, T., P. Prazeller, D. Mayr, A. Jordan, J. Rieder, R. Fall and W. Lindinger, 2001. Human breath isoprene and its relation to blood cholesterol levels: New measurements and modeling. *Journal of Applied Physiology* 91(2): 762–770.

Kavolelis, B. 2003. Influence ventilation rate on ammonia concentration and emission in animal house. *Polish Journal of Environmental Studies* 12(6): 709-712

Kirkup, L. and R. B. Frenkel. 2006. *An Introduction to Uncertainty Measurement Using the GUM*. 1st ed. New York, N.Y.: Cambridge University Press.

Kirschvink, N., D. Marlin, F. Delvaux, J. Leemans, C. Clercx, A. Sparkes and P. Gustin. 2005. Collection of exhaled breath condensate and analysis of hydrogen peroxide as a potential marker of lower airway inflammation in cats. *Veterinary Journal* 169(3): 385-396.

Knutson, M. D. and F. E. Viteri. 1996. Concentrating breath samples using liquid nitrogen: a reliable method for the simultaneous determination of ethane and pentane. *Analytical Biochemistry* 242(1): 129-135.

Kostikas, K., G. Papatheodorou, K. Psathakis, P. Panagou and S. Loukides. 2003. Oxidative stress in expired breath condensate of patients with COPD. *Chest* 124(4): 1373-1380.

Lin, C.C., E R. Smith, N. Ichikawa, T. Baba, and M. Itow. 1991. Decomposition of hydrogen peroxide in aqueous solutions at elevated temperatures. International *Journal of Chemical Kinetics* 23: 971-987.

Liu, J., D. H. Conrad, S. Chow, V. H. Tran, D. H. Yates and P. S. Thomas. 2007. Collection devices influence the constituents of exhaled breath condensate. *European Respiratory Journal* 30(4): 807-808.

Lord, H., Y. F. Yu, A. Segal and J. Pawliszyn. 2002. Breath analysis and monitoring by membrane extraction with sorbent interface. *Analytical Chemistry* 74(21): 5650–5657.

Loukides, S., D. Bouros, G. Papatheodorou, P. Panagou and N. M. Siafakas. 2002. The relationships among hydrogen peroxide in expired breath condensate, airway inflammation, and asthma severity. *Chest* 121(2): 338-346.

Loukides S, I. Horváth, T. Wodehouse, P. J. Cole, P. J. Barnes. 1998. Elevated levels of expired breath hydrogen peroxide in bronchiectasis. *American Journal of Respiratory and Critical Care Medicine* 158 (3): 991–994.

Loukides, S., P. Bakakos and K. Kostikas. 2010. Chapter 12. Exhaled breath condensate: Hydrogen peroxide. *European Respiratory Monograph* 49:162-172.

Loyola, B. R., A. Bhushan, M. Schivo, N. J. Kenyon and C. E. Davis. 2008. Temperature changes in exhaled breath condensate collection devices affect observed acetone concentrations. *Journal of Breath Research* 2: 037005 (7pp).

Machado, R.F., D. Laskowski, O. Deffenderfer, T. Burgh, S. Zheng, P.J. Mazzone, T. Mekhail, C. Jennings, J. K. Stoller, J. Pyle, J. Duncan, R. A. Dweik and S. C. Erzurum. 2005. Detection of lung cancer by sensor array analysis of exhaled breath. *American Journal of Respiratory and Critical Care Medicine*171 (11): 1286–1291.

Miekisch, W., J. K. Schubert and G. F. E. Noeldge-Schomburg. 2004. Diagnostic potential of breath analysis—focus on volatile organic compounds. *Clinica Chimica Acta* 347(1-2): 25-39.

Montusch, P. 2007. Analysis of exhaled breath condensate in respiratory medicine: methodological aspects and potential clinical applications. *Therapeutic Advances in Respiratory Disease* 1(1): 5–23.

Motulsky H. and A. Christopoulos. 2004. *Fitting Models to Biological Data Using Linear and Nonlinear Regression: A Practical Guide to Curve Fitting*. New York, N.Y.: Oxford University Press.

Mueller, W., J. Schubert, A. Benzing and K. Geiger. 1998. Method for analysis of exhaled air by microwave energy desorption coupled with gas chromatography–flame ionization detection–mass spectrometry. *Journal of Chromatography B: Biomedical Sciences and Applications* 716(1-2): 27-38.

Mutlu, J. M., K. W. Garey, R. A. Robbins, L. H. Danziger and L. Rubinstein. 2001. Collection and analysis of exhaled breath condensate in humans, *American Journal of Respiratory and Critical Care Medicine* 164 (5): 731–737.

NIST. 2000. Uncertainty of Measurement Results. Gaithersburg, Md.: National Institute for Standards and Technology. Available at: http://physics.nist.gov/cuu/Uncertainty/index.html. Accessed 15 August 2011.

Nowak, D. 1998. Cigarette smoking does not increase hydrogen peroxide levels in expired breath condensate of patients with stable COPD. *Monaldi Archives for Chest Disease* 53(3): 268-273.

Nowak, D., M. Kasielski, A. Antczak, T. Pietras and P. Bialasiewicz. 1999. Increased content of thiobarbituric acid-reactive substances and hydrogen peroxide in the expired breath condensate of patients with stable chronic obstructive pulmonary disease: No significant effect of cigarette smoking. *Respiratory Medicine* 93(6): 389-396.

Nowak, D., S. Kalucka, P. Bialasiewicz and M. Król. 2001. Exhalation of H2O2 and thiobarbituric acid reactive substances (TBARs) by healthy subjects. *Free Radical Biology and Medicine* 30(2): 178-186.

Oudijk, E. D., W. B. M. Gerritsen, E. H. J. Nijhuis, D. Kanters, B. L. P. Maesen, J. J. Lammers and L. Koenderman. 2006. Expression of priming-associated cellular markers on neutrophils during an exacerbation of COPD. *Respiratory Medicine* 100(10): 1791-1799.

Palmer, T. 2001. Chapter 20: Biotechnological application of enzymes. In *Enzymes: biochemistry, biotechnology and clinical chemistry*. West Sussex, UK: Horwood Publishing.

Phillips, M. and J. Greenberg. 1991. Method for the collection and analysis of volatile compounds in the breath. *Journal of Chromatography B: Biomedical Sciences and Applications* 564(1): 242-249

Prieto, L., A. Ferrer, J. Palop, J. Domenech, R. Llusar and R. Rojas. 2007. Differences in exhaled breath condensate pH measurements between samples obtained with two commercial devices. *Respiratory Medicine* 101: 1715–1720.

Refaeilzadeh P., L. Tang and H. Liu. 2009. Cross-validation. In *Encyclopedia of Database Systems*, 532–538.Liu, L and M. T. Ozsu, ed. US: Springer.

Reinhold, P. and H. Knobloch. 2010. Exhaled breath condensate: lessons learned from veterinary medicine. *Journal of Breath Research* 4(1): 017001 (15 pp.).

Reinhold, P., J. Jaeger and C. Schroeder. 2006. Evaluation of methodological and biological influences on the collection and composition of exhaled breath condensate. *Biomarkers* 11(2): 118-142.

Risby, P.R., B. Novak, D. Nemet, C. Rose-Gottron, D.M. Cooper, S. Meinardi, R. Newcomb, F. Zaldivar and D. Blake. 2005. Breath ethanol and acetone as indicators of serum glucose levels: An initial report, *Diabetes Technology & Therapeutics* 7(1): 115–123.

Risby, T. H. 2001. Chapter 3: Volatile Organic Compounds as Markers in Normal and Diseases States. In *Disease markers in exhaled breath: basic mechanisms and clinical applications*, 113-122. N. Marczin and Yacoub, M. H., ed. Burke, Va.: IOS Press.

Roller, C., K. Namjou, J. Jeffers, W. Potter, P. J. McCann and J. Grego. 2002. Simultaneous NO and CO_2 measurement in human breath with a single IV-VI mid-infrared laser. *Optics Letters* 27(2): 107–109.

Romero, P.V., B. Rodríguez, S. Martínez, R. Cañizares, D. Sepúlveda and F. Manresa. 2006. Analysis of oxidative stress in exhaled breath condensate from patients with severe pulmonary infections. *Archivos de Bronconeumologia* 42(3): 113-119.

Roper, T. 2000. Ammonia Volatilization. Madison, Wis.: Cranberry Crop Management Library. Available at: http://www.hort.wisc.edu/cran/pubs_archive/newsletters/2000/7_5_00%20newsletter.pdf. Accessed 12 April 2010.

Rosias P. P., C. M. Robroeks, A. Kester, G. J. den Hartog, W. K. Wodzig, G. T. Rijkers, L. J. Zimmermann, C. P. van Schayck, Q. Jöbsis, E. Dompeling. 2008. Biomarker reproducibility in exhaled breath condensate collected with different condensers. *European Respiratory Journal* 31(5): 934–42.

Rosias P. P., C. M. Robroeks, H. J. Niemarkt, A. D. Kester, J. H. Vernooy, J. Suykerbuyk, J. Teunissen, J. Heynens, H. J. Hendriks, Q. Jöbsis, E. Dompeling. 2006. Breath condenser coatings affect measurement of biomarkers in exhaled breath condensate. *European Respiratory Journal* 28(5): 1036–41.

Ross B. M. 2008. Sub-parts per billion detection of trace volatile chemicals in human breath using selected ion flow tube mass spectrometry. *BMC Research Notes* 1: 41.

Sander, R. 1999. Compilation of Henry's Law Constants for Inorganic and Organic Species of Potential Importance in Environmental Chemistry (Version 3). Germany: Max-Planck Institute of Chemistry. Available at: http://www.henrys-law.org. Accessed 30 April 2010.

Sawyer, J. 2008. Surface Waters: Ammonium is Not Ammonia. Ames, Iowa: Iowa State University Extension. Available at: http://www.extension.iastate.edu/CropNews/2008/0421JohnSawyer.htm. Accessed 12 April 2010.

Schleiss, M. B., O. Holz, M. Behnke, K. Richter, H. Magnussen and R.A. Jörres. 2000. The concentration of hydrogen peroxide in exhaled air depends on expiratory flow rate. *European Respiratory Journal* 16: 1115-1118.

Skeldon, K. D., C. Patterson, C. A. Wyse, G. M. Gibson, M. J. Padgett, C. Longbottom and L. C. McMillan. 2005. The potential offered by real-time, high-sensitivity monitoring of ethane in breath and some pilot studies using optical spectroscopy. *Journal of Optics A: Pure and Applied Optics* 7(6): S376–S384.

Smith, D. and P. Španěl. 2005. Selected ion flow tube mass spectrometry (SIFT-MS) for online trace gas analysis. *Mass Spectrometry Reviews* 24(5): 661–700.

Smith, D., T. Wang, A. Pysanenko and P. Španěl. 2008. A selected ion flow tube mass spectrometry study of ammonia in mouth- and nose-exhaled breath and in the oral cavity. *Rapid Communications in Mass Spectrometry* 22: 783-789.

Soyer, O. U., E. A. Dizdar, O. Keskin, C. Lilly and O. Kalayci. 2006. Comparison of two methods for exhaled breath condensate collection. *Allergy* 61: 1016–1018.

Španel, P., K. Dryahina and D. Smith. 2007. The concentration distributions of some metabolites in the exhaled breath of young adults. *Journal of Breath Research* 1: 026001 (8 pp).

Španěl, P., S. Davies, and D. Smith. 1999. Quantification of breath isoprene using the selected ion flow tube mass spectrometric analytical method. *Rapid Communications in Mass Spectrometry* 13(17): 1733–1738.

Stellman, J. M. 1998. Peroxides, organic and inorganic. In *Encyclopaedia of Occupational Health and Safety: Guides, indexes, directory*, 906. London, UK: International Labour Office.

Taqieddin, E. and M. Amiji. 2004. Enzyme immobilization in novel alginate–chitosan core-shell microcapsules. *Biomaterials* 25: 1937–1945.

Turner, C., P. Španěl and D. Smith. 2006a. A longitudinal study of methanol in the exhaled breath of 30 healthy volunteers using selected ion flow tube mass spectrometry, SIFT-MS. *Physiological Measurement* 27: 637-648.

Turner, C., P. Španěl and D. Smith. 2006b. A longitudinal study of ethanol and acetaldehyde in the exhaled breath of healthy volunteers using selected ion flow tube mass spectrometry. *Communications in Mass Spectrometry* 20: 61-68.

Turner, C., P. Španěl and D. Smith. 2006c. A longitudinal study of breath isoprene in healthy volunteers using selected ion flow tube mass spectrometry, SIFT-MS. *Physiological Measurement* 27: 13-22.

Turner, C., P. Španěl and D. Smith. 2006d. A longitudinal study of ammonia, acetone, and propanol in the exhaled breath of 30 subjects using selected ion flow tube mass spectrometry, SIFT-MS. *Physiological Measurement* 27: 321-337.

Ultman, J. S. 1985. Gas Transport in the Conducting Airway. In *Gas Mixing and Distribution in the Lung*, 63-136. Engel, L. A. and M. Paiva, ed. New York, N.Y.: Marcel Dekker Inc.

van Beurden, W. J. C., G. A. Harff, P. N. R. Dekhuijzen, van Den Bosch, M. J. A., Creemers, J. P. H. M. and Smeenk, F. W. J. M. 2002. An efficient and reproducible method for measuring hydrogen peroxide in exhaled breath condensate. *Respiratory medicine* 96(3): 197-203.

Van Hoydonck, P.G., W.A. Wuyts, B.M. Vanaudenaerde, E.G. Schouten, L.J. Dupont and E.H. Temme. 2004. Quantitative analysis of 8-isoprostane and hydrogen peroxide in exhaled breath condensate. *European Respiratory Journal* 23: 189–192.

Vaughan, J., L. Ngamtrakulpanit, T. N. Pajewski, R. Turner, T. Nguyen, A. Smith, P. Urban, S. Hom, B. Gaston and J. Hunt. 2003. Exhaled breath condensate pH is a robust and reproducible assay of airway acidity. *European Respiratory Journal* 22(6): 889-894.

Wang, C. J., S. T. Scherrer and D. Hossain. 2004. Measurements of cavity ringdown spectroscopy of acetone in the ultraviolet and near-infrared spectral regions: Potential for development of a breath analyzer. *Applied Spectroscopy* 58(7): 784–791.

Williams, J., U. Poschl, P. J. Crutzen, A. Hansel, R. Holzinger, C. Warneke, W. Lindinger and J. Lelieveld. 2001. An atmospheric chemistry interpretation of mass scans obtained from a proton transfer mass spectrometer flown over the tropical rainforest of Surinam. Journal of Atmospheric Chemistry 38(2): 133–166.

Wilson, A. D. and M. Baiett. 2009. Applications and advances in electronic-nose technologies. *Sensors* 9: 5099-5148.

Yamamoto, K. and M. Ueda. 1972. Studies on breath alcohol analysis for the estimation of blood alcohol levels. *Forensic science* 1(2): 207-224.

APPENDICES

APPENDIX A: EMPIRICAL COEFFICIENTS OF HENRY'S LAW

k_H at 298.15 K and $\Delta_{soln}H/R$ values for ethanol and hydrogen peroxide were estimated using the average values collected from previous studies (Sander, 1999).

Table A.1. k_H at 298.15 K and $\Delta_{soln}H/R$ values of ethanol from previous studies

$k_{H,T=298.15K}$ (M/atm)	$\Delta_{soln}H/R$ (K)	Reference
190		Butler et al., 1935
220		Burnett, 1963
160		Timmermans, 1960
200		Gaffney and Senum, 1984
190	6600	Snider and Dawson, 1985
230		Rohrschneider, 1973
120		Yaws and Yang, 1992
150	6400	Schaffer and Daubert, 1969
200		Meylan and Howard, 1991
184	6500	(average)

Table A.2. k_H at 298.15 K and $\Delta_{soln}H/R$ values of H_2O_2 from previous studies

$k_{H,T=298.15K}$ (M/atm)	$\Delta_{soln}H/R$ (K)	Reference
71000	7000	Martin and Damschen, 1981
71000	7300	Hoffmann and Jacob, 1984
14000		Yoshizumi et al., 1984
97000	6600	Chameides, 1984
69000	7900	Hwang and Dasgupta, 1985
86000	6500	Zhou and Lee, 1992
110000	7500	Staffelbach and Kok, 1993
100000	6300	Lind and Kok, 1994
83000	7400	O'Sullivan et al., 1996
77889	7062.5	(Average)

APPENDIX B: EVALUATION OF NON-IMMOBILIZED AND IMMOBILIZED SPCE

Both assays contained: 1.2 µl AOX (400 units/ml), 0.6 µl BSA (40 mg/ml), and 0.2 µl glutaraldehyde (1.5% (v/v)).

Immobilized assay: the mixture was dropcoated on the working electrode of CoPC SPCE and drying for 2-2.5 hrs. Non-immobilized assay: the mixture was dropcoated on the working electrode of CoPC SPCE and ready for testing without drying time.

Ethanol solutions at concentrations of 0, 0.005, 0.006, 0.010, 0.013% (w/w) were used to produce equivalent vapor concentrations at 0, 4, 5, 7.5, 10 ppm at 310 K to test the current responses.

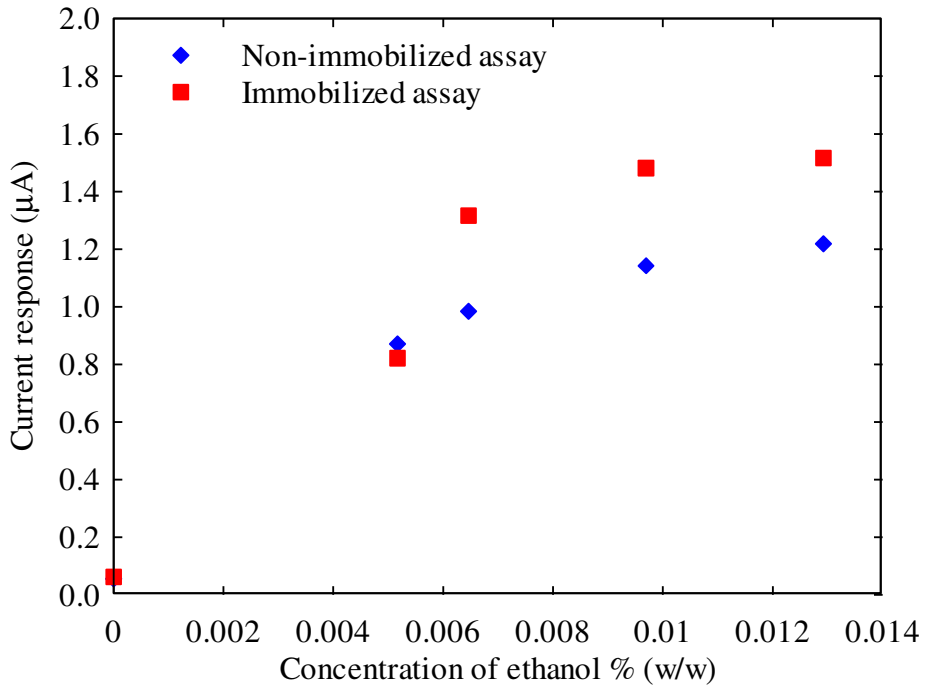

Figure B.1. Immobilized assay had higher current responses than non-immobilized assay in ethanol detection.

APPENDIX C: EVALUATION OF THE CONCENTRATION OF GLUTARALDEHYDE IN AOX-CONTAINED MIXTURE SOLUTIONS

Immobilized AOX assay contained: 1.2 µl AOX (400 units/ml), 0.6 µl BSA (40 mg/ml), and 0.2 µl glutaraldehyde (1.0, 1.5, 2.0% (v/v)).

The mixture was dropcoated on a working electrode of CoPC SPCE for 2-2.5 hrs.

Current responses were measured for 0, 0.0025, 0.005% (w/w) ethanol solutions.

Table C.1. Current measurements from three glutaraldehyde concentrations and three ethanol concentrations (unit: µA)

Glutaraldehyde Concentration	Concentration of ethanol % (v/v)		
% (w/w)	0	0.0025	0.005
1.0	0.0234	0.1798	0.3124
1.5	0.0782	0.1992	0.4434
2.0	0.0782	0.2340	0.3895

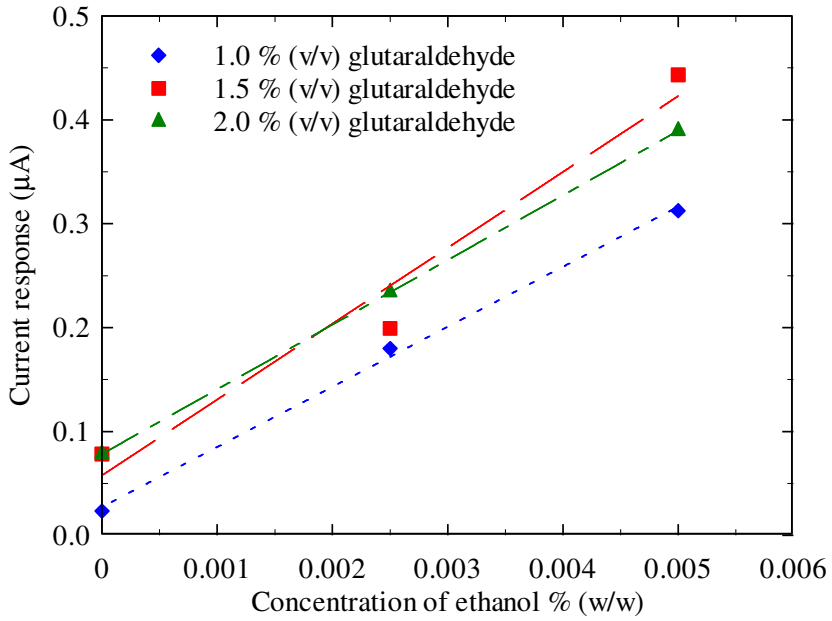

Figure C.1. Higher current responses were measured with AOX immobilized in 1.5% glutaraldehyde than with AOX immobilized in 1.0% glutaraldehyde. There was no significant difference among the assay with 1.5% and 2.0% glutaraldehyde. Dash lines represent regression results.

APPENDIX D: R CODES FOR MODELS FOR MODEL SELECTION AND PREDICTIVE MODEL DEVELOPMENT

D.1 Model Selection for Specific Sensing Time (3, 5, 10 min)

```
library(boot) # For command "glm"

# functions for best model selection
search.for.best.model<-function(data){

# A mapping matrix
ntotal=10
mapping=matrix(NA, 2^ntotal -1, ntotal)
for(x in 1:( 2^ntotal -1)){ flag=x;
	for(step in 1: ntotal) {
		if(x!=0) {
			mapping[flag, ntotal+1-step]=as.logical(x%%2);
			x=x%/%2}
		else{
			mapping[flag, ntotal+1-step]=FALSE}}}

mapping=cbind(rep(TRUE,2^ntotal-1),mapping)

wholedata=cbind(data,data[,2]*data[,3],data[,2]*data[,4],data[,2]*data[,5],
		data[,3]*data[,4],data[,3]*data[,5],data[,4]*data[,5])
name.whole=names(data)
name.whole=c(name.whole,paste(name.whole[2],"*",name.whole[3],sep=""),
		paste(name.whole[2],"*",name.whole[4],sep=""),
		paste(name.whole[2],"*",name.whole[5],sep=""),
		paste(name.whole[3],"*",name.whole[4],sep=""),
		paste(name.whole[3],"*",name.whole[5],sep=""),
		paste(name.whole[4],"*",name.whole[5],sep=""))
colnames(wholedata)=name.whole

# Remove those with interaction but no single term
list=NULL;
for(step in 1:(2^10-1)) {
```

```
        if(mapping[step,6]==TRUE & sum(mapping[step,c(2,3)])!=2) list<-c(list,step)
        if(mapping[step,7]==TRUE & sum(mapping[step,c(2,4)])!=2) list<-c(list,step)
        if(mapping[step,8]==TRUE & sum(mapping[step,c(2,5)])!=2) list<-c(list,step)
        if(mapping[step,9]==TRUE & sum(mapping[step,c(3,4)])!=2) list<-c(list,step)
        if(mapping[step,10]==TRUE & sum(mapping[step,c(3,5)])!=2) list<-c(list,step)
        if(mapping[step,11]==TRUE & sum(mapping[step,c(4,5)])!=2) list<-c(list,step)}

list=unique(list)
mapping=mapping[-list,]

AIC<-rep(NA,dim(mapping)[1])
BIC<-rep(NA,dim(mapping)[1])
CV<-rep(NA,dim(mapping)[1])
AICmin= ntotal^ ntotal
BICmin= ntotal^ ntotal
CVmin= ntotal^ ntotal

for(step in 1:dim(mapping)[1]){
        Z=wholedata[,mapping[step,]]
        fit=lm(I~.,data=Z)
        gfit=glm(I~.,data=Z)
        CVfitresult=cv.glm(Z,gfit,K=10)
        if(sum(is.na(fit$coefficients))==0){
                AIC[step]<- extractAIC(fit)[2]
                BIC[step]<- extractAIC(fit,k=log(dim(Z)[1]))[2]
                CV[step]<-CVfitresult$delta[1]
                if(AIC[step]<AICmin) {
                        AICmin=AIC[step]; AICfit=fit; AICstep=step}
                if(BIC[step]<BICmin) {
                        BICmin=BIC[step]; BICfit=fit; BICstep=step}
                if(CV[step]<CVmin)    {
                        CVmin=CV[step]; CVfit=fit; CVstep=step}}}

list(AIClist=AIC,BIClist=BIC, CVlist=CV,
     AICmin=AICmin, BICmin=BICmin, CVmin=CVmin,
     AICfit=AICfit, BICfit=BICfit, CVfit=CVfit,
```

```
    AICstep=AICstep, BICstep=BICstep, CVstep=CVstep)
}

# Feed data and run model selection function
# FilePath example: C:/Documents and Settings/chen143/My Documents/My
Dropbox/20110915 EtOH testing/Data/raw/corrected data (dT and
V)/vapor_3_sub_reciprocal.csv

data=read.csv("FilePath",header=T)
data=data[,c(1,2:5)]
result=search.for.best.model(data)
result
```

D.2 Model Selection for Full Time (Time Series, 3-10 min)

```
library(boot)

search.for.best.model<-function(data){
    ntotal=15
    mapping=matrix(NA,2^ntotal -1, ntotal)
    for(x in 1:(2^ ntotal -1)){
        flag=x;
        for(step in 1: ntotal) {
            if(x!=0) {
                mapping[flag, ntotal+1 -step]=as.logical(x%%2);
                x=x%/%2}
            else {mapping[flag, ntotal+1 -step]=FALSE}}}
mapping=cbind(rep(TRUE,2^ntotal-1),mapping)

wholedata=cbind(data,data[,2]*data[,3],data[,2]*data[,4],data[,2]*data[,5],
                data[,2]*data[,6],data[,3]*data[,4],data[,3]*data[,5],data[,3]*data[,6],
                data[,4]*data[,5],data[,4]*data[,6],data[,5]*data[,6])
name.whole=names(data)
name.whole=c(name.whole,paste(name.whole[2],"*",name.whole[3],sep=""),
                        paste(name.whole[2],"*",name.whole[4],sep=""),
                        paste(name.whole[2],"*",name.whole[5],sep=""),
```

```
                                paste(name.whole[2],"*",name.whole[6],sep=""),
                                paste(name.whole[3],"*",name.whole[4],sep=""),
                                paste(name.whole[3],"*",name.whole[5],sep=""),
                                paste(name.whole[3],"*",name.whole[6],sep=""),
                                paste(name.whole[4],"*",name.whole[5],sep=""),
                                paste(name.whole[4],"*",name.whole[6],sep=""),
                                paste(name.whole[5],"*",name.whole[6],sep=""))
colnames(wholedata)=name.whole

list=NULL;
for(step in 1:(2^ntotal -1)) {
    if(mapping[step,7]==TRUE & sum(mapping[step,c(2,3)])!=2) list<-c(list,step)
    if(mapping[step,8]==TRUE & sum(mapping[step,c(2,4)])!=2) list<-c(list,step)
    if(mapping[step,9]==TRUE & sum(mapping[step,c(2,5)])!=2) list<-c(list,step)
    if(mapping[step,10]==TRUE & sum(mapping[step,c(2,6)])!=2) list<-c(list,step)
    if(mapping[step,11]==TRUE & sum(mapping[step,c(3,4)])!=2) list<-c(list,step)
    if(mapping[step,12]==TRUE & sum(mapping[step,c(3,5)])!=2) list<-c(list,step)
    if(mapping[step,13]==TRUE & sum(mapping[step,c(3,6)])!=2) list<-c(list,step)
    if(mapping[step,14]==TRUE & sum(mapping[step,c(4,5)])!=2) list<-c(list,step)
    if(mapping[step,15]==TRUE & sum(mapping[step,c(4,6)])!=2) list<-c(list,step)
    if(mapping[step,16]==TRUE & sum(mapping[step,c(5,6)])!=2) list<-c(list,step)}

list=unique(list)
mapping=mapping[-list,]

AIC<-rep(NA,dim(mapping)[1])
BIC<-rep(NA,dim(mapping)[1])
CV<-rep(NA,dim(mapping)[1])
AICmin= ntotal^ ntotal
BICmin= ntotal^ ntotal
CVmin= ntotal^ ntotal

for(step in 1:dim(mapping)[1]){
    Z=wholedata[,mapping[step,]]
    fit=lm(I~.,data=Z)
    gfit=glm(I~.,data=Z)
```

```
        CVfitresult=cv.glm(Z,gfit,K=15)
        if(sum(is.na(fit$coefficients))==0){
            AIC[step]<- extractAIC(fit)[2]
            BIC[step]<- extractAIC(fit,k=log(dim(Z)[1]))[2]
            CV[step]<-CVfitresult$delta[1]
            if(AIC[step]<AICmin) {
                AICmin=AIC[step]; AICfit=fit; AICstep=step}
            if(BIC[step]<BICmin) {
                BICmin=BIC[step]; BICfit=fit; BICstep=step}
            if(CV[step]<CVmin)    {
                CVmin=CV[step]; CVfit=fit; CVstep=step}}}

list(AIClist=AIC,BIClist=BIC, CVlist=CV,
    AICmin=AICmin, BICmin=BICmin, CVmin=CVmin,
    AICfit=AICfit, BICfit=BICfit, CVfit=CVfit,
    AICstep=AICstep, BICstep=BICstep, CVstep=CVstep)
}

data=read.csv("FilePath",header=T)
data=data[,c(1,2:6)]
result=search.for.best.model(data)
result
```

D.3 Test the significance of each variables in the model

Example: model selection result of AIC model from 5 min ethanol vapor sample

```
data1=read.csv("FilePath",header=T)

#Original result from AIC model selection: I ~ Tb1 + Cv + Tb1*Cv
#Tb1=1/Tb
fit1=lm(I ~ Tb1 + Cv + Tb1*Cv,data=data1)

#Test the significance of the intercept
fit2=lm(I ~ Tb1 + Cv + Tb1*Cv-1,data=data1)
anova(fit1,fit2)
#Test the significance of the interaction term “Tb1*Cv”
```

```
fit3=lm(I ~ Tb1 + Cv -1,data=data1)
anova(fit2,fit3)

#Test the significance of the term “Cv”
fit4=lm(I ~ Tb1 + Tb1*Cv-1,data=data1)
anova(fit2,fit4)

#Test the significance of the term “Tb1”
fit5=lm(I ~ Cv + Tb1*Cv-1,data=data1)
anova(fit2,fit4)
```

APPENDIX E: VAPOR SENSING OF H_2O_2 SAMPLES

E.1 Decomposition of H_2O_2 in the Vapor

The decomposition of H_2O_2 in vapor samples at 295 K decreased significantly when sampled after 5 and 10 min ($p = 0.001$). In the 10 min sampling time, the amperometric responses were higher because the longer sampling time increased the chances of H_2O_2 molecules depositing on electrode surface (Figure E.1). In spite of part of the data showing a decreasing trend with time, the current responses were lower than 100 nA at elevated temperatures. It was close to or even lower than the detection limit (80 nA) of the potentiostat. Therefore, the current responses need to be further amplified to provide more credible measurements in order to better differentiate the signal from the noise.

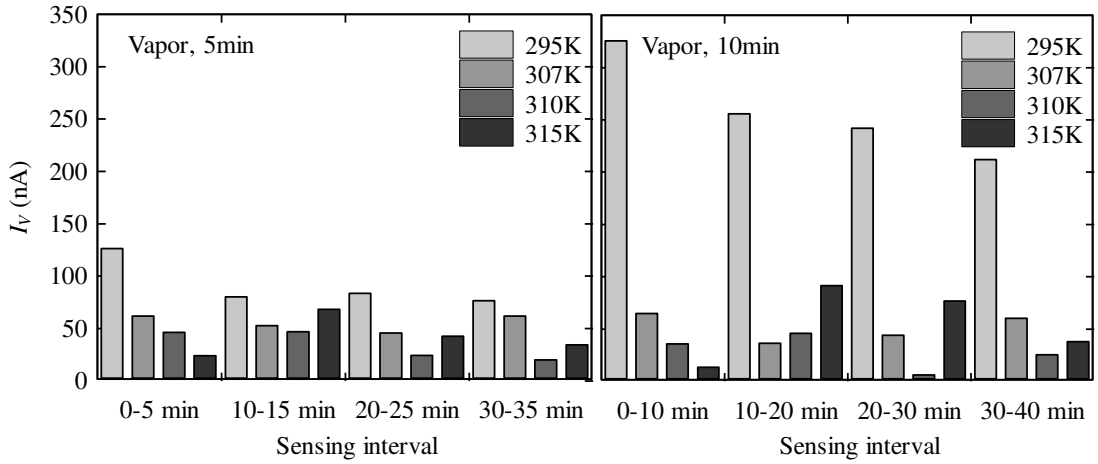

Figure E.1. The decomposition of H_2O_2 in vapor samples was determined by monitoring the current responses in 5 min and 10 min intervals for a period of 35-40 min at different bubbler temperatures and 3.438 LPM. The data represent one replication.

E.2 Current Response of H_2O_2 in the Vapor Samples at Changing Breath Temperature

Current responses measured from vapor sample were too low to determine any appreciable trend in 5 min or 10 min sensing duration at elevated T_b (Figure E.2). The amperometric responses will need to be further amplified, either by increasing the electrode surface or the enzyme loading for vapor sample detection.

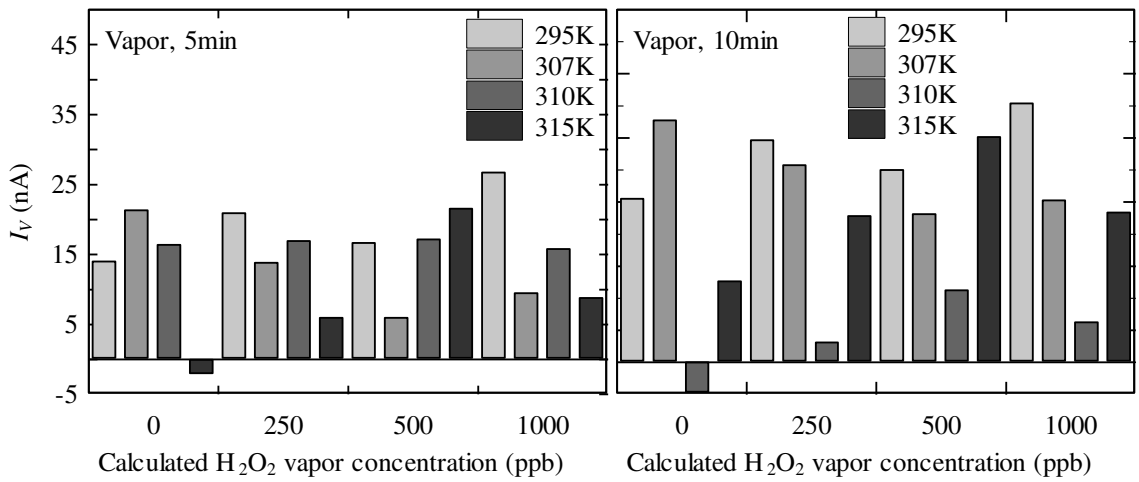

Figure E.2. Amperometric tests were performed to monitor the effect of simulated EB temperature (T_b= 295. 307, 310, 315 K, $\dot{V}$=3.438 LPM) in 5 min and 10 min H_2O_2 vapor sample measurement. The data represent one replication.

E.3 Current Response of H_2O_2 in the Vapor Samples at Changing Breath Rate

Increasing flow rate favored the reaction and raised the current levels, but no trend was found between current and increased H_2O_2 vapor concentration (Figure E.3). Current measurements were still too low for further inference.

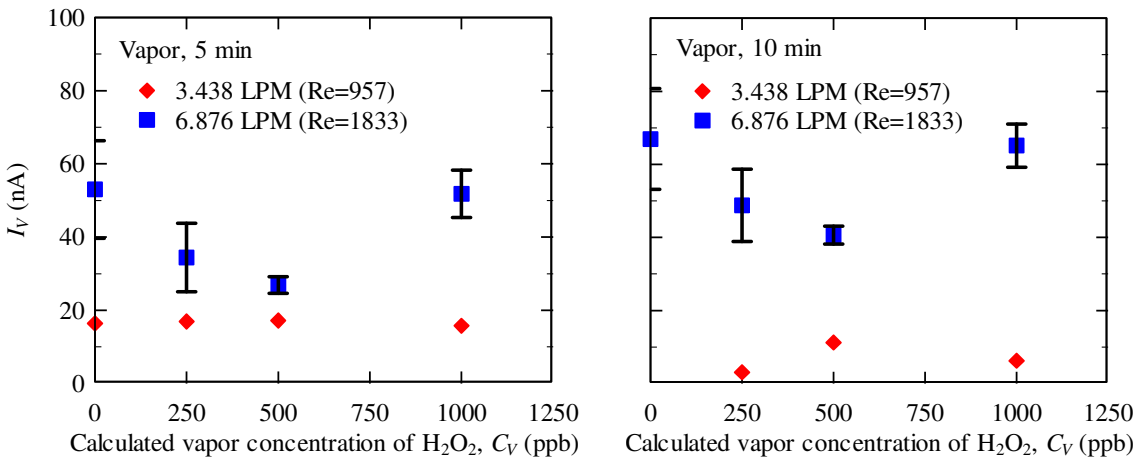

Figure E.3. Amperometric tests were performed to monitor the effect of flow rate change with $\dot{V}$= 3.438 and 6.876 LPM at T_b = 310 K in H_2O_2 vapor samples. Three replicate samples were measured for samples taken from $\dot{V}$= 3.438 and one was from $\dot{V}$= 6.876 LPM. Error bars represent ± one S.E.

APPENDIX F: DETAILED INFORMATION OF UNCERTAINTY ANALYSES

F.1 Systematic Uncertainties (Uncertainties of BOS)

Percentage uncertainties in this section were calculated as:

$$\text{Percentage uncertainty} = \frac{\text{Expanded uncertainty } (U)}{\text{The measurement result} - 273.15} \tag{F.1}$$

The percentage uncertainties were shown in the scale of degree Celsius.

F.1.1 Simulated Breath Temperature

Table F.1. Uncertainty analysis for T_b = 295 K and $\dot{V}$ = 1.779 LPM

T_b = 295 K (22°C), $\dot{V}$ = 1.779 LPM					
Source of uncertainty		Value (K)	Probability distribution	Divisor	Standard uncertainty (K)
Water bath	calibration (±)	0.5	Normal, 2σ	2	0.25
	resolution	0.1	Rectangular	$\sqrt{12}$	0.03
Thermometer	calibration (±)	1.04	Normal, 2σ	2	0.52
	resolution	0.1	Rectangular	$\sqrt{12}$	0.03
	correction	0.03			
SE from 11 repeated readings		0.015	Normal, 1σ	1	0.015
Combined standard uncertainty, u_c					**0.58**
Coverage factor, $k_{coverage}$			2		
Expanded uncertainty, U					1.16
Mean from 11 repeated readings		295.41			
The measurement result and the uncertainty			295.44	±	1.16
Percentage uncertainty					5.21%

Table F.2. Uncertainty analysis for T_b = 307 K and $\dot{V}$ = 1.779 LPM

T_b = 307 K (34°C), $\dot{V}$ = 1.779 LPM					
Source of uncertainty		Value (K)	Probability distribution	Divisor	Standard uncertainty (K)
Water bath	calibration (±)	0.5	Normal, 2σ	2	0.25
	resolution	0.1	Rectangular	$\sqrt{12}$	0.03
Thermometer	calibration (±)	1.07	Normal, 2σ	2	0.53
	resolution	0.1	Rectangular	$\sqrt{12}$	0.03
	correction	0.03			
SE from 11 repeated readings		0.037	Normal, 1σ	1	0.037
Combined standard uncertainty, u_c					**0.59**
Coverage factor, $k_{coverage}$			2		
Expanded uncertainty, U					1.18
Mean from 11 repeated readings		307.36			
The measurement result and the uncertainty			307.39	±	1.18
Percentage uncertainty					3.46%

Table F.3. Uncertainty analysis for T_b = 310 K and $\dot{V}$ = 1.779 LPM

T_b = 310 K (37°C), $\dot{V}$ = 1.779 LPM					
Source of uncertainty		Value (K)	Probability distribution	Divisor	Standard uncertainty (K)
Water bath	calibration (±)	0.5	Normal, 2σ	2	0.25
	resolution	0.1	Rectangular	$\sqrt{12}$	0.03
Thermometer	calibration (±)	1.07	Normal, 2σ	2	0.54
	resolution	0.1	Rectangular	$\sqrt{12}$	0.03
	correction	0.03			
SE from 11 repeated readings		0.08	Normal, 1σ	1	0.08
Combined standard uncertainty, u_c					**0.60**
Coverage factor, $k_{coverage}$			2		
Expanded uncertainty, U					1.20
Mean from 11 repeated readings		310.31			
The measurement result and the uncertainty			310.34	±	1.20
Percentage uncertainty					3.22%

Table F.4. Uncertainty analysis for T_b = 315K and $\dot{V}$ = 1.779 LPM

T_b = 315K (42°C), $\dot{V}$ = 1.779 LPM					
Source of uncertainty		Value (K)	Probability distribution	Divisor	Standard uncertainty (K)
Water bath	calibration (±)	0.5	Normal, 2σ	2	0.25
	resolution	0.1	Rectangular	$\sqrt{12}$	0.03
Thermometer	calibration (±)	1.08	Normal, 2σ	2	0.54
	resolution	0.1	Rectangular	$\sqrt{12}$	0.03
	correction	0.03			
SE from 11 repeated readings		0.128	Normal, 1σ	1	0.128
Combined standard uncertainty, u_c					**0.61**
Coverage factor, $k_{coverage}$			2		
Expanded uncertainty, U					1.22
Mean from 11 repeated readings		315.01			
The measurement result and the uncertainty			315.04	±	1.22
Percentage uncertainty					2.92%

Table F.5. Uncertainty analysis for T_b = 310 K and $\dot{V}$ = 3.407 LPM

T_b = 310 K (37°C), $\dot{V}$ = 3.407 LPM					
Source of uncertainty		Value (K)	Probability distribution	Divisor	Standard uncertainty (K)
Water bath	calibration (±)	0.5	Normal, 2σ	2	0.25
	resolution	0.1	Rectangular	$\sqrt{12}$	0.03
Thermometer	calibration (±)	1.08	Normal, 2σ	2	0.54
	resolution	0.1	Rectangular	$\sqrt{12}$	0.03
	correction	0.03			
SE from 11 repeated readings		0.072	Normal, 1σ	1	0.072
Combined standard uncertainty, u_c					**0.60**
Coverage factor, $k_{coverage}$			2		
Expanded uncertainty, U					1.20
Mean from 11 repeated readings		310.65			
The measurement result and the uncertainty			310.68	±	1.20
Percentage uncertainty					3.19%

F.1.2 Flow rate

Table F.6. Uncertainty analysis for $\dot{V}$ = 1.779 LPM

Flow rate ($\dot{V}$) = 1.779 LPM				
Source of uncertainty	Value (LPM)	Probability distribution	Divisor	Standard uncertainty (LPM)
Error from rotameter				
calibration (±)	0.036	Normal, 2σ	2	0.018
resolution	0.029	Rectangular	$\sqrt{12}$	0.008
Combined standard uncertainty, u_c				**0.0196**
Coverage factor, $k_{coverage}$		2		
Expanded uncertainty, U				0.04
The measurement result and the uncertainty		1.779	±	0.039
Percentage uncertainty				2.20%

Table F.7. Uncertainty analysis for $\dot{V}$ = 3.407 LPM

Flow rate ($\dot{V}$) = 3.407 LPM				
Source of uncertainty	Value (LPM)	Probability distribution	Divisor	Standard uncertainty (LPM)
Error from rotameter				
calibration (±)	0.068	Normal, 2σ	2	0.034
resolution	0.138	Rectangular	$\sqrt{12}$	0.040
Combined standard uncertainty, u_c				**0.0524**
Coverage factor, $k_{coverage}$		2		
Expanded uncertainty, U				0.10
The measurement result and the uncertainty		3.407	±	0.105
Percentage uncertainty				3.08%

F.1.3 Temperature Drop (for vapor samples)

Table F.8. Uncertainty analysis for ΔT from 295 K (22°C), $\dot{V}$ = 1.779 LPM

ΔT from 295 K (22°C), $\dot{V}$ = 1.779 LPM				
Source of uncertainty	Value (K)	Probability distribution	Divisor	Standard uncertainty (K)
Error from T_b				
correction	0.03			
mean from 11 repeated readings	295.41			
corrected mean	295.44			
combined uncertainty: $u(T_b)$				*0.58*
Error from T_{SC}				
calibration (±)	0.5	Normal, 2σ	2	0.25
resolution	0.1	Rectangular	$\sqrt{12}$	0.03
SE from 11 repeated readings	0.03	Normal, 1σ	1	0.03
correction	0.03			
mean from 11 repeated readings	295.48			
corrected mean	295.52			
combined uncertainty: $u(T_{SC})$				*0.25*
Combined standard uncertainty, u_c				**0.63**
Coverage factor, $k_{coverage}$		2		
Expanded uncertainty, U				1.27
Mean from 11 repeated readings	-0.08			
The measurement result and the uncertainty		-0.08	±	1.27
Percentage uncertainty				-1622.80%[1]

[1]Uncertainties of this magnitude was due to the relatively small value (-0.08), which was the divisor when calculating the percentage uncertainty, from the measurement results.

Table F.9. Uncertainty analysis for ΔT from 307 K (34°C), $\dot{V}$ = 1.779 LPM

ΔT from 307 K (34°C), $\dot{V}$ = 1.779 LPM				
Source of uncertainty	Value (K)	Probability distribution	Divisor	Standard uncertainty (K)
Error from T_b				
correction	0.03			
mean from 11 repeated readings	307.36			
corrected mean	307.39			
combined uncertainty: $u(T_b)$				*0.59*
Error from T_{SC}				
calibration (±)	0.5	Normal, 2σ	2	0.25
resolution	0.1	Rectangular	$\sqrt{12}$	0.03
SE from 11 repeated readings	0.18	Normal, 1σ	1	0.18
correction	0.03			
mean from 11 repeated readings	303.00			
corrected mean	303.04			
combined uncertainty: $u(T_{SC})$				*0.31*
Combined standard uncertainty, u_c				**0.67**
Coverage factor, $k_{coverage}$		2		
Expanded uncertainty, U				1.33
Mean from 11 repeated readings	4.35			
The measurement result and the uncertainty		4.35	±	1.33
Percentage uncertainty				30.62%

Table F.10. Uncertainty analysis for ΔT from 310 K (37°C), $\dot{V}$ = 1.779 LPM

ΔT from 310 K (37°C), $\dot{V}$ = 1.779 LPM				
Source of uncertainty	Value (K)	Probability distribution	Divisor	Standard uncertainty (K)
Error from T_b				
correction	0.03			
mean from 11 repeated readings	310.31			
corrected mean	310.34			
combined uncertainty: $u(T_b)$				*0.6*
Error from T_{SC}				
calibration (±)	0.5	Normal, 2σ	2	0.25
resolution	0.1	Rectangular	$\sqrt{12}$	0.03
SE from 11 repeated readings	0.23	Normal, 1σ	1	0.23
correction	0.03			
mean from 11 repeated readings	305.25			
corrected mean	305.29			
combined uncertainty: $u(T_{SC})$				*0.34*
Combined standard uncertainty, u_c				**0.69**
Coverage factor, $k_{coverage}$		2		
Expanded uncertainty, U				1.38
Mean from 11 repeated readings	5.0525			
The measurement result and the uncertainty		5.05	±	1.38
Percentage uncertainty				27.26%

Table F.11. Uncertainty analysis for ΔT from 315 K (42°C), $\dot{V}$ = 1.779 LPM

ΔT from 315 K (42°C), $\dot{V}$ = 1.779 LPM				
Source of uncertainty	Value (K)	Probability distribution	Divisor	Standard uncertainty (K)
Error from T_b				
correction	0.03			
mean from 11 repeated readings	315.01			
corrected mean	315.04			
combined uncertainty: $u(T_b)$				*0.61*
Error from T_{SC}				
calibration (±)	0.5	Normal, 2σ	2	0.25
resolution	0.1	Rectangular	$\sqrt{12}$	0.03
SE from 11 repeated readings	0.24	Normal, 1σ	1	0.24
correction	0.03			
mean from 11 repeated readings	308.07			
corrected mean	308.10			
combined uncertainty: $u(T_{SC})$				*0.35*
Combined standard uncertainty, u_c				**0.70**
Coverage factor, $k_{coverage}$		2		
Expanded uncertainty, U				1.41
Mean from 11 repeated readings	6.94			
The measurement result and the uncertainty		6.94	±	1.41
Percentage uncertainty				20.28%

Table F.12. Uncertainty analysis for ΔT from 310 K (37°C), $\dot{V}$ = 3.407 LPM

ΔT from 310 K (37°C), $\dot{V}$ = 3.407 LPM				
Source of uncertainty	Value (K)	Probability distribution	Divisor	Standard uncertainty (K)
Error from T_b				
correction	0.03			
mean from 11 repeated readings	310.65			
corrected mean	310.68			
combined uncertainty: $u(T_b)$				*0.6*
Error from T_{SC}				
calibration (±)	0.5	Normal, 2σ	2	0.25
resolution	0.1	Rectangular	$\sqrt{12}$	0.03
SE from 11 repeated readings	0.17	Normal, 1σ	1	0.17
correction	0.03			
mean from 11 repeated readings	306.06			
corrected mean	306.09			
combined uncertainty: $u(T_{SC})$				*0.30*
Combined standard uncertainty, u_c				**0.67**
Coverage factor, $k_{coverage}$		2		
Expanded uncertainty, U				1.34
Mean from 11 repeated readings	4.59			
The measurement result and the uncertainty		4.59	±	1.34
Percentage uncertainty				29.29%

F.1.4 Condensing Temperature (for condensate samples)

Table F.13. Uncertainty analysis for T_C = 274 K (1°C)

T_C = 274 K (1°C)				
Source of uncertainty	Value (K)	Probability distribution	Divisor	Standard uncertainty (K)
Ice bath				
calibration (±)	0.5	Normal, 2σ	2	0.25
Thermometer				
calibration (±)	1.00	Normal, 2σ	2	0.50
resolution	0.1	Rectangular	$\sqrt{12}$	0.03
correction	0.03			
SE from 11 repeated readings	0.16	Normal, 1σ	1	0.16
Combined standard uncertainty, u_c				**0.53**
Coverage factor, $k_{coverage}$		2		
Expanded uncertainty, U				1.06
Mean from 11 repeated readings	274.37			
The measurement result and the uncertainty		274.40	±	1.06
Percentage uncertainty				84.53%

Table F.14. Uncertainty analysis for T_C = 256 K (-17°C)

T_C = 256 K (-17°C)				
Source of uncertainty	Value (K)	Probability distribution	Divisor	Standard uncertainty (K)
Ice bath				
calibration (±)	0.5	Normal, 2σ	2	0.25
Thermometer				
calibration (±)	0.97	Normal, 2σ	2	0.48
resolution	0.1	Rectangular	$\sqrt{12}$	0.03
correction	0.03			
SE from 11 repeated readings	0.13	Normal, 1σ	1	0.13
Combined standard uncertainty, u_c				**0.50**
Coverage factor, $k_{coverage}$		2		
Expanded uncertainty, U				1.00
Mean from 11 repeated readings	256.09			
The measurement result and the uncertainty		256.11	±	1.00
Percentage uncertainty				-5.88%

F.2 Uncertainties of Ethanol in Simulated Exhaled Breath

In this section, rectangular probability distribution was considered as $\sqrt{3}$ because the value of ± range was already included in shown numbers.

Table F.15. Uncertainty analysis of producing 4 ppm ethanol vapor at 295 K

Ethanol solution preparation for producing 4 ppm ethanol vapor at 295 K					
Source of uncertainty		Value ± (µl)	Probability distribution	Divisor	Standard uncertainty (µl)
A (solute, use 0.1% (v/v) ethanol solution)					4135
4000 µl	calibration from pipette	40	Rectangular	$\sqrt{3}$	23.09
	uncertainty from 0.1% ethanol				28.22
	combined uncertainty				*36.47*
135 µl	calibration from pipette	1.6	Rectangular	$\sqrt{3}$	0.92
	uncertainty from 0.1% ethanol				0.95
	combined uncertainty				*1.33*
Combined standard uncertainty $u_c(A)$					*36.49*
B (solvent, use buffer)					75865
75 ml	calibration from graduate cylinder	600	Rectangular	$\sqrt{3}$	346.41
865 µl	calibration from pipette	8	Rectangular	$\sqrt{3}$	4.62
Combined standard uncertainty $u_c(B)$					*346.44*
Standard uncertainty of ethanol solution $u(P)$					**0.00049**
Coverage factor, $k_{coverage}$			2		
The measurement result and the uncertainty (in 0.1% ethanol based)			0.0517	±	0.0010
Percentage uncertainty					**1.88%**

Table F.16. Uncertainty analysis of producing 5 ppm ethanol vapor at 295 K

Ethanol solution preparation for producing 5 ppm ethanol vapor at 295 K					
	Source of uncertainty	Value ± (µl)	Probability distribution	Divisor	Standard uncertainty (µl)
A (solute, use 0.1% (v/v) ethanol solution)					5168
5000 µl	calibration from pipette	40	Rectangular	$\sqrt{3}$	23.09
	uncertainty from 0.1% ethanol				35.28
	combined uncertainty				*42.17*
168 µl	calibration from pipette	1.6	Rectangular	$\sqrt{3}$	0.92
	uncertainty from 0.1% ethanol				1.19
	combined uncertainty				*1.50*
Combined standard uncertainty $u_c(A)$					*42.19*
B (solvent, use buffer)					74832
74 ml	calibration from graduate cylinder	600	Rectangular	$\sqrt{3}$	346.41
800 µl	calibration from pipette	8	Rectangular	$\sqrt{3}$	4.62
32 µl	calibration from pipette	0.5	Rectangular	$\sqrt{3}$	0.29
Combined standard uncertainty $u_c(B)$					*346.44*
Standard uncertainty of ethanol solution $u(P)$					**0.00057**
Coverage factor, $k_{coverage}$			2		
The measurement result and the uncertainty (in 0.1% ethanol based)			0.0646	±	0.0011
Percentage uncertainty					**1.76%**

Table F.17. Uncertainty analysis of producing 7.5 ppm ethanol vapor at 295 K

Ethanol solution preparation for producing 7.5 ppm ethanol vapor at 295 K				
Source of uncertainty	Value ± (µl)	Probability distribution	Divisor	Standard uncertainty (µl)
A (solute, use 0.1% (v/v) ethanol solution)				7753
5000 µl calibration from pipette	40	Rectangular	$\sqrt{3}$	23.09
uncertainty from 0.1% ethanol				35.28
combined uncertainty				*42.17*
2000 µl calibration from pipette	40	Rectangular	$\sqrt{3}$	23.09
uncertainty from 0.1% ethanol				14.11
combined uncertainty				*27.06*
710 µl calibration from pipette	8	Rectangular	$\sqrt{3}$	4.62
uncertainty from 0.1% ethanol				5.01
combined uncertainty				*6.81*
43 µl calibration from pipette	0.5	Rectangular	$\sqrt{3}$	0.29
uncertainty from 0.1% ethanol				0.30
combined uncertainty				*0.42*
Combined standard uncertainty $u_c(A)$				*50.57*
B (solvent, use buffer)				72247
72 ml calibration from graduate cylinder	600	Rectangular	$\sqrt{3}$	346.41
200 µl calibration from pipette	8	Rectangular	$\sqrt{3}$	4.62
47 µl calibration from pipette	0.5	Rectangular	$\sqrt{3}$	0.29
Combined standard uncertainty $u_c(B)$				*346.44*
Standard uncertainty of ethanol solution $u(P)$				**0.00071**
Coverage factor, $k_{coverage}$		2		
The measurement result and the uncertainty (in 0.1% ethanol based)		0.0969	±	0.0014
Percentage uncertainty				**1.46%**

Table F.18. Uncertainty analysis of producing 4 ppm ethanol vapor at 307 K

Ethanol solution preparation for producing 4 ppm ethanol vapor at 307 K				
Source of uncertainty	Value ± (µl)	Probability distribution	Divisor	Standard uncertainty (µl)
A (solute, use 0.1% (v/v) ethanol solution)				1814
1000 µl calibration from pipette	8	Rectangular	$\sqrt{3}$	4.62
uncertainty from 0.1% ethanol				7.06
combined uncertainty				*8.43*
700 µl calibration from pipette	8	Rectangular	$\sqrt{3}$	4.62
uncertainty from 0.1% ethanol				4.94
combined uncertainty				*6.76*
114 µl calibration from pipette	1.6	Rectangular	$\sqrt{3}$	0.92
uncertainty from 0.1% ethanol				0.80
combined uncertainty				*1.22*
Combined standard uncertainty $u_c(A)$				*10.88*
B (solvent, use buffer)				78186
78 ml calibration from graduate cylinder	600	Rectangular	$\sqrt{3}$	346.41
100 µl calibration from pipette	1.6	Rectangular	$\sqrt{3}$	0.92
86 µl calibration from pipette	1.6	Rectangular	$\sqrt{3}$	0.92
Combined standard uncertainty $u_c(B)$				*346.41*
Standard uncertainty of ethanol solution *u*(*P*)				**0.00017**
Coverage factor, $k_{coverage}$		2		
The measurement result and the uncertainty (in 0.1% ethanol based)		0.0227	±	0.0003
Percentage uncertainty				**1.46%**

Table F.19. Uncertainty analysis of producing 5 ppm ethanol vapor at 307 K

Ethanol solution preparation for producing 5 ppm ethanol vapor at 307 K					
	Source of uncertainty	Value ± (µl)	Probability distribution	Divisor	Standard uncertainty (µl)
A (solute, use 0.1% (v/v) ethanol solution)					2267
1000 µl	calibration from pipette	8	Rectangular	$\sqrt{3}$	4.62
	uncertainty from 0.1% ethanol				7.06
	combined uncertainty				*8.43*
1000 µl	calibration from pipette	8	Rectangular	$\sqrt{3}$	4.62
	uncertainty from 0.1% ethanol				7.06
	combined uncertainty				*8.43*
200 µl	calibration from pipette	1.6	Rectangular	$\sqrt{3}$	0.92
	uncertainty from 0.1% ethanol				1.41
	combined uncertainty				*1.69*
67 µl	calibration from pipette	1.6	Rectangular	$\sqrt{3}$	0.92
	uncertainty from 0.1% ethanol				0.47
	combined uncertainty				*1.04*
Combined standard uncertainty $u_c(A)$					*12.09*
B (solvent, use buffer)					77733
77 ml	calibration from graduate cylinder	600	Rectangular	$\sqrt{3}$	346.41
700 µl	calibration from pipette	8	Rectangular	$\sqrt{3}$	4.62
33 µl	calibration from pipette	0.5	Rectangular	$\sqrt{3}$	0.29
Combined standard uncertainty $u_c(B)$					*346.44*
Standard uncertainty of ethanol solution $u(P)$					**0.00019**
Coverage factor, $k_{coverage}$			2		
The measurement result and the uncertainty (in 0.1% ethanol based)			0.0283	±	0.0004
Percentage uncertainty					**1.35%**

Table F.20. Uncertainty analysis of producing 7.5 ppm ethanol vapor at 307 K

Ethanol solution preparation for producing 7.5 ppm ethanol vapor at 307 K					
	Source of uncertainty	Value ± (μl)	Probability distribution	Divisor	Standard uncertainty (μl)
A (solute, use 0.1% (v/v) ethanol solution)					3401
3000 μl	calibration from pipette	40	Rectangular	$\sqrt{3}$	23.09
	uncertainty from 0.1% ethanol				21.17
	combined uncertainty				*31.33*
360 μl	calibration from pipette	8	Rectangular	$\sqrt{3}$	4.62
	uncertainty from 0.1% ethanol				2.54
	combined uncertainty				*5.27*
41 μl	calibration from pipette	0.5	Rectangular	$\sqrt{3}$	0.29
	uncertainty from 0.1% ethanol				0.29
	combined uncertainty				*0.41*
Combined standard uncertainty $u_c(A)$					*31.77*
B (solvent, use buffer)					76599
77 ml	calibration from graduate cylinder	600	Rectangular	$\sqrt{3}$	346.41
700 μl	calibration from pipette	8	Rectangular	$\sqrt{3}$	4.62
33 μl	calibration from pipette	0.5	Rectangular	$\sqrt{3}$	0.29
Combined standard uncertainty $u_c(B)$					*346.44*
Standard uncertainty of ethanol solution *u*(*P*)					**0.00042**
Coverage factor, $k_{coverage}$			2		
The measurement result and the uncertainty (in 0.1% ethanol based)			0.0425	±	0.0008
Percentage uncertainty					**1.99%**

Table F.21. Uncertainty analysis of producing 4 ppm ethanol vapor at 310 K

Ethanol solution preparation for producing 4 ppm ethanol vapor at 310 K				
Source of uncertainty	Value ± (μl)	Probability distribution	Divisor	Standard uncertainty (μl)
A (solute, use 0.1% (v/v) ethanol solution)				1478
1000 μl calibration from pipette	8	Rectangular	$\sqrt{3}$	4.62
uncertainty from 0.1% ethanol				7.06
combined uncertainty				*8.43*
450 μl calibration from pipette	8	Rectangular	$\sqrt{3}$	4.62
uncertainty from 0.1% ethanol				3.18
combined uncertainty				*5.60*
28 μl calibration from pipette	0.5	Rectangular	$\sqrt{3}$	0.29
uncertainty from 0.1% ethanol				0.20
combined uncertainty				*0.35*
Combined standard uncertainty $u_c(A)$				*10.13*
B (solvent, use buffer)				78522
78 ml calibration from graduate cylinder	600	Rectangular	$\sqrt{3}$	346.41
500 μl calibration from pipette	8	Rectangular	$\sqrt{3}$	4.62
22 μl calibration from pipette	0.5	Rectangular	$\sqrt{3}$	0.29
Combined standard uncertainty $u_c(B)$				*346.44*
Standard uncertainty of ethanol solution $u(P)$				**0.00015**
Coverage factor, $k_{coverage}$		2		
The measurement result and the uncertainty (in 0.1% ethanol based)		0.0185	±	0.0003
Percentage uncertainty				**1.60%**

Table F.22. Uncertainty analysis of producing 5 ppm ethanol vapor at 310 K

Ethanol solution preparation for producing 5 ppm ethanol vapor at 310 K				
Source of uncertainty	Value ± (µl)	Probability distribution	Divisor	Standard uncertainty (µl)
A (solute, use 0.1% (v/v) ethanol solution)				1874
1000 µl calibration from pipette	8	Rectangular	$\sqrt{3}$	4.62
uncertainty from 0.1% ethanol				7.06
combined uncertainty				*8.43*
800 µl calibration from pipette	8	Rectangular	$\sqrt{3}$	4.62
uncertainty from 0.1% ethanol				5.64
combined uncertainty				*7.29*
74 µl calibration from pipette	1.6	Rectangular	$\sqrt{3}$	0.92
uncertainty from 0.1% ethanol				0.52
combined uncertainty				*1.06*
Combined standard uncertainty $u_c(A)$				*11.20*
B (solvent, use buffer)				78126
78 ml calibration from graduate cylinder	600	Rectangular	$\sqrt{3}$	346.41
126 µl calibration from pipette	8	Rectangular	$\sqrt{3}$	4.62
Combined standard uncertainty $u_c(B)$				*346.44*
Standard uncertainty of ethanol solution $u(P)$				**0.00017**
Coverage factor, $k_{coverage}$		2		
The measurement result and the uncertainty (in 0.1% ethanol based)		0.0234	±	0.0003
Percentage uncertainty				**1.45%**

Table F.23. Uncertainty analysis of producing 7.5 ppm ethanol vapor at 310 K

Ethanol solution preparation for producing 7.5 ppm ethanol vapor at 310 K				
Source of uncertainty	Value ± (µl)	Probability distribution	Divisor	Standard uncertainty (µl)
A (solute, use 0.1% (v/v) ethanol solution)				2771
1000 µl calibration from pipette	8	Rectangular	$\sqrt{3}$	4.62
uncertainty from 0.1% ethanol				7.06
combined uncertainty				*8.43*
1000 µl calibration from pipette	8	Rectangular	$\sqrt{3}$	4.62
uncertainty from 0.1% ethanol				7.06
combined uncertainty				*8.43*
600 µl calibration from pipette	8	Rectangular	$\sqrt{3}$	4.62
uncertainty from 0.1% ethano				4.23
combined uncertainty				*6.27*
171 µl calibration from pipette	1.6	Rectangular	$\sqrt{3}$	0.92
uncertainty from 0.1% ethanol				1.21
combined uncertainty				*1.52*
Combined standard uncertainty $u_c(A)$				*13.56*
B (solvent, use buffer)				77229
77 ml calibration from graduate cylinder	600	Rectangular	$\sqrt{3}$	346.41
200 µl calibration from pipette	1.6	Rectangular	$\sqrt{3}$	0.92
29 µl calibration from pipette	0.5	Rectangular	$\sqrt{3}$	0.29
Combined standard uncertainty $u_c(B)$				*346.41*
Standard uncertainty of ethanol solution *u*(*P*)				**0.00022**
Coverage factor, $k_{coverage}$		2		
The measurement result and the uncertainty (in 0.1% ethanol based)		0.0346	±	0.0004
Percentage uncertainty				**1.28%**

Table F.24. Uncertainty analysis of producing 4 ppm ethanol vapor at 315 K

Ethanol solution preparation for producing 4 ppm ethanol vapor at 315 K					
Source of uncertainty		Value ± (μl)	Probability distribution	Divisor	Standard uncertainty (μl)
A (solute, use 0.1% (v/v) ethanol solution)					1059
1000 μl	calibration from pipette	8	Rectangular	$\sqrt{3}$	4.62
	uncertainty from 0.1% ethanol				7.06
	combined uncertainty				*8.43*
59 μl	calibration from pipette	1.6	Rectangular	$\sqrt{3}$	0.92
	uncertainty from 0.1% ethanol				0.42
	combined uncertainty				*1.01*
Combined standard uncertainty $u_c(A)$					*8.49*
B (solvent, use buffer)					78941
78 ml	calibration from graduate cylinder	600	Rectangular	$\sqrt{3}$	346.41
900 μl	calibration from pipette	8	Rectangular	$\sqrt{3}$	4.62
41 μl	calibration from pipette	0.5	Rectangular	$\sqrt{3}$	0.29
Combined standard uncertainty $u_c(B)$					*346.44*
Standard uncertainty of ethanol solution $u(P)$					**0.00012**
Coverage factor, $k_{coverage}$			2		
The measurement result and the uncertainty (in 0.1% ethanol based)			0.0132	±	0.0002
Percentage uncertainty					**1.80%**

Table F.25. Uncertainty analysis of producing 5 ppm ethanol vapor at 315 K

Ethanol solution preparation for producing 5 ppm ethanol vapor at 315 K					
	Source of uncertainty	Value ± (μl)	Probability distribution	Divisor	Standard uncertainty (μl)
A (solute, use 0.1% (v/v) ethanol solution)					1324
1000 μl	calibration from pipette	8	Rectangular	$\sqrt{3}$	4.62
	uncertainty from 0.1% ethanol				7.06
	combined uncertainty				*8.43*
300 μl	calibration from pipette	8	Rectangular	$\sqrt{3}$	4.62
	uncertainty from 0.1% ethanol				2.12
	combined uncertainty				*5.08*
24 μl	calibration from pipette	0.5	Rectangular	$\sqrt{3}$	0.29
	uncertainty from 0.1% ethanol				0.17
	combined uncertainty				*0.33*
Combined standard uncertainty $u_c(A)$					*9.85*
B (solvent, use buffer)					78676
78 ml	calibration from graduate cylinder	600	Rectangular	$\sqrt{3}$	346.41
600 μl	calibration from pipette	8	Rectangular	$\sqrt{3}$	4.62
76 μl	calibration from pipette	1.6	Rectangular	$\sqrt{3}$	0.92
Combined standard uncertainty $u_c(B)$					*346.44*
Standard uncertainty of ethanol solution $u(P)$					**0.00014**
Coverage factor, $k_{coverage}$			2		
The measurement result and the uncertainty (in 0.1% ethanol based)			0.0166	±	0.0003
Percentage uncertainty					**1.70%**

Table F.26. Uncertainty analysis of producing 7.5 ppm ethanol vapor at 315 K

Ethanol solution preparation for producing 7.5 ppm ethanol vapor at 315 K					
	Source of uncertainty	Value ± (μl)	Probability distribution	Divisor	Standard uncertainty (μl)
A (solute, use 0.1% (v/v) ethanol solution)					1986
1000 μl	calibration from pipette	8	Rectangular	$\sqrt{3}$	4.62
	uncertainty from 0.1% ethanol				7.06
	combined uncertainty				*8.43*
900 μl	calibration from pipette	8	Rectangular	$\sqrt{3}$	4.62
	uncertainty from 0.1% ethanol				6.35
	combined uncertainty				*7.85*
86 μl	calibration from pipette	0.5	Rectangular	$\sqrt{3}$	0.29
	uncertainty from 0.1% ethanol				0.61
	combined uncertainty				*0.67*
Combined standard uncertainty $u_c(A)$					*11.54*
B (solvent, use buffer)					78014
78 ml	calibration from graduate cylinder	600	Rectangular	$\sqrt{3}$	346.41
14 μl	calibration from pipette	0.5	Rectangular	$\sqrt{3}$	0.29
Combined standard uncertainty $u_c(B)$					*346.41*
Standard uncertainty of ethanol solution $u(P)$					**0.00018**
Coverage factor, $k_{coverage}$			2		
The measurement result and the uncertainty (in 0.1% ethanol based)			0.0248	±	0.0004
Percentage uncertainty					**1.43%**

F.3 Uncertainties of H_2O_2 in Simulated Exhaled Breath

"Value" showed in Table F.27.– Table F.38 present uncertainty of calibration from pipette.

Table F.27. Uncertainty analysis of producing 250 ppb H_2O_2 vapor at 295 K

H_2O_2 solution preparation for producing 250 ppb H_2O_2 vapor at 295 K				
Source of uncertainty	Value ± (µl)	Probability distribution	Divisor	Standard uncertainty (µl)
A (solute, use 30% (w/w) H_2O_2 solution)				135
135 µl	1.6	Rectangular	1.732	0.92
Combined standard uncertainty $u_c(A)$				*0.92*
B (solvent, use buffer)				79865
79 ml	600	Rectangular	1.732	346.41
865 µl	8	Rectangular	1.732	4.62
Combined standard uncertainty $u_c(B)$				*346.44*
Standard uncertainty of ethanol solution $u(P)$				**1.36E-05**
Coverage factor, $k_{coverage}$		2		
The measurement result and the uncertainty (µl of 30% (w/w) H_2O_2 solution)		0.0017	±	2.73E-05
The measurement result and the uncertainty (concentration, %)		0.00051	±	8.19E-06
Percentage uncertainty				**1.62%**

Table F.28. Uncertainty analysis of producing 500 ppb H_2O_2 vapor at 295 K

H_2O_2 solution preparation for producing 500 ppb H_2O_2 vapor at 295 K				
Source of uncertainty	Value ± (µl)	Probability distribution	Divisor	Standard uncertainty (µl)
A (solute, use 30% (w/w) H_2O_2 solution)				271
200 µl	8	Rectangular	1.732	4.62
71 µl	1.6	Rectangular	1.732	0.92
Combined standard uncertainty $u_c(A)$				*4.71*
B (solvent, use buffer)				79729
79 ml	600	Rectangular	1.732	346.41
700 µl	8	Rectangular	1.732	4.62
29 µl	0.5	Rectangular	1.732	0.29
Combined standard uncertainty $u_c(B)$				*346.44*
Standard uncertainty of ethanol solution $u(P)$				**6.05E-05**
Coverage factor, $k_{coverage}$		2		
The measurement result and the uncertainty (µl of 30% (w/w) H_2O_2 solution)		0.0034	±	1.21E-04
The measurement result and the uncertainty (concentration, %)		0.00102	±	3.63E-05
Percentage uncertainty				**3.57%**

Table F.29. Uncertainty analysis of producing 1000 ppb H_2O_2 vapor at 295 K

H_2O_2 solution preparation for producing 1000 ppb H_2O_2 vapor at 295 K				
Source of uncertainty	Value ± (µl)	Probability distribution	Divisor	Standard uncertainty (µl)
A (solute, use 30% (w/w) H_2O_2 solution)				542
500 µl	8	Rectangular	1.732	4.62
42 µl	0.5	Rectangular	1.732	0.29
Combined standard uncertainty $u_c(A)$				*4.63*
B (solvent, use buffer)				79458
79 ml	600	Rectangular	1.732	346.41
410 µl	8	Rectangular	1.732	4.62
48 µl	0.5	Rectangular	1.732	0.29
Combined standard uncertainty $u_c(B)$				*346.44*
Standard uncertainty of ethanol solution $u(P)$				**6.45E-05**
Coverage factor, $k_{coverage}$		2		
The measurement result and the uncertainty (µl of 30% (w/w) H_2O_2 solution)		0.0068	±	1.29E-04
The measurement result and the uncertainty (concentration, %)		0.00203	±	3.87E-05
Percentage uncertainty				**1.90%**

Table F.30. Uncertainty analysis of producing 250 ppb H_2O_2 vapor at 307 K

H_2O_2 solution preparation for producing 250 ppb H_2O_2 vapor at 307 K					
Source of uncertainty		Value ± (µl)	Probability distribution	Divisor	Standard uncertainty (µl)
A (solute, use 30% (w/w) H_2O_2 solution)					60
60	µl	1.6	Rectangular	1.732	0.92
	µl		Rectangular	1.732	0.00
Combined standard uncertainty $u_c(A)$					*0.92*
B (solvent, use buffer)					79940
79	ml	600	Rectangular	1.732	346.41
940	µl	8	Rectangular	1.732	4.62
	µl		Rectangular	1.732	0.00
Combined standard uncertainty $u_c(B)$					*346.44*
Standard uncertainty of ethanol solution $u(P)$					**1.20E-05**
Coverage factor, $k_{coverage}$			2		
The measurement result and the uncertainty (µl of 30% (w/w) H_2O_2 solution)			0.0008	±	2.40E-05
The measurement result and the uncertainty (concentration, %)			0.00023	±	7.19E-06
Percentage uncertainty					**3.20%**

Table F.31. Uncertainty analysis of producing 500 ppb H_2O_2 vapor at 307 K

H_2O_2 solution preparation for producing 500 ppb H_2O_2 vapor at 307 K					
Source of uncertainty		Value ± (µl)	Probability distribution	Divisor	Standard uncertainty (µl)
A (solute, use 30% (w/w) H_2O_2 solution)					120
120	µl	1.6	Rectangular	1.732	0.92
	µl		Rectangular	1.732	0.00
Combined standard uncertainty $u_c(A)$					*0.92*
B (solvent, use buffer)					79880
79	ml	600	Rectangular	1.732	346.41
880	µl	8	Rectangular	1.732	4.62
	µl		Rectangular	1.732	0.00
Combined standard uncertainty $u_c(B)$					*346.44*
Standard uncertainty of ethanol solution $u(P)$					**1.32E-05**
Coverage factor, $k_{coverage}$			2		
The measurement result and the uncertainty (µl of 30% (w/w) H_2O_2 solution)			0.0015	±	2.65E-05
The measurement result and the uncertainty (concentration, %)			0.00045	±	7.94E-06
Percentage uncertainty					**1.76%**

Table F.32. Uncertainty analysis of producing 1000 ppb H_2O_2 vapor at 307 K

H_2O_2 solution preparation for producing 1000 ppb H_2O_2 vapor at 307 K				
Source of uncertainty	Value ± (µl)	Probability distribution	Divisor	Standard uncertainty (µl)
A (solute, use 30% (w/w) H_2O_2 solution)				239
200 µl	1.6	Rectangular	1.732	0.92
39 µl	0.5	Rectangular	1.732	0.29
Combined standard uncertainty $u_c(A)$				*0.97*
B (solvent, use buffer)				79761
79 ml	600	Rectangular	1.732	346.41
720 µl	8	Rectangular	1.732	4.62
41 µl	0.5	Rectangular	1.732	0.29
Combined standard uncertainty $u_c(B)$				*346.44*
Standard uncertainty of ethanol solution $u(P)$				**1.77E-05**
Coverage factor, $k_{coverage}$		2		
The measurement result and the uncertainty (µl of 30% (w/w) H_2O_2 solution)		0.0030	±	3.54E-05
The measurement result and the uncertainty (concentration, %)		0.00090	±	1.06E-05
Percentage uncertainty				**1.18%**

Table F.33. Uncertainty analysis of producing 250 ppb H_2O_2 vapor at 310 K

H_2O_2 solution preparation for producing 250 ppb H_2O_2 vapor at 310 K					
Source of uncertainty		Value ± (µl)	Probability distribution	Divisor	Standard uncertainty (µl)
A (solute, use 30% (w/w) H_2O_2 solution)					48
48	µl	0.5	Rectangular	1.732	0.29
	µl		Rectangular	1.732	0.00
Combined standard uncertainty $u_c(A)$					*0.29*
B (solvent, use buffer)					79952
79	ml	600	Rectangular	1.732	346.41
910	µl	8	Rectangular	1.732	4.62
42	µl	0.5	Rectangular	1.732	0.29
Combined standard uncertainty $u_c(B)$					*346.44*
Standard uncertainty of ethanol solution $u(P)$					**4.44E-06**
Coverage factor, $k_{coverage}$			2		
The measurement result and the uncertainty (µl of 30% (w/w) H_2O_2 solution)			0.0006	±	8.89E-06
The measurement result and the uncertainty (concentration, %)			0.00018	±	2.67E-06
Percentage uncertainty					**1.48%**

Table F.34. Uncertainty analysis of producing 500 ppb H_2O_2 vapor at 310 K

H_2O_2 solution preparation for producing 500 ppb H_2O_2 vapor at 310 K					
Source of uncertainty		Value ± (µl)	Probability distribution	Divisor	Standard uncertainty (µl)
A (solute, use 30% (w/w) H_2O_2 solution)					96
96	µl	1.6	Rectangular	1.732	0.92
	µl		Rectangular	1.732	0.00
Combined standard uncertainty $u_c(A)$					*0.92*
B (solvent, use buffer)					79904
79	ml	600	Rectangular	1.732	346.41
860	µl	8	Rectangular	1.732	4.62
44	µl	0.5	Rectangular	1.732	0.29
Combined standard uncertainty $u_c(B)$					*346.44*
Standard uncertainty of ethanol solution $u(P)$					**1.26E-05**
Coverage factor, $k_{coverage}$			2		
The measurement result and the uncertainty (µl of 30% (w/w) H_2O_2 solution)			0.0012	±	2.53E-05
The measurement result and the uncertainty (concentration, %)			0.00036	±	7.59E-06
Percentage uncertainty					**2.11%**

Table F.35. Uncertainty analysis of producing 1000 ppb H_2O_2 vapor at 310 K

H_2O_2 solution preparation for producing 1000 ppb H_2O_2 vapor at 310 K					
Source of uncertainty		Value ± (µl)	Probability distribution	Divisor	Standard uncertainty (µl)
A (solute, use 30% (w/w) H_2O_2 solution)					192
192	µl	1.6	Rectangular	1.732	0.92
	µl		Rectangular	1.732	0.00
Combined standard uncertainty $u_c(A)$					*0.92*
B (solvent, use buffer)					79808
79	ml	600	Rectangular	1.732	346.41
760	µl	8	Rectangular	1.732	4.62
48	µl	0.5	Rectangular	1.732	0.29
Combined standard uncertainty $u_c(B)$					*346.44*
Standard uncertainty of ethanol solution $u(P)$					**1.55E-05**
Coverage factor, $k_{coverage}$			2		
The measurement result and the uncertainty (µl of 30% (w/w) H_2O_2 solution)			0.0024	±	3.10E-05
The measurement result and the uncertainty (concentration, %)			0.00072	±	9.31E-06
Percentage uncertainty					**1.29%**

Table F.36. Uncertainty analysis of producing 250 ppb H_2O_2 vapor at 315 K

H_2O_2 solution preparation for producing 250 ppb H_2O_2 vapor at 315 K					
Source of uncertainty		Value ± (µl)	Probability distribution	Divisor	Standard uncertainty (µl)
A (solute, use 30% (w/w) H_2O_2 solution)					60
34	µl	8	Rectangular	1.732	4.62
	µl		Rectangular	1.732	0.00
Combined standard uncertainty $u_c(A)$					*4.62*
B (solvent, use buffer)					79940
79	ml	600	Rectangular	1.732	346.41
920	µl	8	Rectangular	1.732	4.62
46	µl	0.5	Rectangular	1.732	0.29
Combined standard uncertainty $u_c(B)$					*346.44*
Standard uncertainty of ethanol solution $u(P)$					**5.78E-05**
Coverage factor, $k_{coverage}$			2		
The measurement result and the uncertainty (µl of 30% (w/w) H_2O_2 solution)			0.0008	±	1.16E-04
The measurement result and the uncertainty (concentration, %)			0.00023	±	3.47E-05
Percentage uncertainty					**15.41%**

Table F.37. Uncertainty analysis of producing 500 ppb H_2O_2 vapor at 315 K

H_2O_2 solution preparation for producing 500 ppb H_2O_2 vapor at 315 K					
Source of uncertainty		Value ± (µl)	Probability distribution	Divisor	Standard uncertainty (µl)
A (solute, use 30% (w/w) H_2O_2 solution)					68
68	µl	8	Rectangular	1.732	4.62
	µl		Rectangular	1.732	0.00
Combined standard uncertainty $u_c(A)$					*4.62*
B (solvent, use buffer)					79932
79	ml	600	Rectangular	1.732	346.41
900	µl	8	Rectangular	1.732	4.62
32	µl	0.5	Rectangular	1.732	0.29
Combined standard uncertainty $u_c(B)$					*346.44*
Standard uncertainty of ethanol solution $u(P)$					**5.78E-05**
Coverage factor, $k_{coverage}$			2		
The measurement result and the uncertainty (µl of 30% (w/w) H_2O_2 solution)			0.0009	±	1.16E-04
The measurement result and the uncertainty (concentration, %)			0.00026	±	3.47E-05
Percentage uncertainty					**13.60%**

Table F.38. Uncertainty analysis of producing 1000 ppb H_2O_2 vapor at 315 K

H_2O_2 solution preparation for producing 1000 ppb H_2O_2 vapor at 315 K					
Source of uncertainty		Value ± (µl)	Probability distribution	Divisor	Standard uncertainty (µl)
A (solute, use 30% (w/w) H_2O_2 solution)					136
136	µl	8	Rectangular	1.732	4.62
	µl		Rectangular	1.732	0.00
Combined standard uncertainty $u_c(A)$					*4.62*
B (solvent, use buffer)					79864
79	ml	600	Rectangular	1.732	346.41
820	µl	8	Rectangular	1.732	4.62
44	µl	0.5	Rectangular	1.732	0.29
Combined standard uncertainty $u_c(B)$					*346.44*
Standard uncertainty of ethanol solution $u(P)$					**5.81E-05**
Coverage factor, $k_{coverage}$			2		
The measurement result and the uncertainty (µl of 30% (w/w) H_2O_2 solution)			0.0017	±	1.16E-04
The measurement result and the uncertainty (concentration, %)			0.00051	±	3.49E-05
Percentage uncertainty					**6.84%**

APPENDIX G: TEMPERATURE DROP PROFILE OVER TIME IN VAPOR SENSING

Temperatures in vapor sensing chamber were measured and decreased with increasing sensing time. Therefore the temperature difference (ΔT) between vapor temperature from BOS and the temperature of the vapor sensing chamber, which can be calculated by Equation G.1, also increased:

$$\Delta T = T_b - \text{temperature in sensing chamber} \tag{G.1}$$

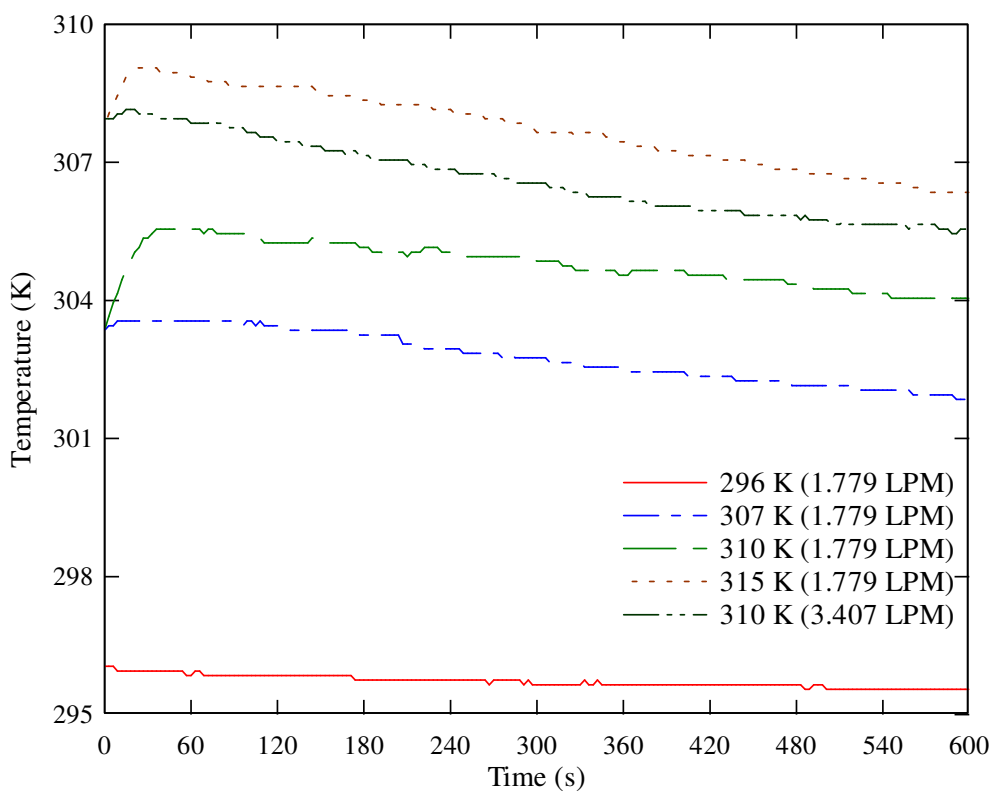

Figure G.1. Temperatures in vapor sensing chamber decreased over time.

APPENDIX H: SCREEN-PRINTED CARBON ELECTRODE COMPARISON

Immobilized AOX assay on each Gwent SPCE contained 1.2 µl AOX (200 units/ml), 0.6 µl BSA (40 mg/ml), and 0.2 µl Glutaraldehyde 1.0% (v/v). Immobilized AOX assay on each DropSens SPCE contained 1.2 µl AOX (400 units/ml), 0.6 µl BSA (80 mg/ml), and 0.2 µl glutaraldehyde 1.0% (v/v). The mixture was dropcoated on a working electrode of CoPC SPCE for 2-2.5 hrs. Current responses for 0, 0.0015, 0.0025, 0.005% (w/w) ethanol solution were recorded.

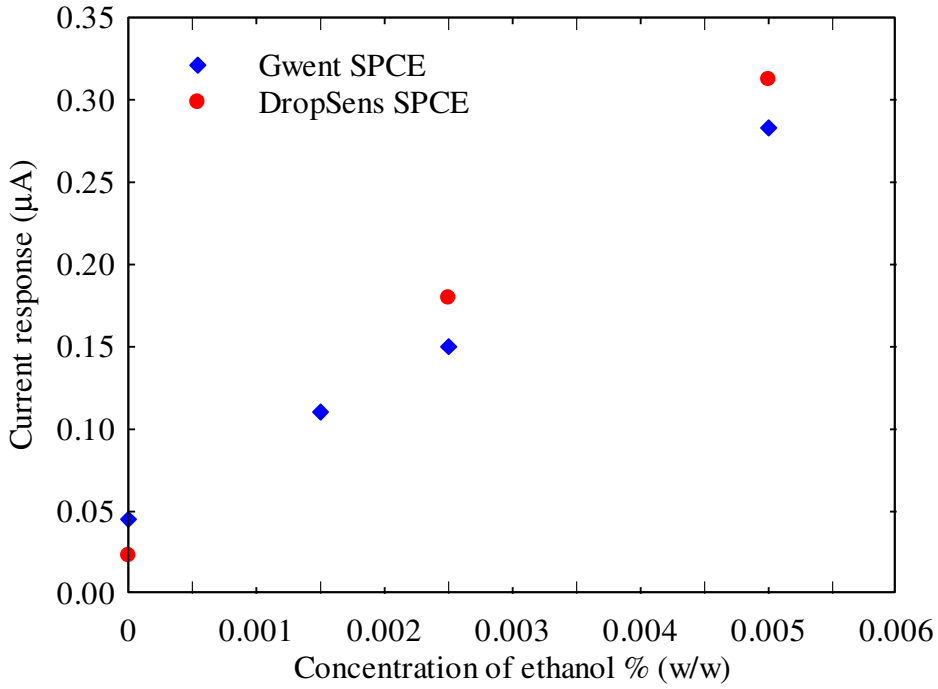

Figure H.1. Current responses from AOX-based biosensors using Gwent SPCEs and DropSens SPCEs were comparable.

APPENDIX I: MONITORING OTHER BIOMARKERS IN BREATH

I.1 Ammonia

Ammonia is a big concern in environmental control and the regulated threshold values of it in work places are 25 ppmv (time-weighted average, TWA), 35ppmv (short-term exposure limit, STEL). The typical ammonia concentration in a livestock facility is 10-25 ppmv (Kavolelis, 2003). Ammonia is not only an odorous compound, but it also causes secondary inorganic aerosols including ammonium nitrate and ammonium sulfate. In breath analysis, ammonia, a metabolite of protein and amino acids degradation is associated with liver or renal dysfunction (Smith et al., 2008).

Simulated exhaled breath containing ammonia was produced using the breath output simulator. An ammonia biosensor was designed by using Meldola's Blue (MB) mediated SPCE and immobilized the enzyme mixture of 1 μl L-glutamate dehydrogenase (GLDH, 1 unit/μl), 8 μL β-nicotinamide adenine dinucleotide (NADH, 2.3 mM), and 8 μL α-ketoglutaric acid (KGA, 34 mM) (Figure I.1). Each ammonia sensor was dropcoated with 40 μl ammonia sample after 3 hr drying time. Ammonia ion standard solution with 0.1M was used for preparing stock solution at 58.8–588 μM (to produce equivalent vapor concentration from 20-240 ppm). A cathodic (reduced) peak around +600 mV vs. Ag/AgCl, resulted in a linear response to increasing concentrations of ammonia in ampeometric measurement (Figure I.2).

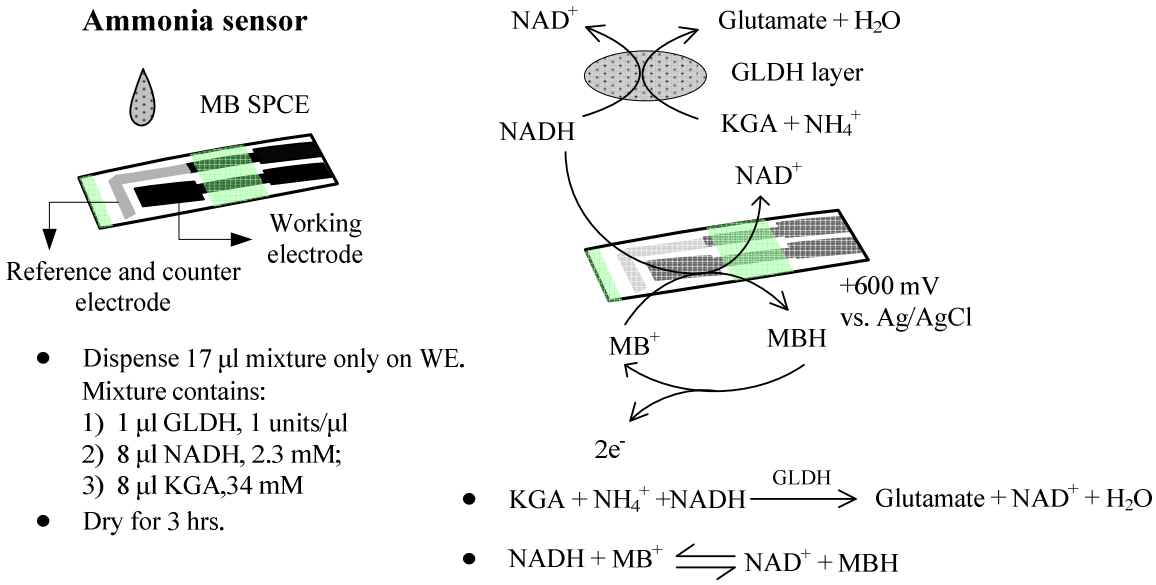

Figure I.1. The measurement of ammonia was based on redox reaction catalyzed by GLDH enzyme.

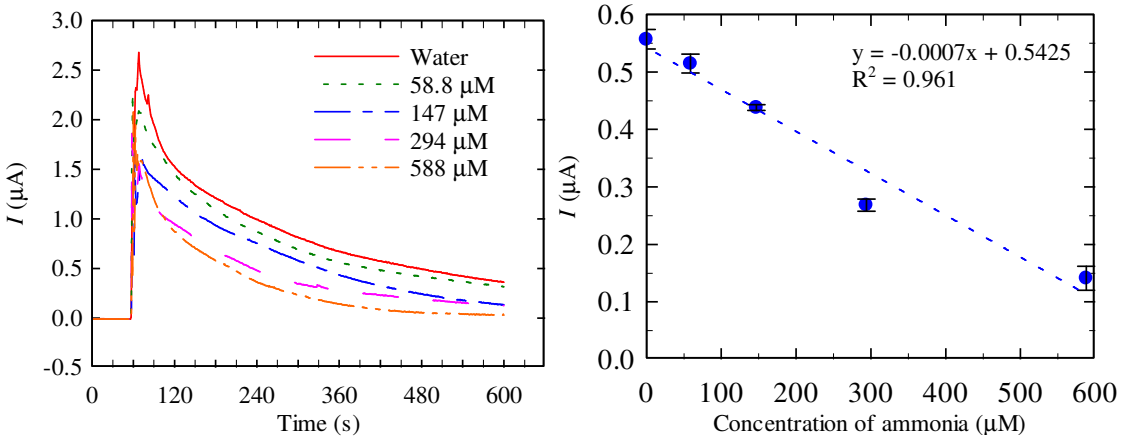

Figure I.2. Amperometric tests showed a decreasing linear trend with increasing ammonia concentration in buffer. Each test contained three replications. Error bars and dashed lines represent ± one S.E and the linear regression results, respectively.

Current responses measure from vapor and condensate sampled from different T_b were conducted. Higher sampling T_b had a smaller current response in vapor samples, but no clear trends were observed between C_V and I_V at 296.5 K or 311.5 K (Figure I.3a). In condensate samples, data taken from T_b at 296.5 K and 315 K displayed decreasing linear

trends, but barely presented the linear trends in data from T_b at 304.5 K and 311.5 K (Figure I.3b). Although part of the data showed linear trend and I_C increased at $C_V = 0$ ppm with increasing temperature, no correlation was found between current and the changing T_b or C_V.

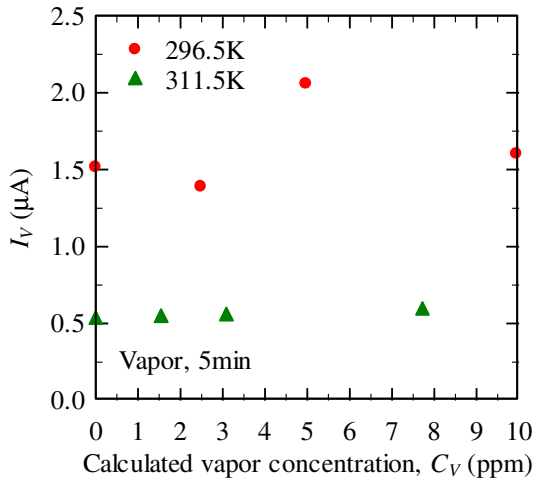

(a)

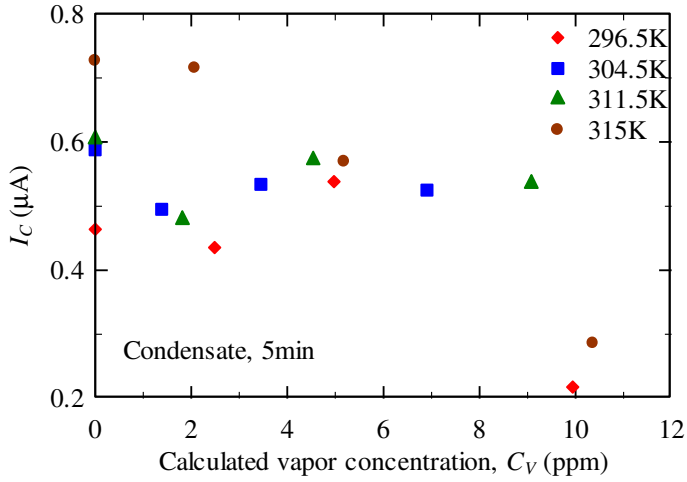

(b)

Figure I.3. Amperometric tests were performed in (a) vapor and (b) condensate samples to conduct sampling temperature (T_b) efffect. No clear trend was found. One replication sample has been measured.

In a validation test of ammonia sensor, dry ammonia at 20-240 ppm was passed through water and the water was later tested with the ammonia biosensor. A linear trend (R^2=0.9049) was found and had 15.91% average error from predictive curve (Figure I.4). Therefore the ammonia sensor was found effective with this sampling procedure.

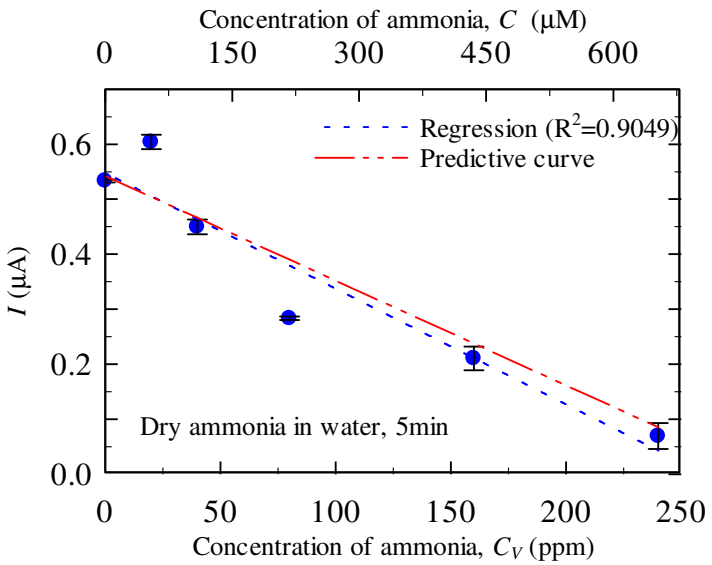

Figure I.4. Ammonia sensor was validated by liquid samples taken from dry ammonia dissolving in water and had 15.91% average error from predictive curve. Error bars and dashed lines represent ± one S.E and linear regression results, respectively.

Another possible cause for inability to see the relation between current response and C_V is that the simulated exhaled breath does not contain the ammonia concentration predicted by Henry's law. Henry's law can be applied when the gas sample fulfills the following three conditions: 1) ideal gas; 2) only dissolves in liquid solvent, not react with it; 3) no dissociation or association with the liquid solvent. In the third required condition, Henry's law may be invalid with ammonia dissolving in water, but it was valid when ammonia dissolving in benzene, because ammonia had a high solubility in water but barely dissolving in benzene.

Moreover, Roper (2000) and Sawyer (2008) mentioned that pH was a critical factor in the conversion between ammonium ion and ammonia.

$$NH_4^+ + OH^- \leftrightarrow NH_3 + H_2O \tag{I.1}$$

When pH is less than 6.0, the ammonium ion is very stable and ammonia molecules are hardly released; at pH 9.0 to 9.5, the conversion between ammonium ion and ammonia molecule is close to 1:1. The pH effect was also conducted and confirmed in measurement of condensate samples (Figure I.5). For simulating mammalian condition, pH 7.4 was set in our experiments. Under this setting, ammonium ion was also limited converted to be ammonia from our breath output simulator.

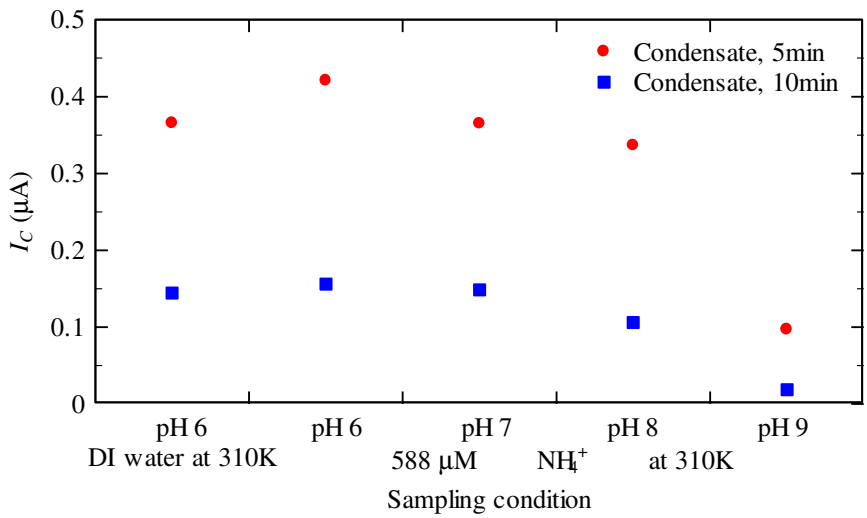

Figure I.5. Higher pH favored ammonium ion to be converted to ammonia and a decreasing current response were present when increasing pH in stock solution.

Therefore for effectively simulating ammonia in exhaled breath, mixing method for preparing certain amount of ammonia concentration in vapor (RH > 95%) needs to be further studied and the sampling effect could be discussed on this basis.

I.2 Crosstalk between Metabolites in Alcohol Metabolism — Interferences from Acetone, Acetaldehyde and Methanol in Ethanol Sensing

Acetone, acetaldehyde, methanol and ethanol are present in EB. These biomarkers can be catalyzed, and electrochemically sensed, using alcohol dehydrogenase, but only ethanol and methanol are catalyzed by alcohol oxidase (Table I.1). For enhanced specificity and simplicity, alcohol oxidase was chosen as the catalyzing enzyme in sensor fabrication in this study. For further understanding of the practical effect in simulated EB sensing, such as how much noise will be made from the presence of acetone and acetaldehyde, how much current increase will be induced by the presence of methanol, the crosstalk experiment will provide related information to improve sensor design and help signal interpretation.

Table I.1. Available enzymes and mechanisms in acetaldehyde, acetone, ethanol and methanol sensing

Biomarker	Enzyme	Mechanism
Acetaldehyde	alcohol dehydrogenase	acetaldehyde + NADH + H^+ ↔ ethanol + NAD^+
		acetaldehyde + NADPH + H^+ ↔ ethanol + $NADP^+$
Acetone	alcohol dehydrogenase	acetone + NADH ↔ isopropanol + NAD^+
		acetone + NADH + H^+ ↔ propan-2-ol + NAD^+
		acetone + NADPH ↔ 2-propanol + $NADP^+$
		acetone + NADPH + H^+ ↔ propan-2-ol + $NADP^+$
Ethanol	alcohol dehydrogenase	ethanol + NAD^+ ↔ acetaldehyde + NADH + H^+
		ethanol + $NADP^+$ ↔ acetaldehyde + NADPH + H^+
	alcohol oxidase	ethanol + O_2 ↔ acetaldehyde + H_2O_2
Methanol	alcohol dehydrogenase	methanol + NAD^+ ↔ formaldehyde + NADH + H^+
		methanol + $NADP^+$ ↔ formaldehyde + NADPH + H^+
	alcohol oxidase	methanol + O_2 ↔ formaldehyde + H_2O_2

A preliminary experiment was conducted to test liquid phase mixture (which is called stock solution in previous sections). The concentrations of each constituent in mixture were prepared using Henry's law (Table I.2).

Table I.2. Properties of acetaldehyde, acetone, ethanol, and methanol

Biomarker	**k_H at 310K (M/atm)**	**F.W. (g/mol)**	**Density (g/ml)**	**Aqueous Concentration (%)**	**Vapor Concentration (ppm)**
Acetaldehyde	7.05	44.05	0.788	0.00016	4
				0.00020	5
				0.00030	7.5
Acetone	14.58	58.08	0.793	0.00043	4
				0.00053	5
				0.00080	7.5
Ethanol	79.09	46.07	0.789	0.00185	4
				0.00231	5
				0.00346	7.5
Methanol	101.03	32.04	0.792	0.00164	4
				0.00204	5
				0.00307	7.5

A mixture of methanol/ethanol had the highest current response than mixtures of acetone/ethanol, acetaldehyde/ethanol, or ethanol only sample (Figure I.6). Moreover, only the result from methanol/ethanol mixture had a significant difference (p=0.093) from the ethanol only sample.

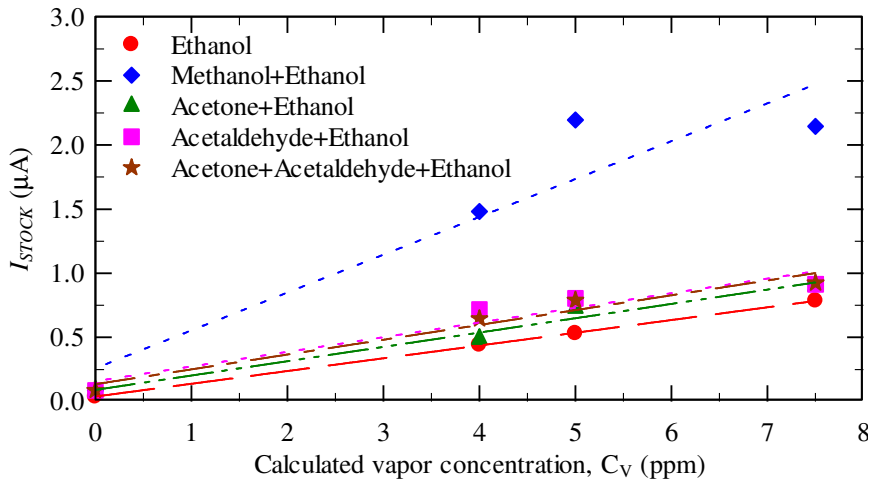

Figure I.6. Amperometric measurements of mixtures of acetaldehyde, acetone, ethanol, and methanol were taken in stock solution. One replication sample has been measured. Dashed lines represent linear regression results

Further studies need to be done to determine how each biomarker would present in vapor and condensate samples and the effect of different sampling conditions, such as sampling temperature and flow rate, on sensing a mixture of biomarkers.